ARL-TR-93-20

Copy No. 3

NATIVE I VLF Signal Analysis

Final Report under Contract N00039-91-C-0082
TD No. 01A1019, NATIVE I VLF Experiment Data Research and Analysis

Scott J. Levinson
Stephen K. Mitchell
Nancy R. Bedford
Joan C. Lange

Applied Research Laboratories
The University of Texas at Austin
P. O. Box 8029 Austin, TX 78713-8029

20 October 1993

Final Report

15 April 1991 - 31 October 1992

Approved for public release;
distribution is unlimited.

Prepared for:
Naval Research Laboratory
Stennis Space Center, MS 39529-5004

Monitored by:
Space and Naval Warfare Systems Command
Department of the Navy
Washington, D.C. 20363-5100

DISCLAIMER NOTICE

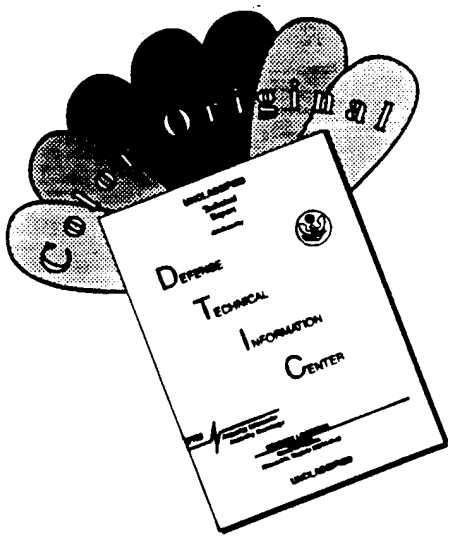

THIS DOCUMENT IS BEST QUALITY AVAILABLE. THE COPY FURNISHED TO DTIC CONTAINED A SIGNIFICANT NUMBER OF COLOR PAGES WHICH DO NOT REPRODUCE LEGIBLY ON BLACK AND WHITE MICROFICHE.

REPORT DOCUMENTATION PAGE

Form Approved
OMB No. 0704-0188

1. AGENCY USE ONLY (Leave blank)	2. REPORT DATE	3. REPORT TYPE AND DATES COVERED
	20 October 1993	final 15 Apr 91 - 31 Oct 92

4. TITLE AND SUBTITLE

NATIVE I VLF Signal Analysis, Final Report under Contract N00039-91-C-0082, TD No. 01A1019, NATIVE I VLF Experiment Data Research and Analysis

5. FUNDING NUMBERS

N00039-91-C-0082,
TD No. 01A1019

6. AUTHOR(S)

Levinson, Scott J.
Bedford, Nancy R.
Mitchell, Stephen K.
Lange, Joan C.

7. PERFORMING ORGANIZATION NAMES(S) AND ADDRESS(ES)

Applied Research Laboratories
The University of Texas at Austin
P.O. Box 8029
Austin, Texas 78713-8029

8. PERFORMING ORGANIZATION REPORT NUMBER

ARL-TR-93-20

9. SPONSORING/MONITORING AGENCY NAME(S) AND ADDRESS(ES)

Commanding Officer
Naval Research Laboratory
Stennis Space Center, MS 39529-5004

Space and Naval Warfare Systems Command
Department of the Navy
Washington, DC 20363-5100

10. SPONSORING/MONITORING AGENCY REPORT NUMBER

11. SUPPLEMENTARY NOTES

12a. DISTRIBUTION/AVAILABILITY STATEMENT

Approved for public release;
distribution is unlimited.

12b. DISTRIBUTION CODE

13. ABSTRACT (Maximum 200 words)

During the NATIVE I experiment conducted in the Blake Plateau area, very low frequency (VLF) sound waves transmitted at 7 and 10 Hz from a source towed at a depth of 122 m were sampled over the bottom half of the water column by an 18-element vertical hydrophone array anchored on the bottom (3170 m deep). Analysis included the comparison of measured beam levels with corresponding eigenray and adiabatic normal mode models at short (0.7 km - 20 km) and long (35-60 km) ranges. At short ranges, the VLF measurements and both models were consistent in indicating easily distinguishable direct, bottom, bottom-surface, and bottom-surface-bottom interacting arrivals. At longer range, the arrivals typically consisted of three from the surface and three from the bottom, corresponding to two, three, and four bottom interactions. An anomalous bottom loss observed at 30-34° at 7 Hz appears to be the result of a slow hydrate layer in the sediment. Except for these angles, VLF bottom loss was low compared to typical values at higher frequency, and consistent with conventional modeled loss calculations for the pre-assessed geoacoustic parameters of the sediment.

14. SUBJECT TERMS

VLF
NATIVE I
bottom loss
hydrate layer
normal mode model
ray model
VEDABS measurements
beam signal level

15. NUMBER OF PAGES

86

16. PRICE CODE

17. SECURITY CLASSIFICATION OF REPORT	18. SECURITY CLASSIFICATION OF THIS PAGE	19. SECURITY CLASSIFICATION OF ABSTRACT	20. LIMITATION OF ABSTRACT
UNCLASSIFIED	UNCLASSIFIED	UNCLASSIFIED	SAR

NSN 7540-01-280-5500

Standard Form 298 (Rev. 2-89)
Prescribed by ANSI Std. 239-18
298-102

This page intentionally left blank.

TABLE OF CONTENTS

This page intentionally left blank.

LIST OF FIGURES

PREFACE

This report is the final report on work that ARL:UT was tasked to do under Contract N00039-91-C-0082, TD No. 01A1019, entitled NATIVE I VLF Experiment Data Research and Analysis. Overall sponsorship of the NATIVE I experiment and the processing and analysis of the data was provided by the Advanced Environmental Acoustic Support (AEAS) Program of the Office of Naval Research.

This page intentionally left blank.

1. INTRODUCTION

In recent years it has become apparent that antisubmarine warfare (ASW) systems must be developed to exploit different portions of the source signal spectrum depending on the particular environment and source operating mode. Some promising results have been obtained with systems focusing on the very low frequency (VLF) regime (1-30 Hz). However, the research community has only limited knowledge of environmental acoustic parameters at very low frequencies. Several things will be required for optimal design and utilization of VLF based systems: an improved understanding of VLF propagation under various oceanographic and geologic conditions, the development of VLF databases, and the design of VLF performance prediction models.

In this report we present our analysis of the VLF continuous wave (cw) acoustic data collected during Event 1 of the NATIVE I Exercise.[1] Our objectives here are to examine the arrival structure of the cw signal propagation, and to establish and validate the corresponding geoacoustic profile in the sediment. Our approach is to compare the arrival structure and acoustic levels measured at the VEDABS 1 array with those predicted by model calculations based on pre-assessed and measured geoacoustic parameters.

We first use the range invariant GAMARAY model[2] to describe an ocean 3300 m in depth and having no bottom loss. These ray calculations are then used to compare the measurements with the coherent transmission loss (TL) at short ranges (~20 km) for 18 receiver depths between 1565 m and 3140 m. This model, we have observed, provides a useful, intuitive picture of the propagation. A more refined analysis of the ~0.5° sloping bottom in the NATIVE exercise area is also conducted using adiabatic normal mode calculations from NEMESIS[3] to quantitatively investigate the acoustic arrival structure and the sediment's sound speed and attenuation profiles.

This report is organized as follows. The NATIVE I Exercise is outlined in Section 2 and the environment is described in Section 3. In Section 4 we investigate the omnidirectional arrivals at short ranges (0-12 km) by comparing

the measured TL at each hydrophone in the array to corresponding model calculations which incorporate no bottom attenuation. These comparisons are performed to confirm source-receiver ranges and to validate the VLF transmission loss within RAP range, as calculated using the reported source level and receiver sensitivities. Both range and level corrections were required in this analysis. In Section 5, we investigate the arrival structure at ranges to about 20 km by comparing the beam levels from the ray and mode models with those measured during Event 1. We then investigate the geoacoustic properties of the bottom in Section 6 by comparing the measurements with modeled beam and bottom loss estimates based on two distinctive sets of geoacoustic parameters. In Section 7, we investigate the arrival structure and bottom loss at ranges between 35-60 km; because of their increased sensitivity to environmental uncertainties, we have statistically analyzed these longer range measurement-model comparisons. In Section 8, VLF propagation and bottom loss are summarized.

2. NATIVE I EVENT 1 DESCRIPTION

A 12 kHz narrowbeam echo sounder aboard the R/V Gyre was used to collect pertinent bathymetric data during NATIVE I,[4] and the extremely low frequency (ELF) acoustic source[5] was used to project cw signals. Figure 2.1 is an overview of the NATIVE I exercise cw track for Event 1.[5] The curves illustrate where the "short range" and "long range" 7 and 10 Hz signals were projected relative to the VEDABS receiving array (V1 array). Figure 2.2 is a plot of the measurements and the bathymetry used in calculations. The measurements have been used to model the ocean depth at nine ranges in a piecewise linear fashion. The bathymetry used in calculations is symmetric at "short ranges" about V1, and has been incorporated in the range variable, normal mode calculations that will be presented later. (Figure 2.1 indicates that the bathymetry measurements were conducted on a track slightly different from the track used in the acoustic measurements. Although the resulting bathymetry errors are probably small, comparison of the model and the measurements indicates that these errors have likely affected the degree of certainty that can be given to bottom loss and attenuation profile estimates.)

The VEDABS 1 array, shown schematically in Fig. 2.3, was located on the Blake Outer Ridge where the ocean is 3170 m in depth, and the array covered approximately half of the water column. Acoustic data have been collected, and corresponding transmission loss has been calculated at every working receiver. Four of the receivers were not usable for cw measurements since three of them (Nos. 2, 15, and 17) were not working, and the fourth (No. 12) was desensitized by 40 dB for SUS analysis. The ELF projector was towed at a depth of 122 ±7 m by the R/V Gyre, with projected cw tones at 7, 10, and 16 Hz.[6] Our analysis of the arrival structure focuses on the 7 and 10 Hz components since the VEDABS 1 array was designed for 10 Hz and is aliased at higher frequencies.

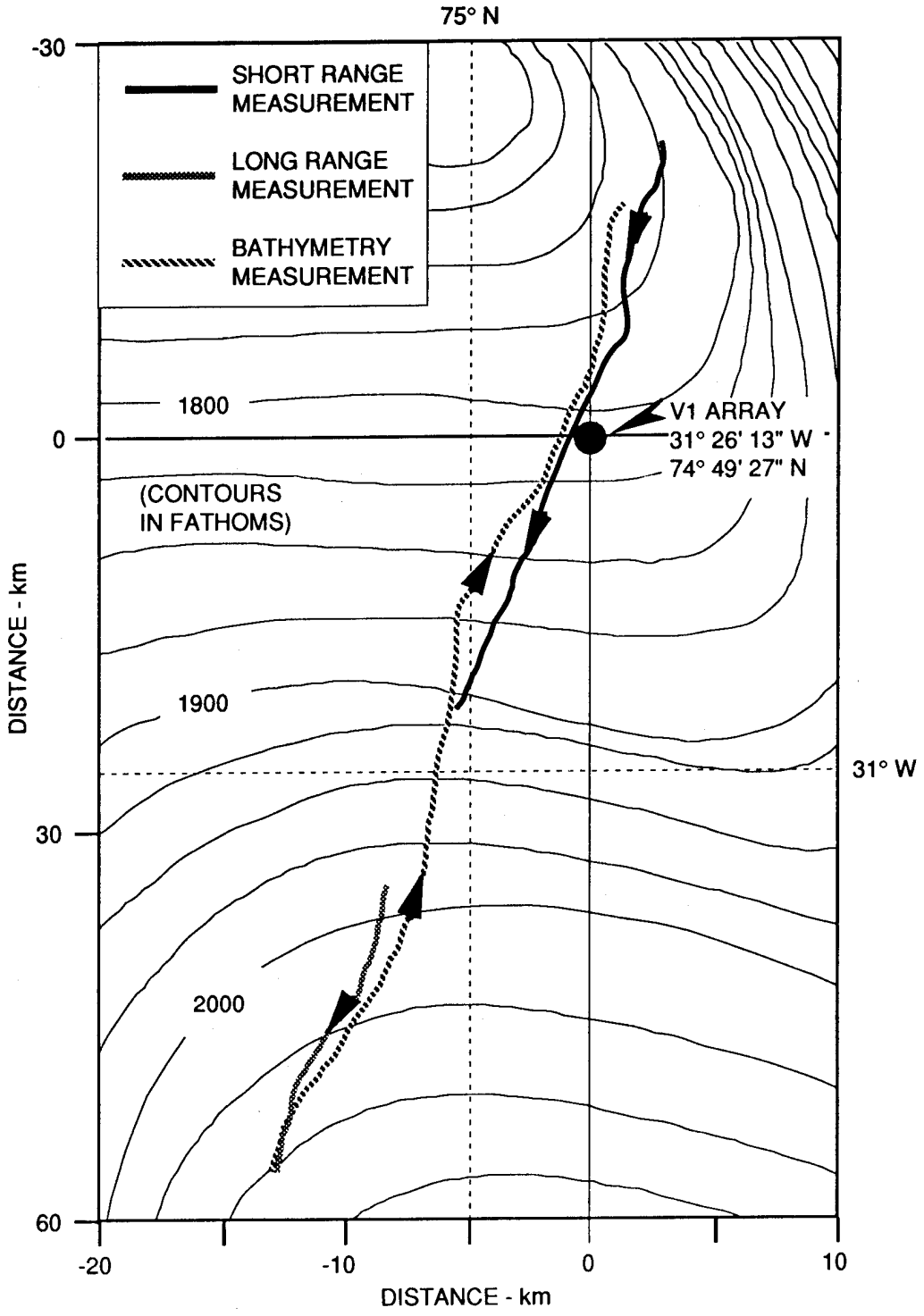

FIGURE 2.1
NATIVE I NAVIGATION AND BATHYMETRY
FOR 7 AND 10 Hz cw EXERCISE (EVENT 1)

ARL - UT
AS-93-543
SJL/RFO
10-93/hd2

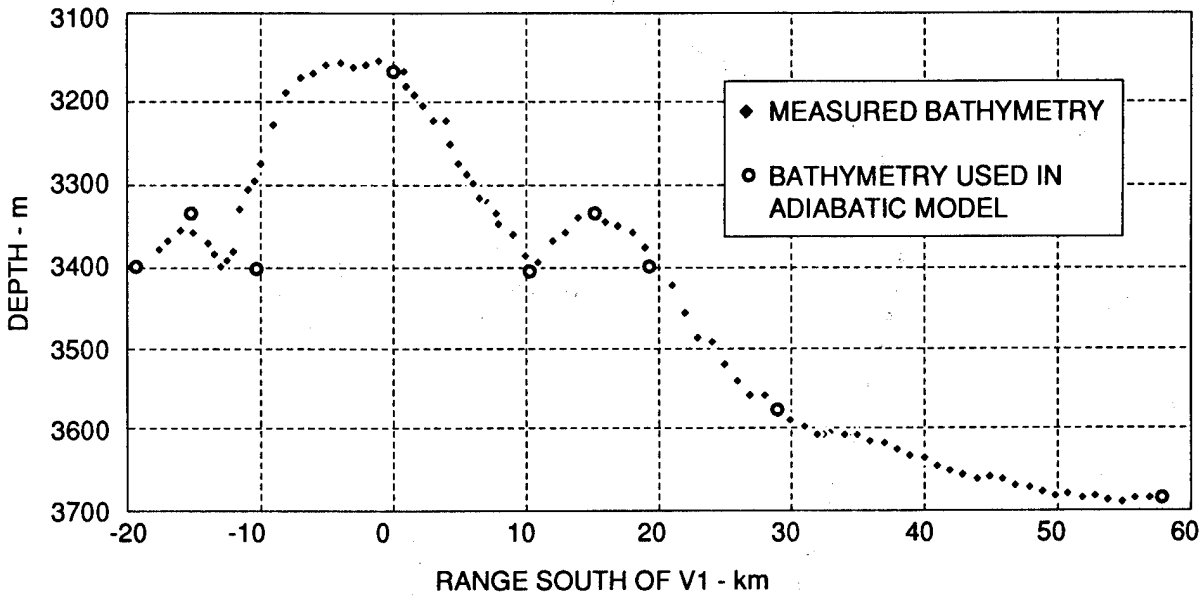

FIGURE 2.2
BATHYMETRY AS MEASURED AND USED IN ADIABATIC MODEL

ARL - UT
AS-93-544
SJL/RFO
10-93/hd2

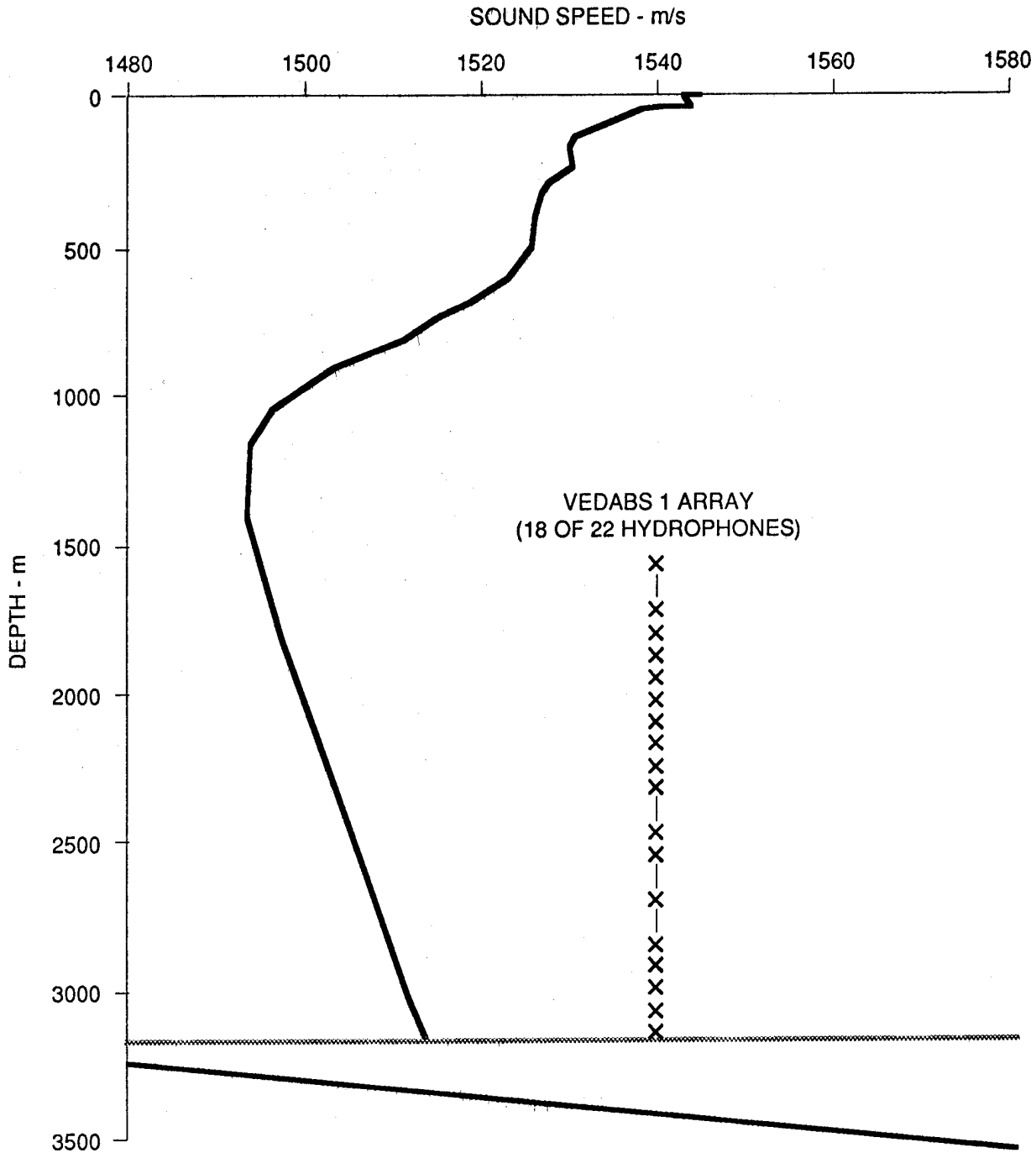

FIGURE 2.3
NATIVE I SOUND VELOCITY PROFILE
IN THE VICINITY OF THE VEDABS 1 HYDROPHONE ARRAY

ARL - UT
AS-93-545
SJL/RSFO
10-93/hd2

3. ACOUSTIC ENVIRONMENTAL DESCRIPTION

The sound velocity profile (SVP) was measured using bathythermograph and conductivity-temperature-depth casts deployed from the R/V Gyre.[4] The SVP for the ocean in the vicinity of the VEDABS array is shown in Fig. 2.3. Note that the SVP indicates a bottom-limited acoustic environment.

Event 1 occurred on the Blake Outer Ridge, which is formed by soft, current deposited, hemipalagic sediments.[4] The acoustic properties of this sediment type are described[1] by the GAM 1 SVP and attenuation curves shown in Fig. 3.1. The Blake Outer Ridge region is also known to contain gas hydrates, which affect the "short range" arrivals.[4,7] Due to increasing temperature with increasing depth, gas hydrates often decompose (forming free gas) below a given depth, resulting in a sound velocity inversion,[8] as shown by the GAM 2 curves[9] in Fig. 3.1.

In Sections 5 and 6, the sediment will be modeled acoustically as a fluid, overlying a semi-infinite solid substrate using GAM 1 and GAM 2 sediment profiles. To ascertain the geometric spreading loss, we model the sediment with the compressional sound speed of GAM 1 but without attenuation (GAM 0). The high shear attenuation and low shear sound speeds shown in Fig. 3.1 (relative to their compressional counterparts) lead to insignificant shear wave excitation. Bottom loss calculations which consider shear waves have been performed, but these have shown that shear effects are, indeed, negligible. Thus, only the fluid properties of the sediment (with solid substrate properties) will be analyzed with normal mode calculations in this work. In such calculations, the sediment is first considered to exhibit the smooth, positive compressional sound speed gradient shown in Fig. 3.1, but with no attenuation (GAM 0), so that only the geometric spreading loss is indicated. The GAM 1 compressional attenuation profile will be modeled with normal mode calculations to compare the measurements with expected bottom loss estimates when no hydrate layer is present. Finally, the GAM 2 profile,[9] which describes a gas hydrate layer 300-340 m deep into the sediment having a reduced compressional SVP, will be modeled with normal mode calculations of the "short range" arrivals.

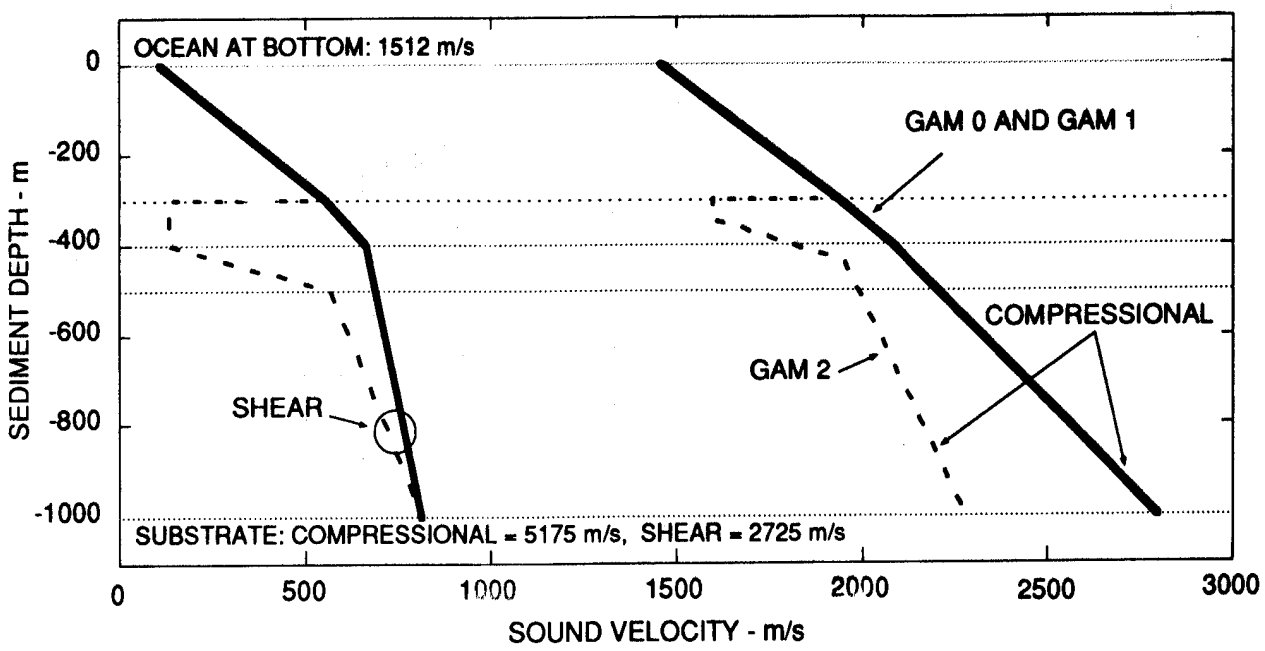

(a) SEDIMENT SVP

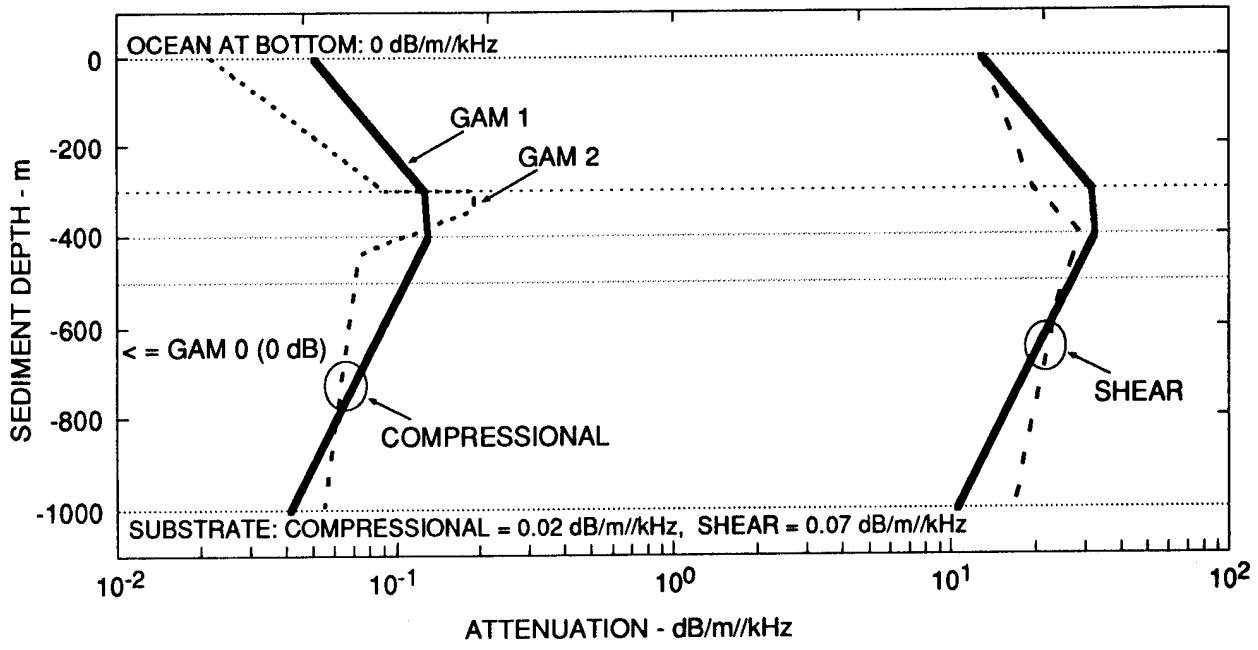

(b) SEDIMENT ATTENUATION

FIGURE 3.1
SOUND VELOCITY AND ATTENUATION PROFILES OF THE SEDIMENT USED IN MODELS

ARL - UT
AS-93-546
SJL/RFO
10-93/hd2

4. SHORT RANGE OMNIDIRECTIONAL ARRIVALS

The measured omnidirectional hydrophone levels at 7 Hz are shown as a colorscale plot in Fig. 4.1. The levels for each hydrophone are plotted as a function of source-receiver range, with negative ranges when the source is approaching the VEDABS array from the north, and positive ranges when the source is moving south away from the array. At short ranges (<7 km), note how the interference peaks and nulls advance smoothly in range with increasing depth. As shown by a similar colorscale plot in Fig. 4.2, these qualitative features are well simulated by corresponding ray model calculations, which are based on a sediment described by GAM 0.

More quantitative comparisons of measured and calculated omnidirectional transmission loss (TL) are given for specific hydrophones. Examples of 7 Hz TL calculations using ray modeling and normal mode modeling at the reported ranges[1] are shown in Fig. 4.3 for the shallowest hydrophone (z_1 = 1565 m). Also shown are corresponding TL measurements determined by subtracting the received levels from the reported source level[5] (164 dB). A superior resemblance of the model to the measurements is clearly obtained if the range and level scales are translated to align the calculated and measured peaks occurring near R = 2 km. Such translations correspond to a 0.5 km increase in the measurement ranges and a 4 dB increase in the 7 Hz source level (or a corresponding decrease in the receiver sensitivity). These range and source level translations have been applied to the received level from each hydrophone in the array, and excellent model simulations of the measurements have verified this 0.5 km range scale increase and 4 dB level change.

Model-measurement comparisons are shown in Fig. 4.4 for the shallowest depth (1565 m), a mid-depth (2240 m), and the deepest (3140 m) hydrophones in the array. Comparisons from both GAMARAY ray and NEMESIS normal mode calculations to the omnidirectional measurements are shown in this figure out to 12 km in range. The variable ocean depth is also shown to provide a perspective. A comparison of the ray calculations with the measurements shows that the correspondence is strong at the shortest ranges (R <7 km) where direct paths dominate.

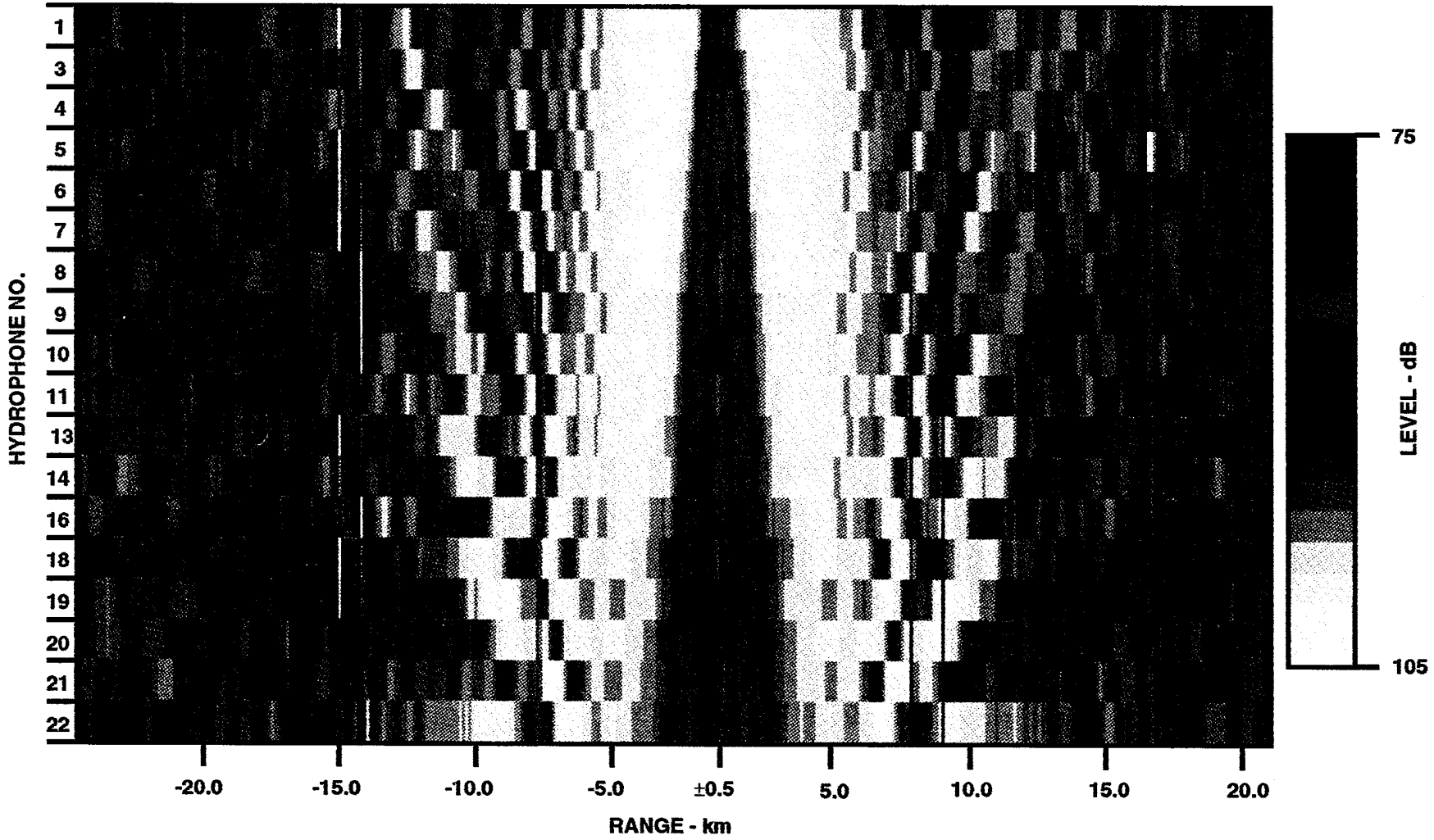

FIGURE 4.1
SHORT RANGE MEASURED 7 Hz OMNIDIRECTIONAL ACOUSTIC LEVELS versus RECEIVER AND RANGE

ARL:UT
AS-93-547
SJL - RFG
10-93uncl2

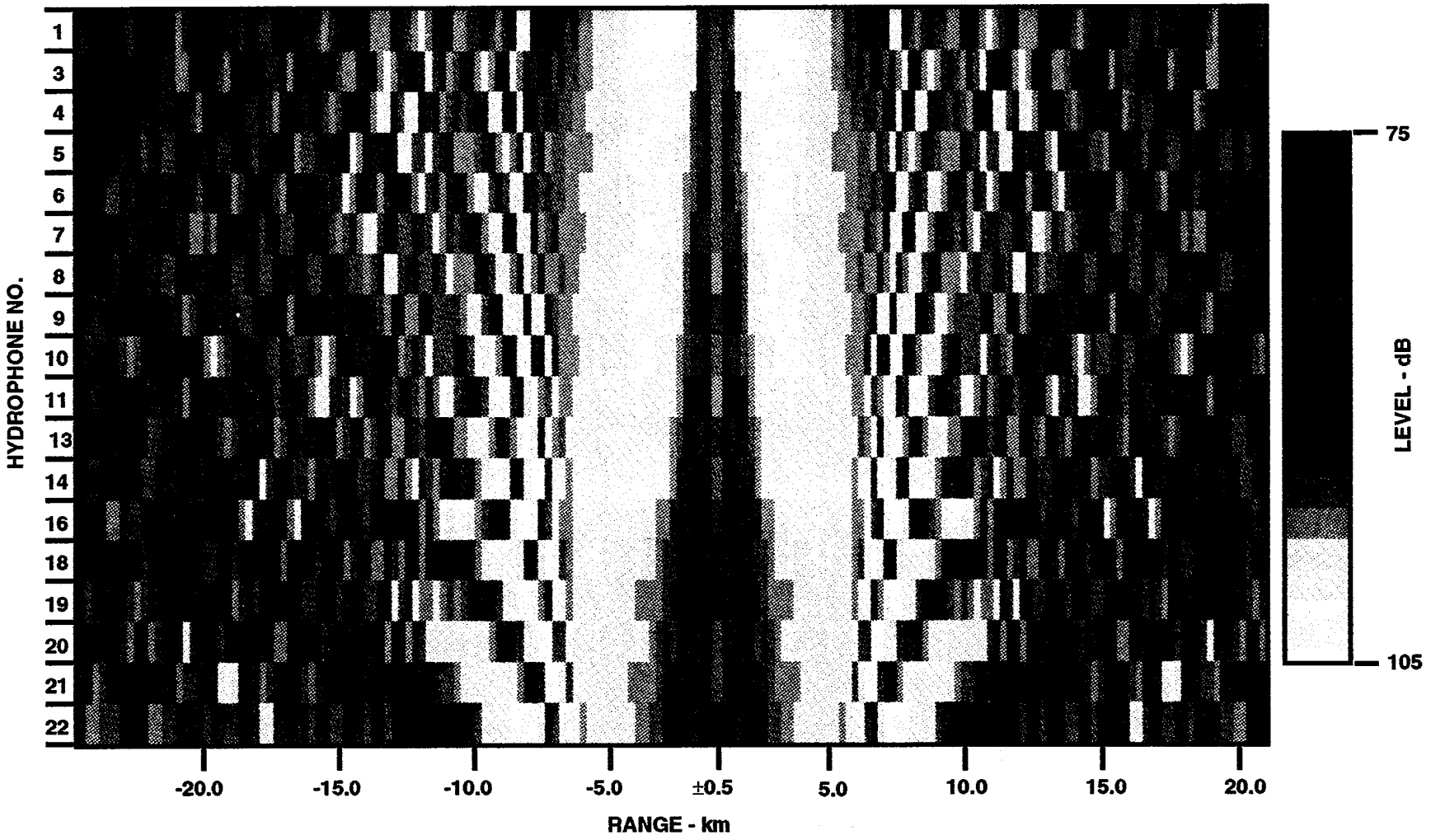

FIGURE 4.2
SHORT RANGE RAY MODELED 7 Hz OMNIDIRECTIONAL LEVELS (GAM 0 SEDIMENT PROPERTIES) versus RECEIVER AND RANGE

ARL-UT
AS-93-548
SJL - RFG
10-93uncl2

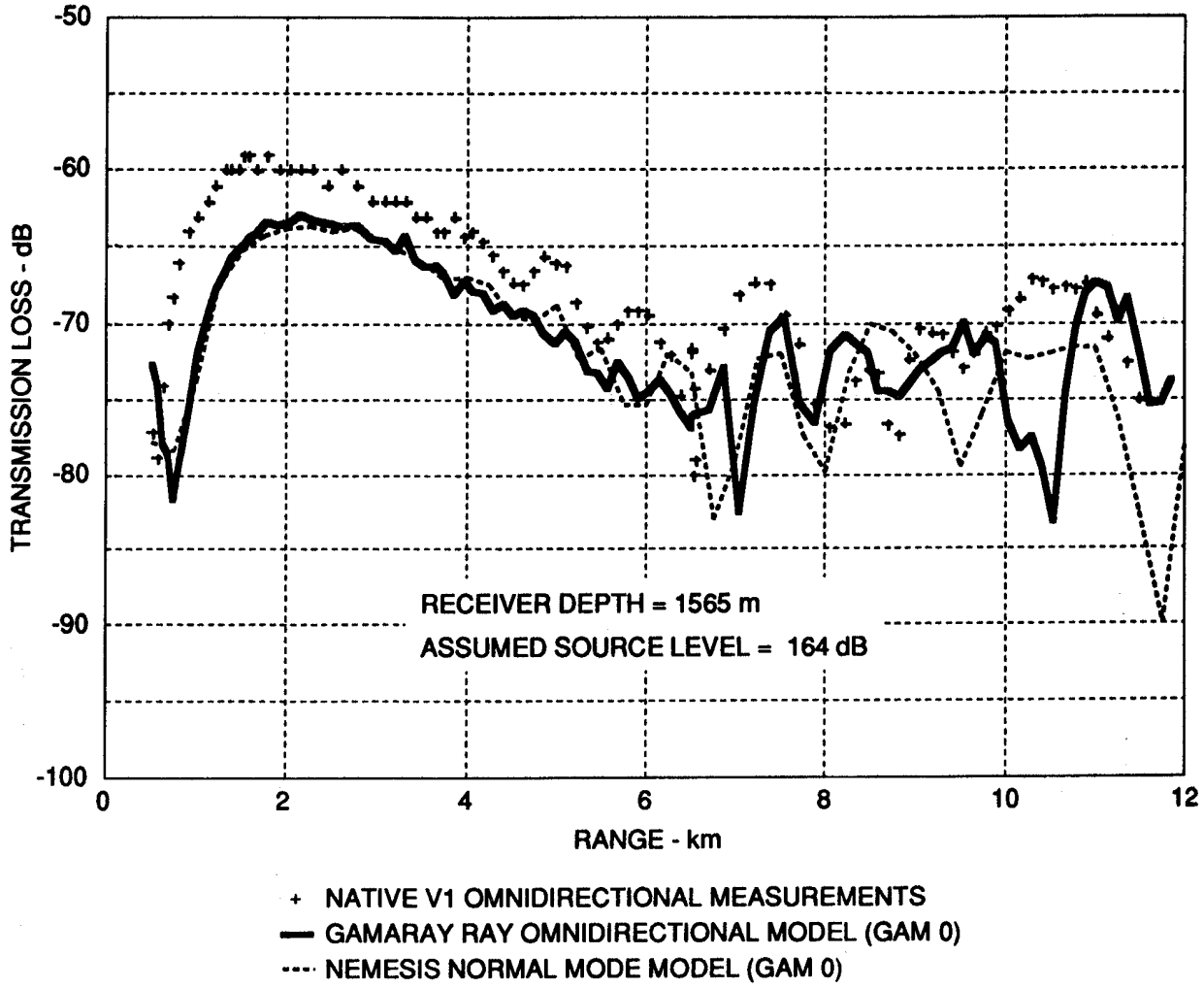

FIGURE 4.3
7 Hz OMNIDIRECTIONAL TRANSMISSION LOSS

ARL - UT
AS-93-549
SJL/RFO
10-93/hd2

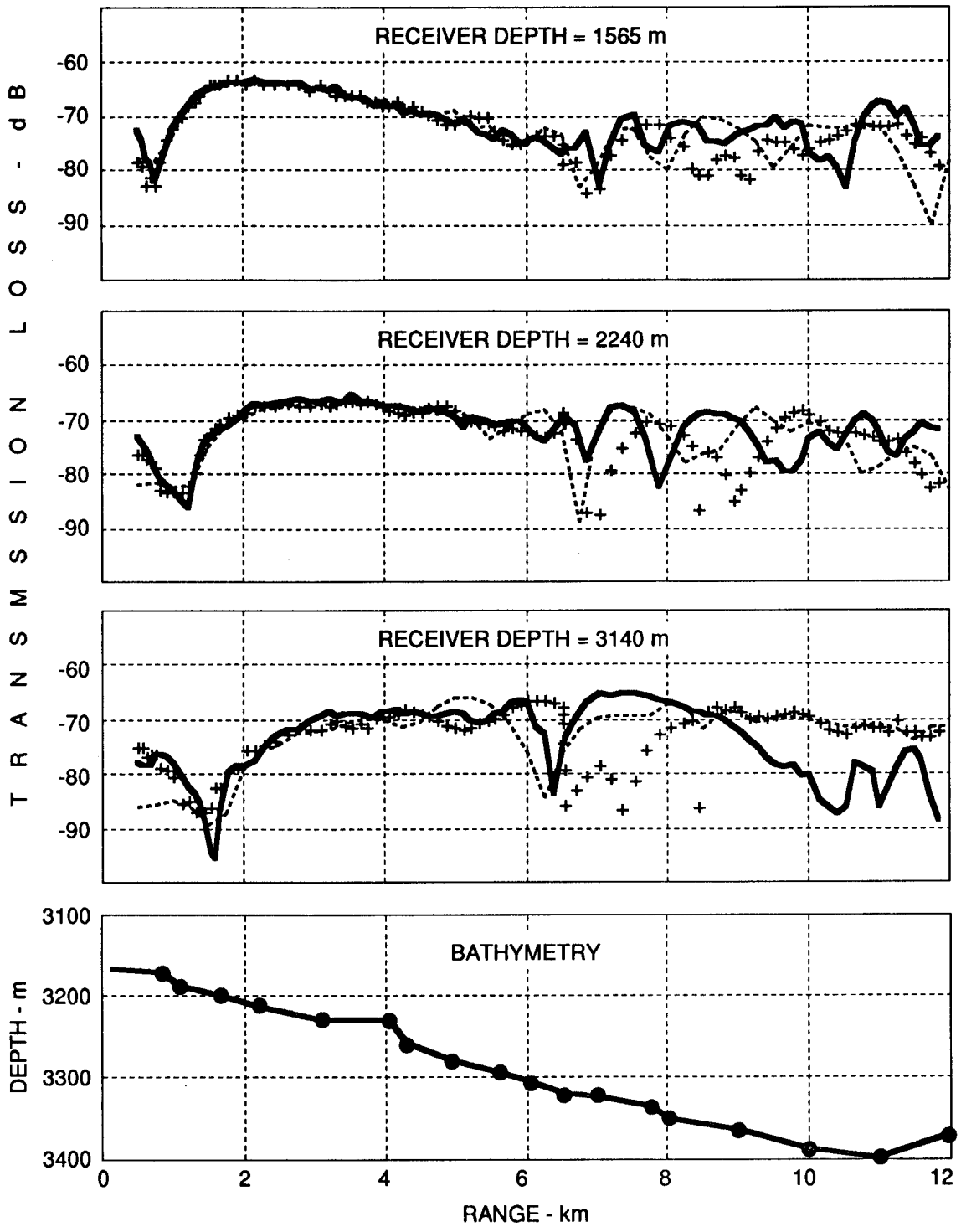

FIGURE 4.4
MEASURED AND MODELED (ASSUMING NO SEDIMENT ATTENUATION)
7 Hz OMNIDIRECTIONAL TRANSMISSION LOSS
AT RANGES TO 12 km

ARL - UT
AS-93-550
SJL/RFO
10-93/hd2

At longer ranges, the significance of the bottom reflections increases, and the associated arrival times and interference patterns are increasingly dependent on bathymetry. Thus differences between measurements and modeling result from the range invariant and "bottom-loss-less" features of the ray model calculations. The normal mode calculations corresponded well to the measurements between 2 km and 7 km. However, high angle arrivals (>60°) are not well simulated by the normal mode calculations; thus poor correspondence exists at ranges where high angle arrivals dominate: those less than 2 km. As a result of the ability to incorporate depth variability, the adiabatic normal mode calculations arguably simulate the measurements better at longer ranges than corresponding ray calculations. However, both models have neglected bottom loss; thus better simulations occur at shorter ranges and shallower receiver depths, as shown in Fig. 4.4. More sophisticated (and accurate) simulations of the beam measurements will be discussed in the next section, where different bottom attenuations will be incorporated in normal mode beam calculations.

The revised range and level scales determined from the omnidirectional levels are used for all subsequent 7 Hz evaluations. We believe that the requirement of a range scale translation for the measurements may result from an unsynchronized timing standard for the projector tow ship and the VEDABS 1 array. The apparent 4 dB level error may be attributed to either a source level that is too low, or to receiving sensitivities that are too high. Comparison with data from other receivers indicates that the receiving sensitivity is more likely the problem. Fortunately, the loss estimates to be discussed are unaffected if either the source level or receiver level is properly compensated.

Measured and ray modeled omnidirectional levels at 10 Hz are shown in Figs. 4.5 and 4.6, respectively. The general features of the measurements are again well simulated by the corresponding model calculations, which are similar to those of the 7 Hz omnidirectional levels (Figs. 4.1 and 4.2).

Figure 4.7 shows both the measured and modeled 10 Hz TL for hydrophone 1 which was determined using the reported 10 Hz source level (166 dB). As with 7 Hz, superior model-measurement correspondence is

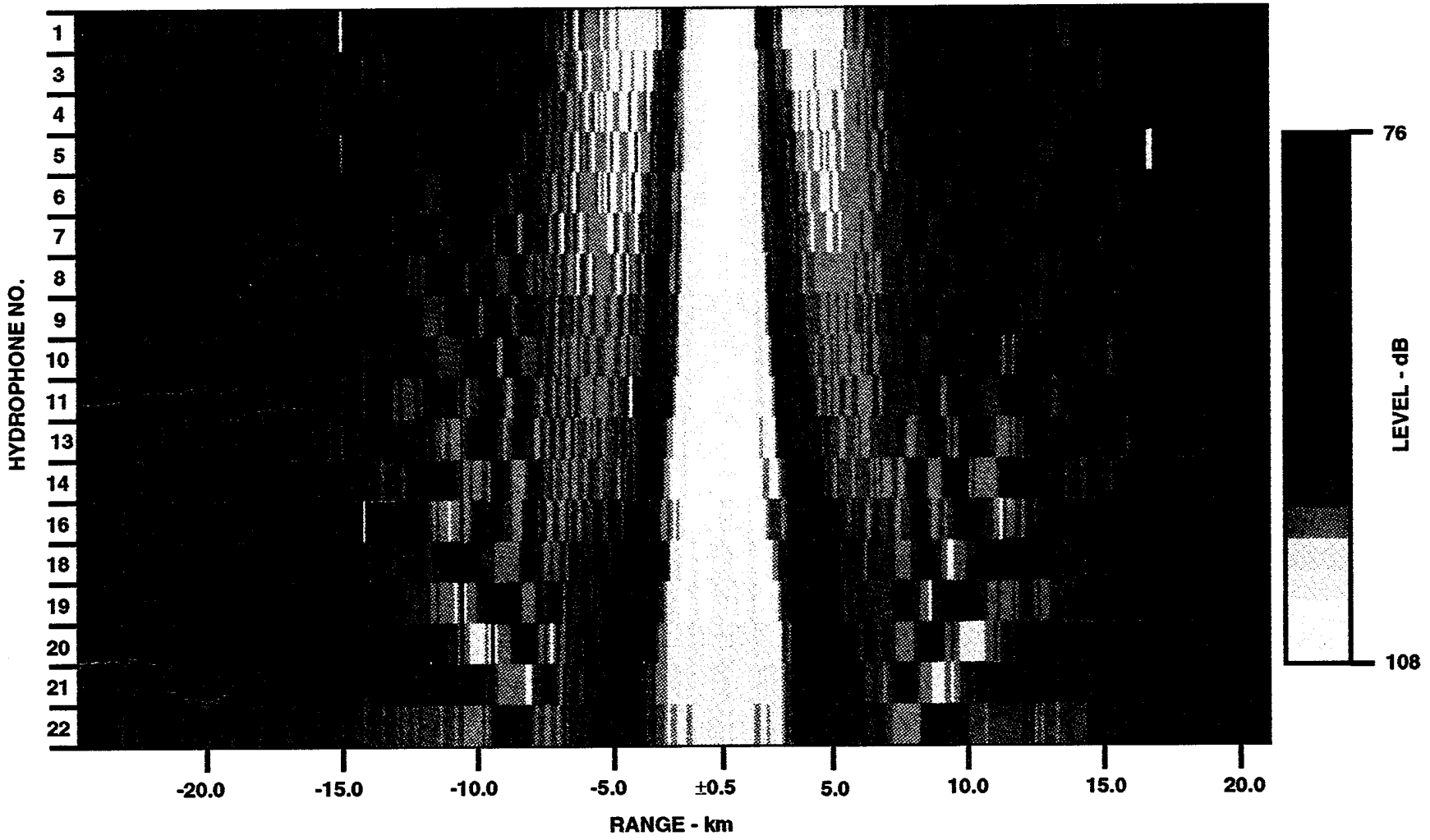

FIGURE 4.5
SHORT RANGE MEASURED 10 Hz OMNIDIRECTIONAL ACOUSTIC LEVELS versus RECEIVER AND RANGE

ARL:UT
AS-93-551
SJL - RFG
10-93uncl2

This page intentionally left blank.

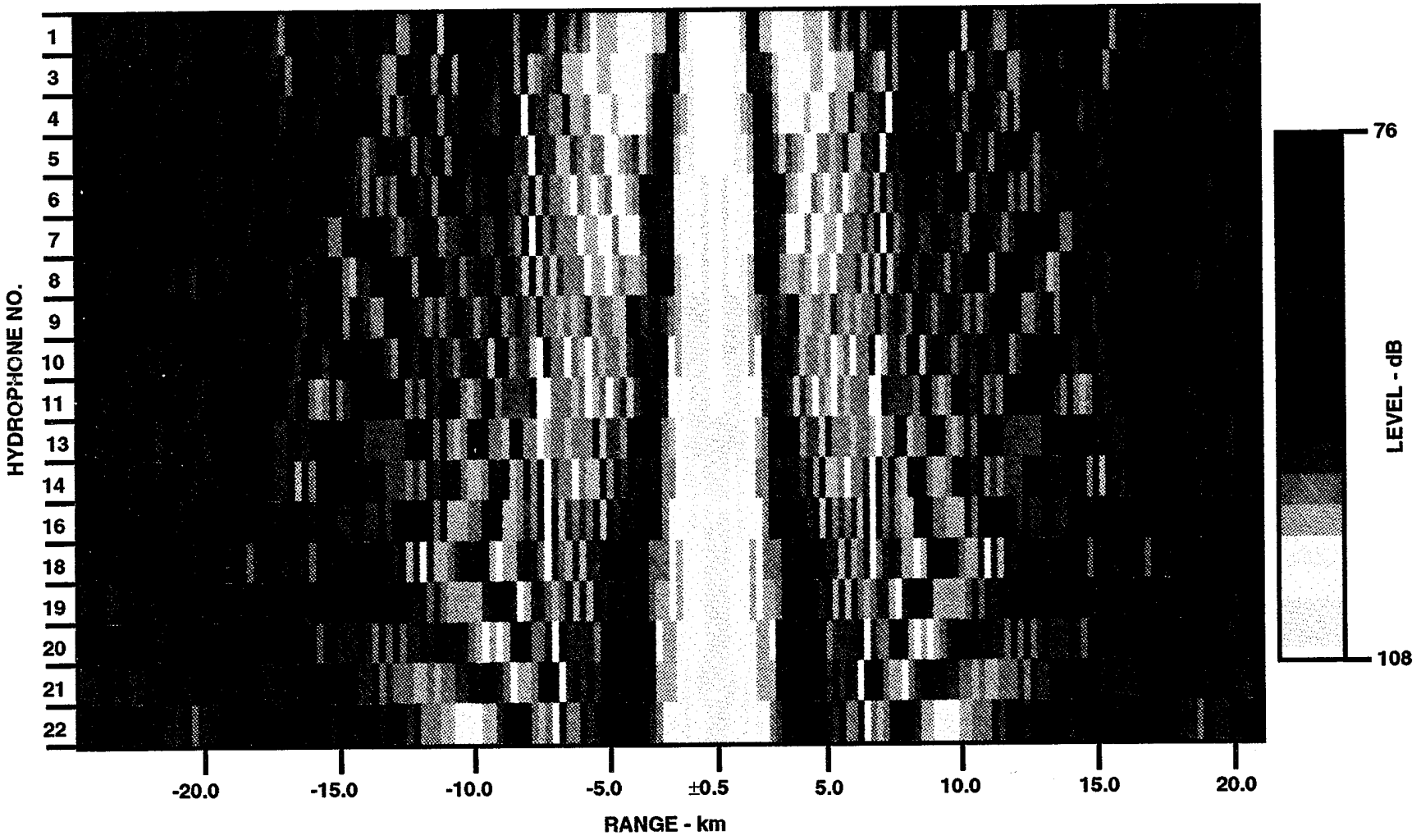

FIGURE 4.6
SHORT RANGE RAY MODELED 10 Hz OMNIDIRECTIONAL LEVELS (GAM 0 SEDIMENT PROPERTIES) versus RECEIVER AND RANGE

ARL:UT
AS-93-552
SJL - RFG
10-93umcl2

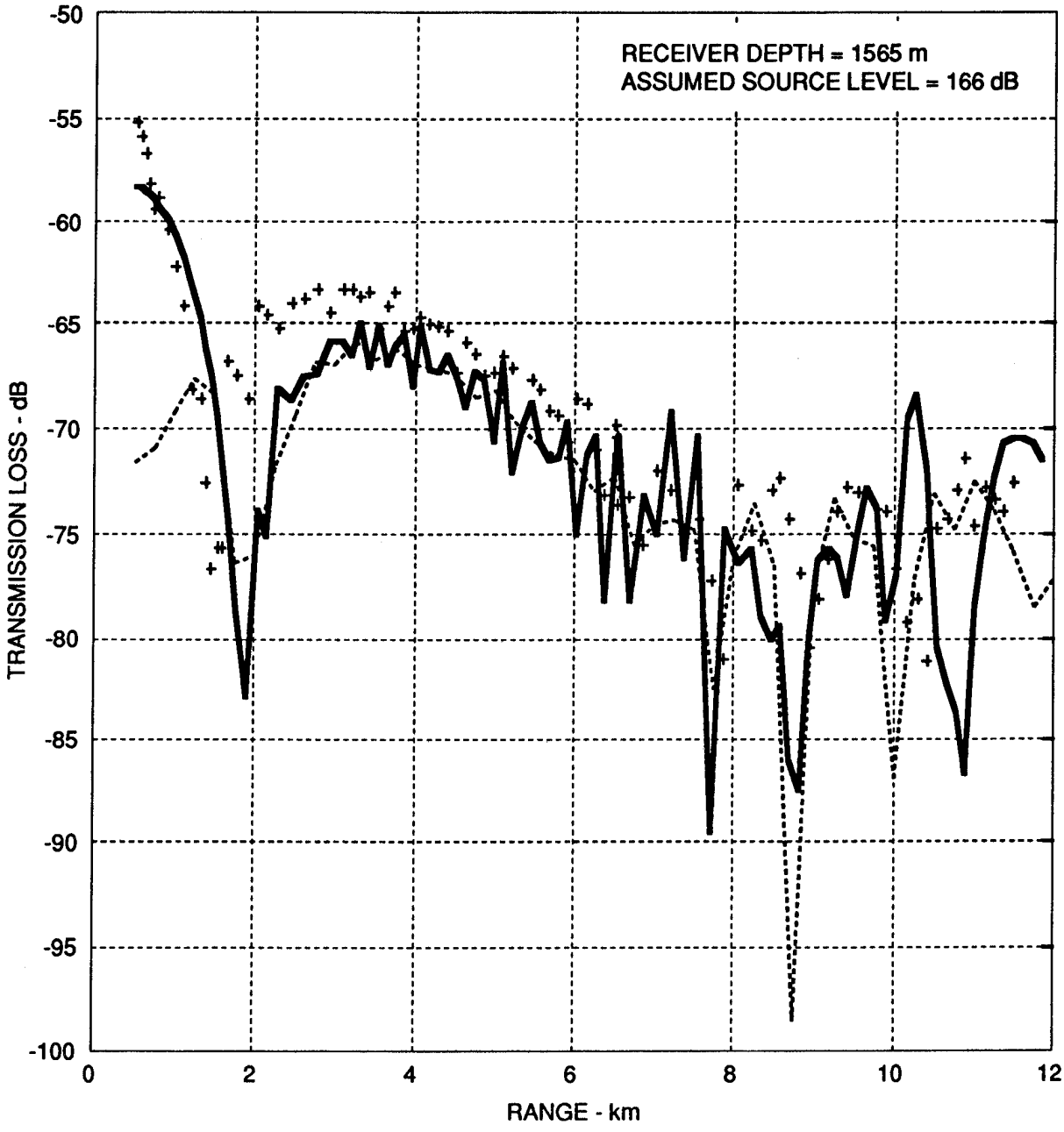

FIGURE 4.7
10 Hz OMNIDIRECTIONAL TRANSMISSION LOSS

ARL - UT
AS-93-553
SJL/RFO
10-93/hd2

obtained when the range and level scales are translated to align the short range, highest level features. For 10 Hz this occurs near R = 3 km, as shown in Fig. 4.7. A 2 dB level change is indicated at 10 Hz, and the 0.5 km range scale translation requirement is consistent with (i.e., the same as) that required at 7 Hz. As illustrated by the omnidirectional levels of three of the receivers in Fig. 4.8, this translation of the range and source levels gives satisfactory 10 Hz model simulations of the omnidirectional measurements. These translations have been applied to the data in Figs. 4.5 and 4.6, and will apply to all subsequent 10 Hz analysis.

Measured omnidirectional levels at 16 Hz are shown as a colorscale plot in Fig. 4.9. The 16 Hz source was projected from a different location than that for 7 and 10 Hz. Thus, the 16 Hz range scale is different, but the general features of the measurements are again well simulated by corresponding model calculations - which are similar to those of 7 and 10 Hz shown in Figs. 4.2 and 4.6, respectively.

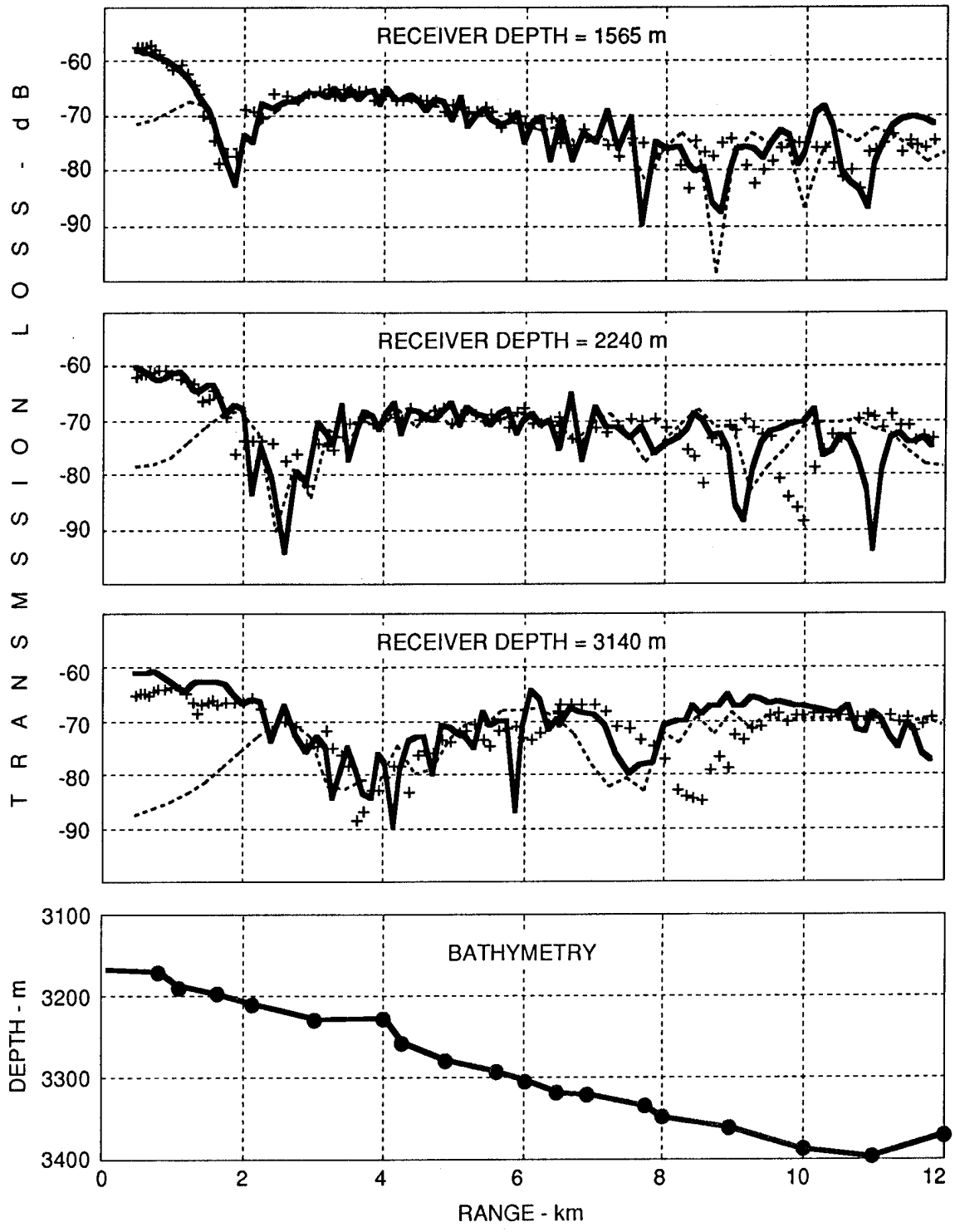

FIGURE 4.8
MEASURED AND MODELED (ASSUMING NO SEDIMENT ATTENUATION)
10 Hz OMNIDIRECTIONAL TRANSMISSION LOSS
AT RANGES TO 12 km

ARL - UT
AS-93-554
SJL/RFO
10-93/hd2

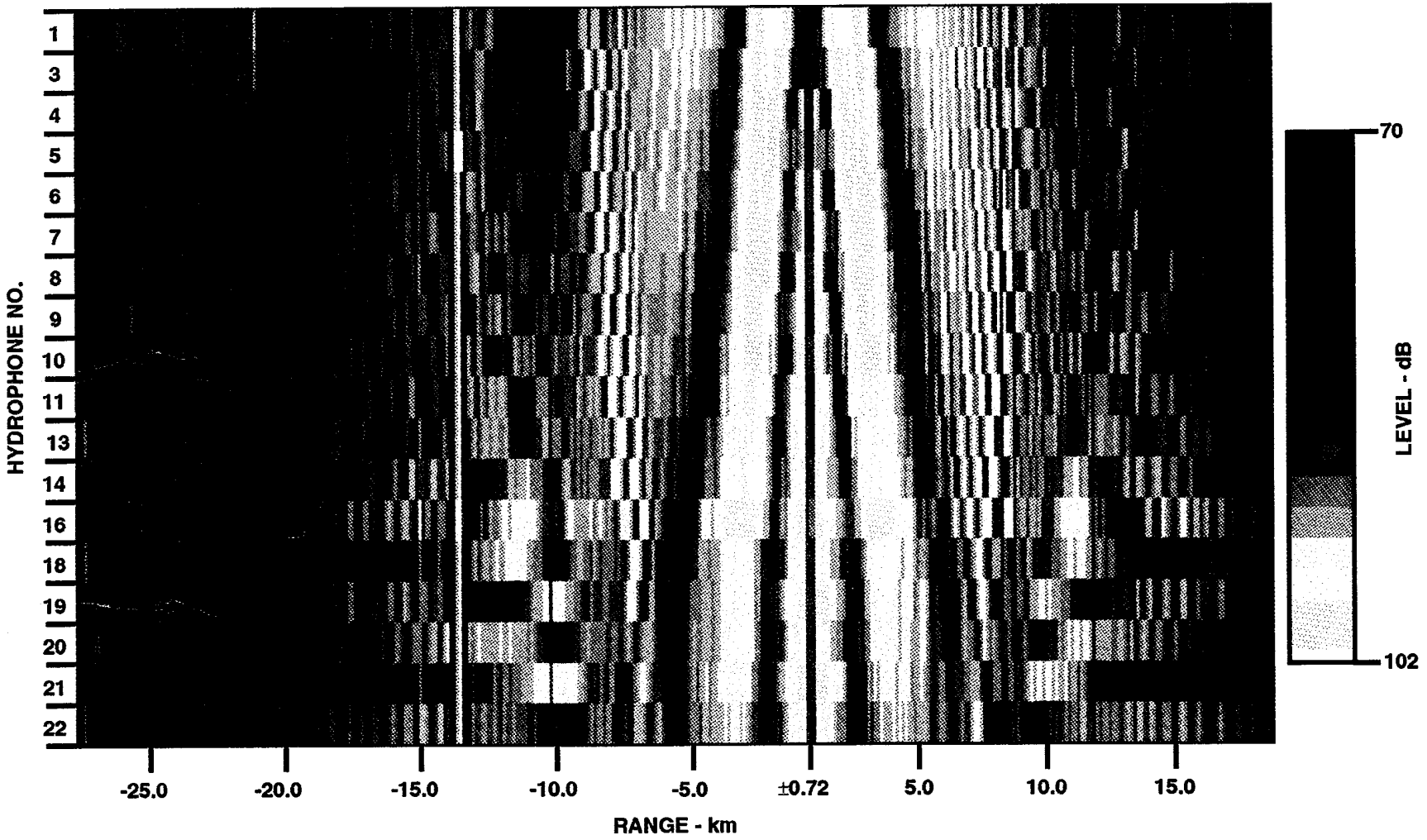

FIGURE 4.9
MEASURED 16 Hz OMNIDIRECTIONAL LEVELS versus RECEIVER AND RANGE

ARL:UT
AS-93-555
SJL - RFG
10-93umcl2

This page intentionally left blank.

5. SHORT RANGE BEAM ARRIVAL STRUCTURE

In this section the arrival structure and transmission loss within 20 km of the VEDABS 1 array are investigated using beams steered at grazing angles from -90° to 90° in 1° steering increments. As a result of the failure of some receivers in the array, standard uniformly spaced shading procedures (such as Dolph-Chebychev or Taylor methods) are unsatisfactory. Consequently, the receiver shading coefficients were selected using an in-house optimization technique at each frequency. Broadside beam patterns at 7, 10, and 16 Hz, which correspond to the optimized shading coefficients developed in this work, are shown in Fig. 5.1.

Several arrival orders are readily observable in the 7 Hz beam data of Fig. 5.2. Strong, direct arrivals (>90 dB), for example, may be recognized at positive grazing angles at short ranges (|R| < ~12 km). Bottom reflections occurring at negative grazing angles (-15° > q > -40°) are recognizable at ranges ~7 km < |R| < ~20 km, as are bottom-surface reflections occurring at grazing angles 22° < q <50° at ranges ~12 km < |R| < ~20 km. Double bottom reflecting arrivals are even discernible near -30° at ranges greater than 18 km. Range intervals showing an equally low level across all angles correspond to a calibration time period or a processing artifact.

Figures 5.3 and 5.4 show 7 Hz beams determined from the coherent TL calculations using the adjusted source level with GAM 0 sediment properties. These modeled beams are comparable to the measured beams shown in Fig. 5.2. Specifically, Fig. 5.3 represents range-invariant GAMARAY ray calculations (depth = 3300 m) for each of the 18 receivers. Figure 5.4 shows corresponding NEMESIS, adiabatic normal mode calculations using the bathymetry shown in Fig. 2.2. It is worth noting that all of the significant features found in the measurements in Fig. 5.2 may also be observed using both models in Figs. 5.3 and 5.4 except at ranges corresponding to processing artifacts. The arrivals are direct, bottom reflected, bottom-surface reflected, and double bottom reflected in the models at approximately the same ranges and angles as those in the data.

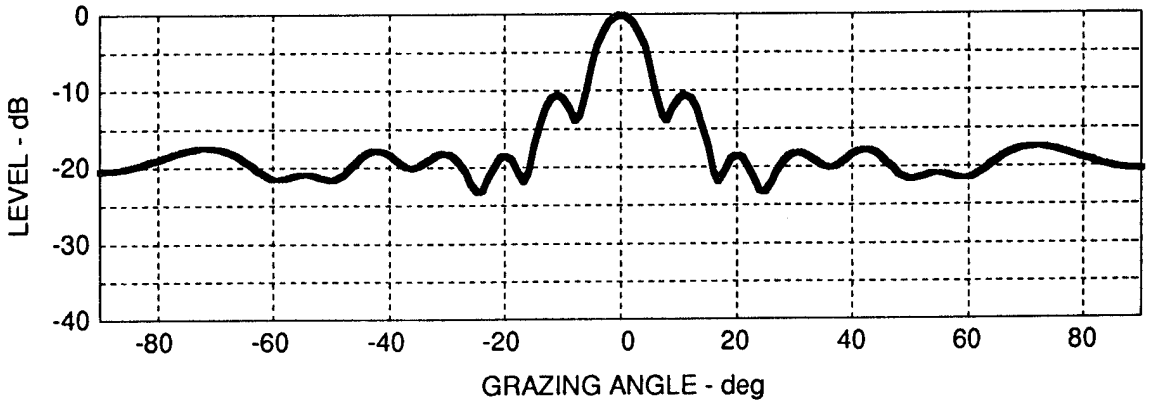

(a) 7 Hz OPTIMIZED BEAM PATTERN

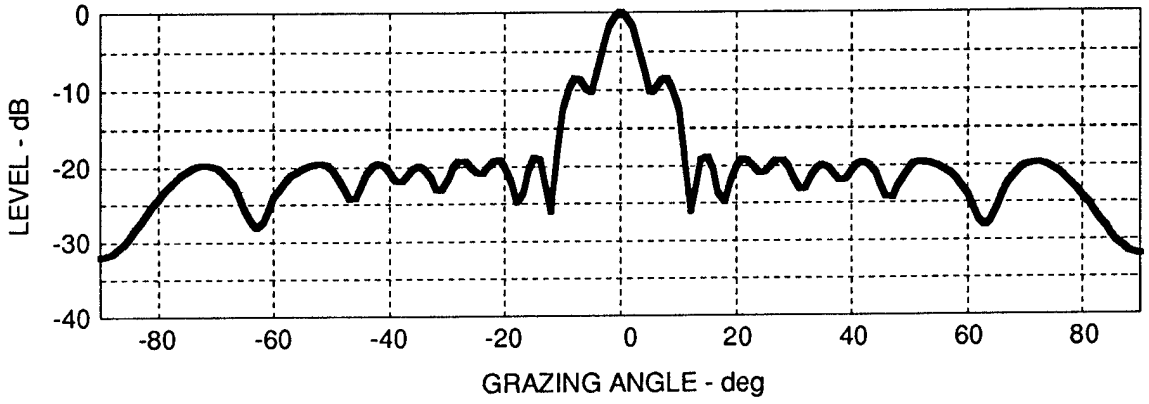

(b) 10 Hz OPTIMIZED BEAM PATTERN

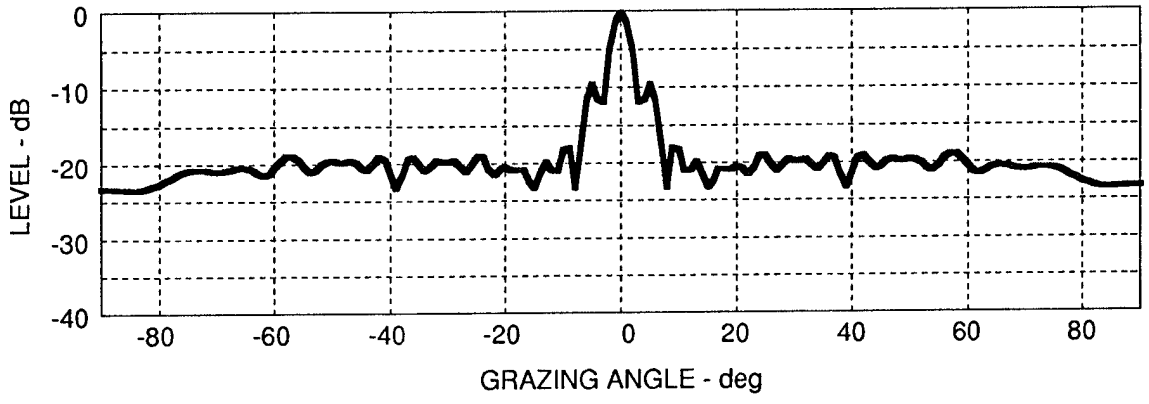

(c) 16 Hz OPTIMIZED BEAM PATTERN

FIGURE 5.1
OPTIMIZED BEAM PATTERN (STEERED TO 0°)
FOR 7, 10, AND 16 Hz BEAM ANALYSES

ARL - UT
AS-93-556
SJL/RFO
10-93/hd2

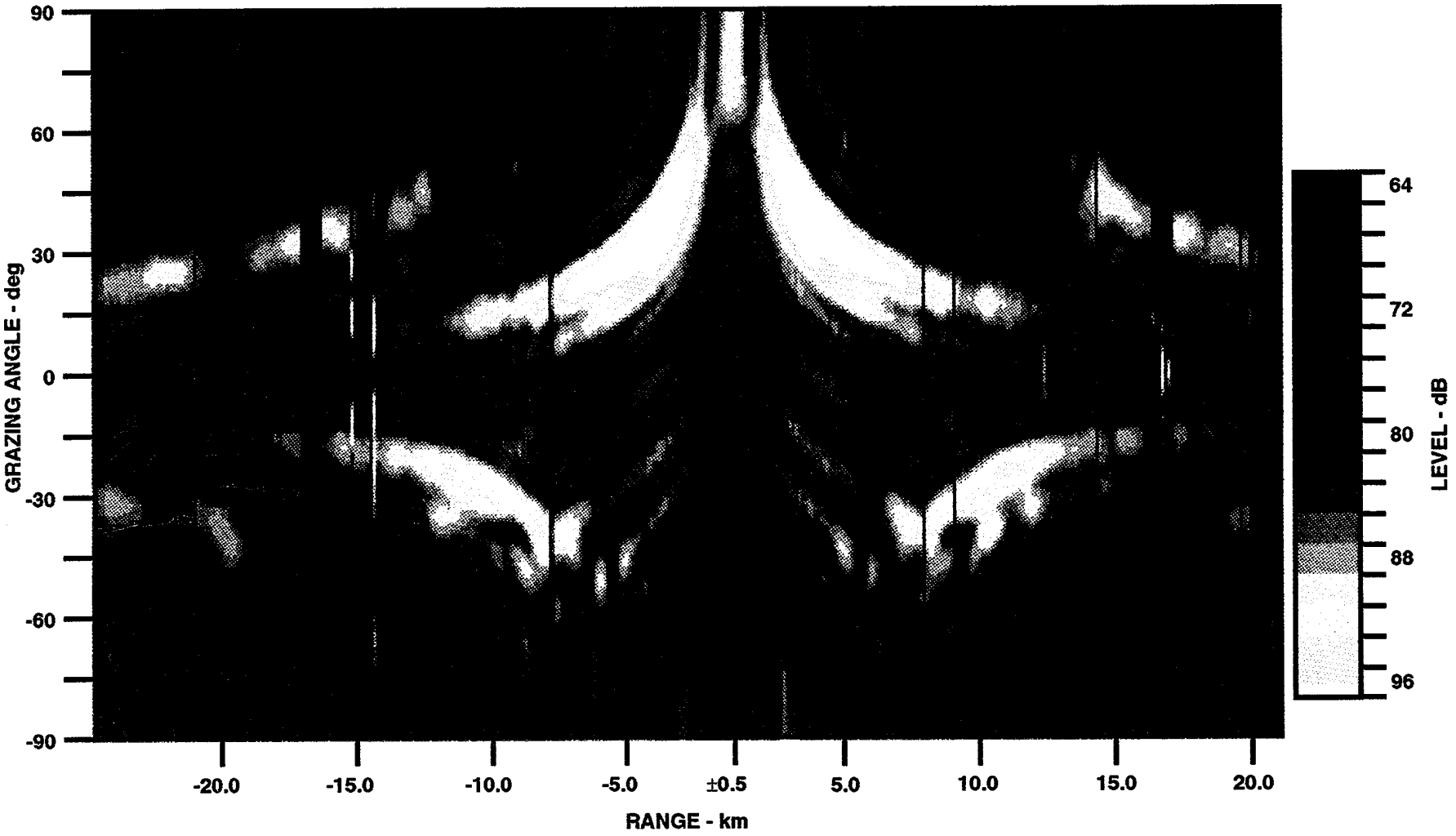

FIGURE 5.2
SHORT RANGE 7 Hz MEASURED BEAM LEVELS versus GRAZING ANGLE AND RANGE

ARL:UT
AS-93-557
SJL - RFG
10-93urncl2

This page intentionally left blank.

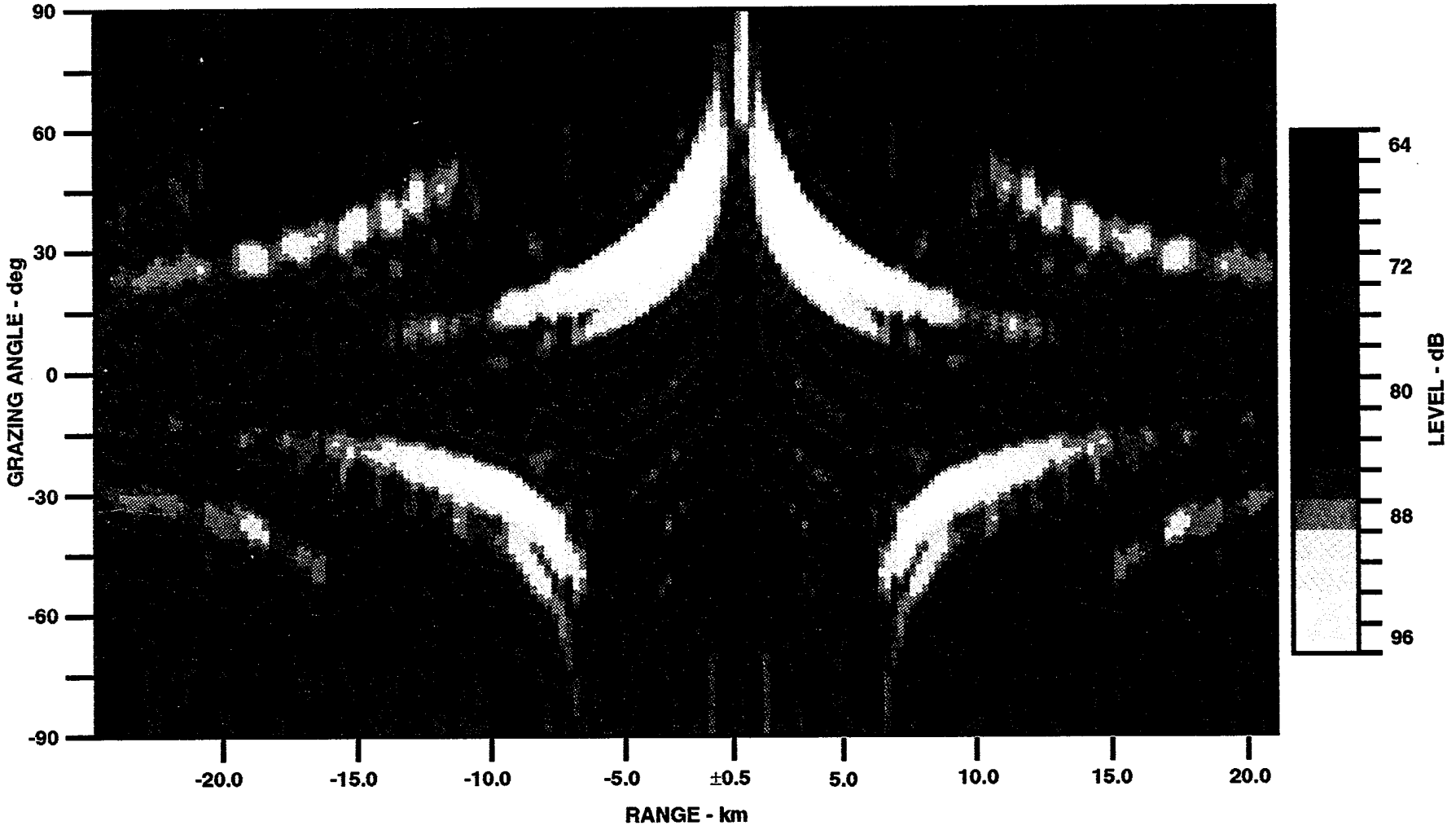

FIGURE 5.3
SHORT RANGE 7 Hz RAY MODELED BEAM LEVELS versus GRAZING ANGLE AND RANGE (GAM 0 SEDIMENT PARAMETERS)

ARL:UT
AS-93-558
SJL - RFG
10-93uncl2

This page intentionally left blank.

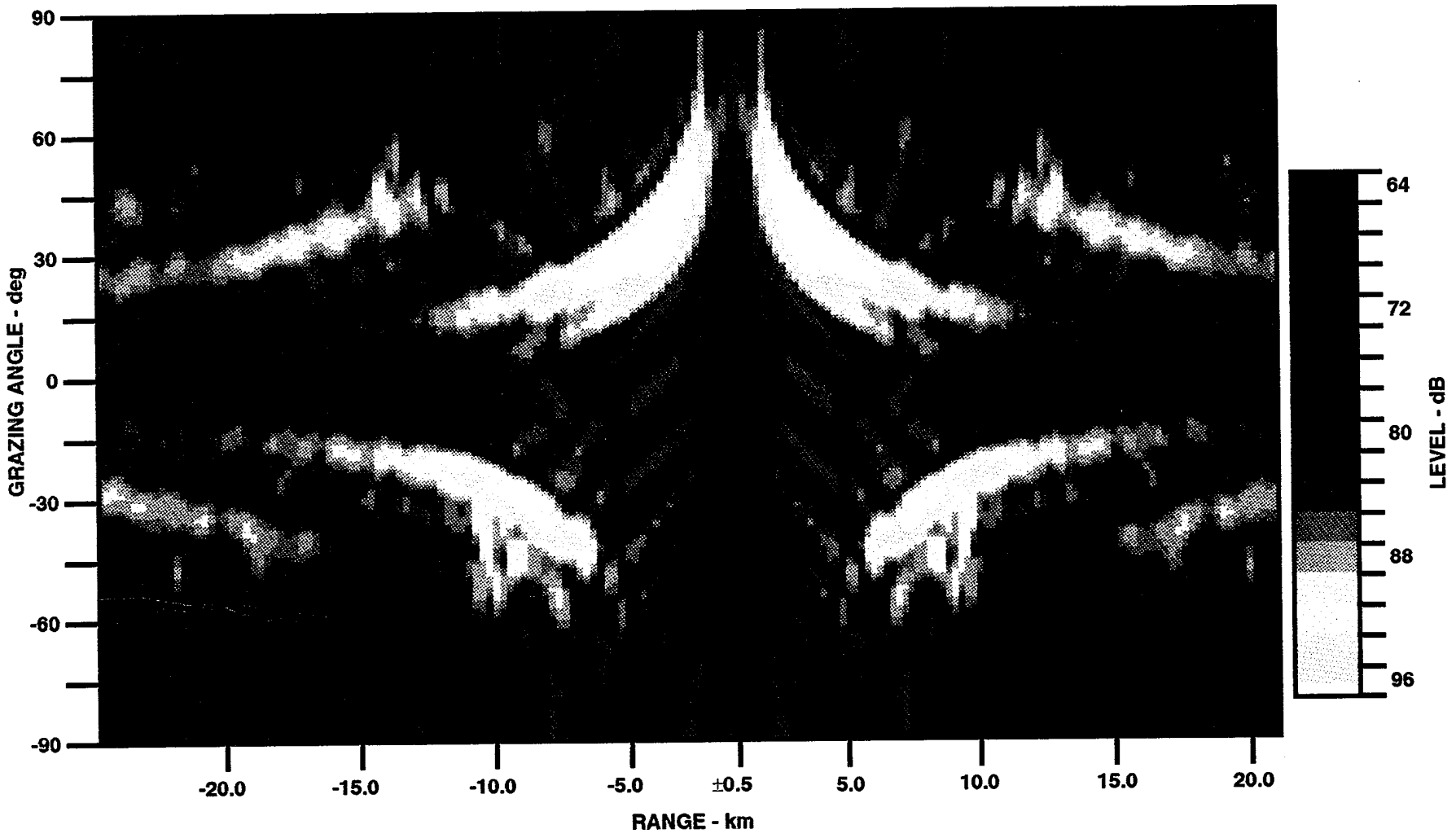

FIGURE 5.4
SHORT RANGE 7 Hz ADIABATIC NORMAL MODE MODELED BEAM LEVELS (GAM 0 SEDIMENT PARAMETERS) versus GRAZING ANGLE AND RANGE

ARL:UT
AS-93-559
SJL - RFG
10-93unc12

Beamforming is based on the assumption of plane wave arrivals. Thus, at ranges shorter than 7 km, the farfield plane wave approximation is significantly violated, and direct arrivals also appear on sidelobes. Observe that the calculations in Figs. 5.3 and 5.4 also show negative grazing angle arrivals at these ranges which are similar to the corresponding arrivals in the data in Fig. 5.2. These arrivals, which at first might appear to be the result of interactions with the bottom at high negative grazing angles are, in fact, the result of direct arrivals received on sidelobes. This assessment may be verified by comparing the arrivals in Fig. 5.2 with similar appearing arrivals found in Fig. 5.5, which were modeled using only waterborne rays in GAMARAY calculations.

Measured 10 Hz beams are shown in Fig. 5.6. The same arrival orders observed at 7 Hz may also be seen in this figure. Calculated 10 Hz beams using the ray and mode models (using GAM 0 sediment properties) are shown in Figs. 5.7 and 5.8, respectively. Note that these also exhibit the same qualitative features as the measurements shown in Fig. 5.6.

Measured 16 Hz beams are shown in Fig. 5.9. The arrival orders observed at 7 and 10 Hz are also present in this figure. Since the 16 Hz features are similar, and because corresponding aliased lobes prevent reliable interpretation of the 16 Hz arrivals in a careful analysis, no further analysis has been attempted.

When comparing the data at 7 and 10 Hz with ray and mode calculations for ranges shorter than 2 km, we note that the ray calculations better simulate the measured high angle arrivals ($\geq 60°$). On the other hand, the measured arrivals at longer ranges are observed predominantly at angles $\leq 50°$, where the adiabatic normal mode calculations achieve higher accuracy. This is principally because range dependent bathymetry is incorporated in them. Thus, we use the NEMESIS model to systematically investigate the VLF arrival structure and bottom loss. These features will be investigated in this section by quantitatively comparing the peak arrivals of the measurements with corresponding adiabatic, normal mode calculations from NEMESIS using the GAM 0 and GAM 1 geoacoustic profiles of the sediment shown in Fig. 3.1.

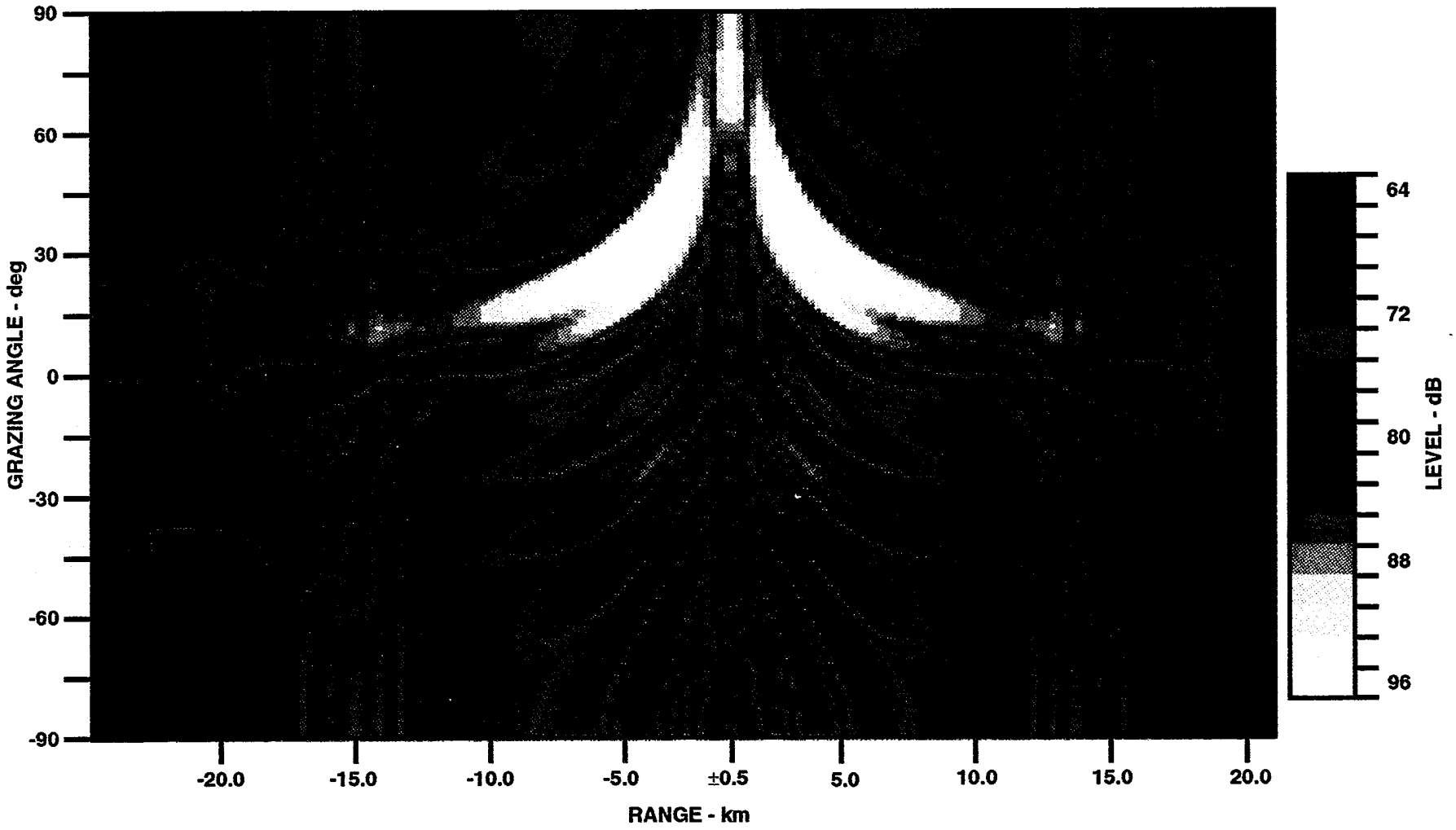

FIGURE 5.5
SHORT RANGE 7 Hz RAY MODELED BEAM LEVELS
FOR DIRECT ARRIVALS versus GRAZING ANGLE AND RANGE

ARL:UT
AS-93-560
SJL - RFG
10-93uncl2

This page intentionally left blank.

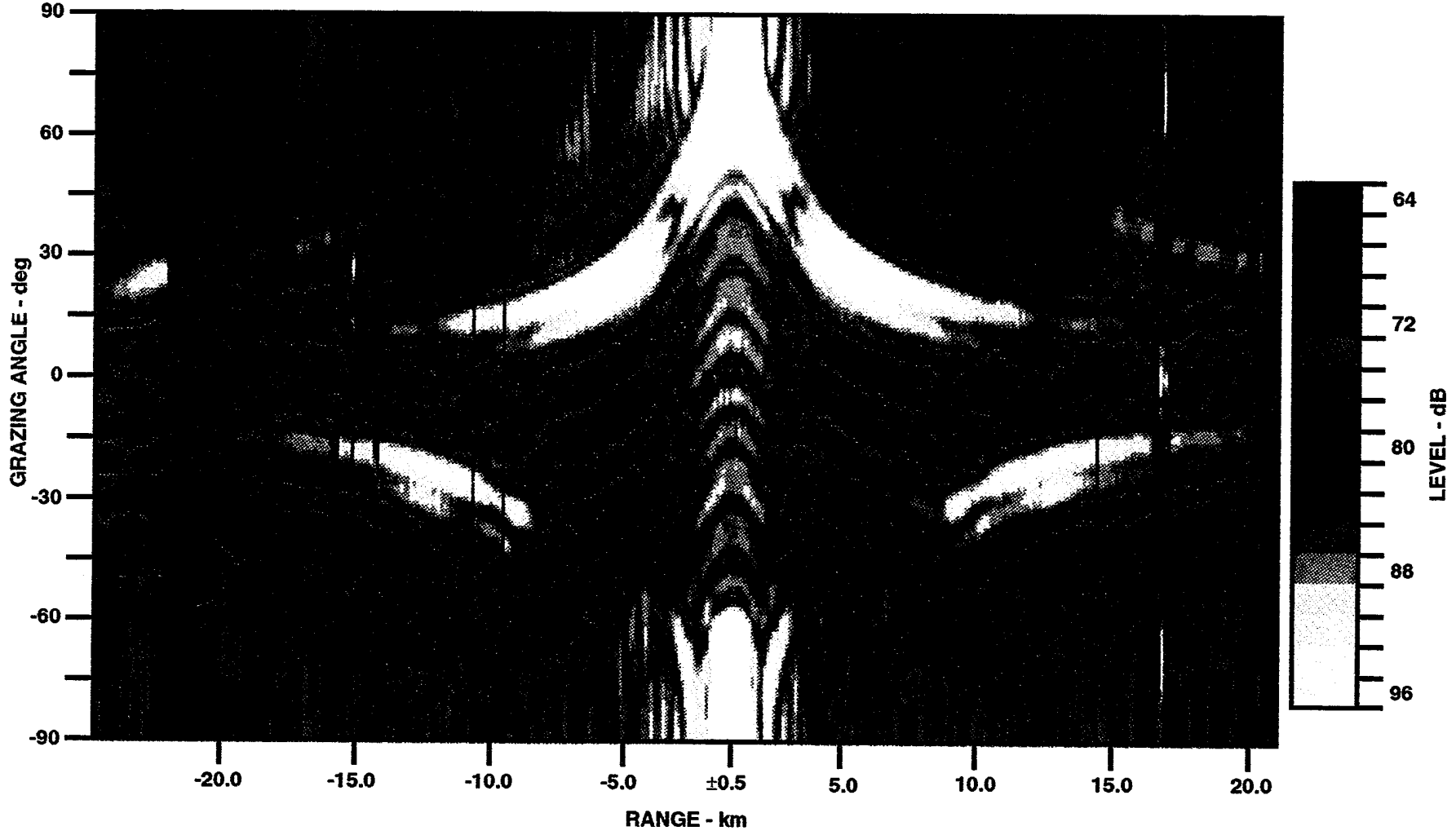

FIGURE 5.6
SHORT RANGE 10 Hz MEASURED BEAM LEVELS versus GRAZING ANGLE AND RANGE

ARL:UT
AS-93-561
SJL - RFG
10-93uncl2

This page intentionally left blank.

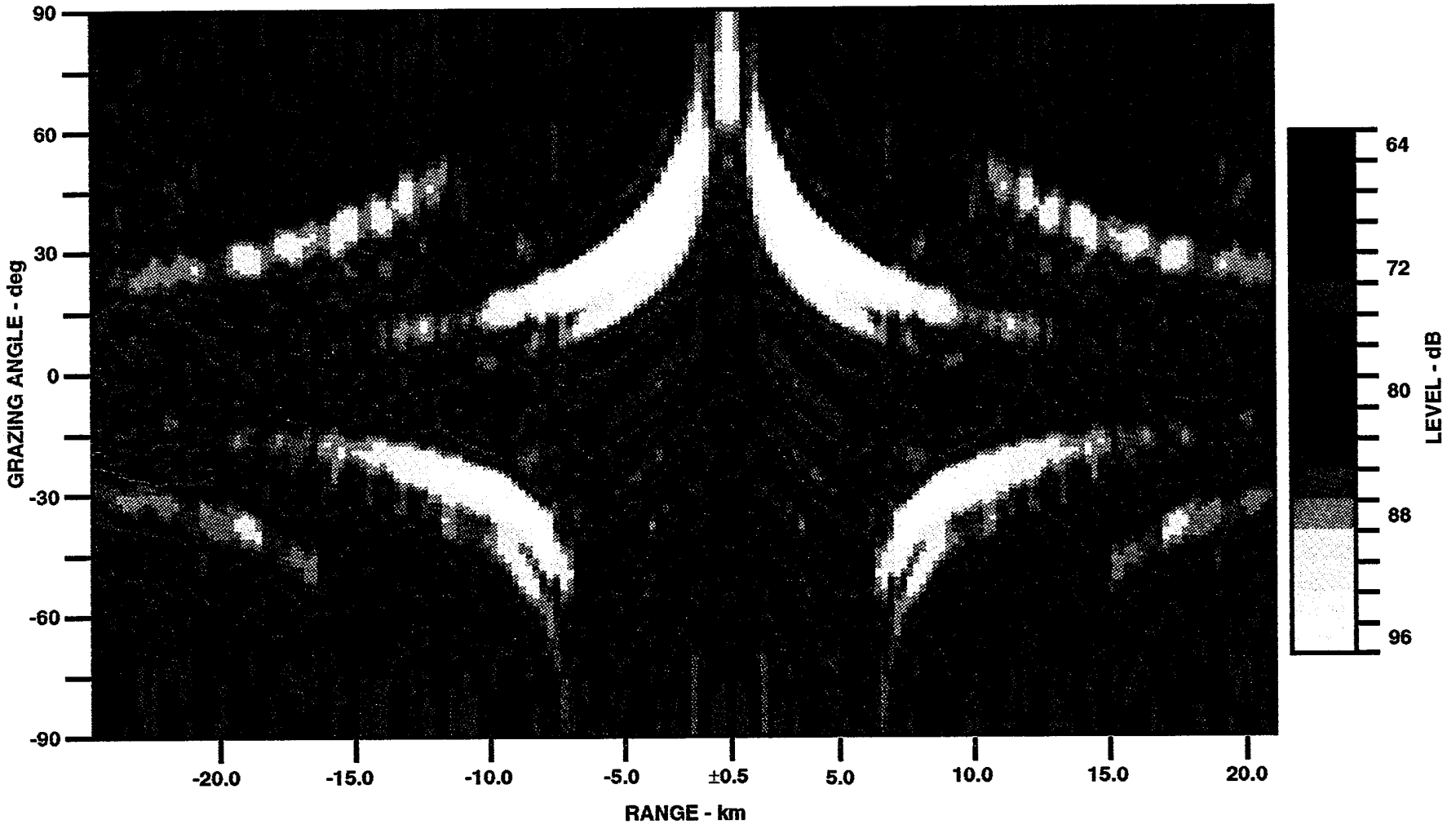

FIGURE 5.7
SHORT RANGE 10 Hz RAY MODELED BEAM LEVELS
(GAM 0 SEDIMENT PARAMETERS) versus GRAZING ANGLE AND RANGE

ARL:UT
AS-93-562
SJL - RFG
10-93umcl2

This page intentionally left blank.

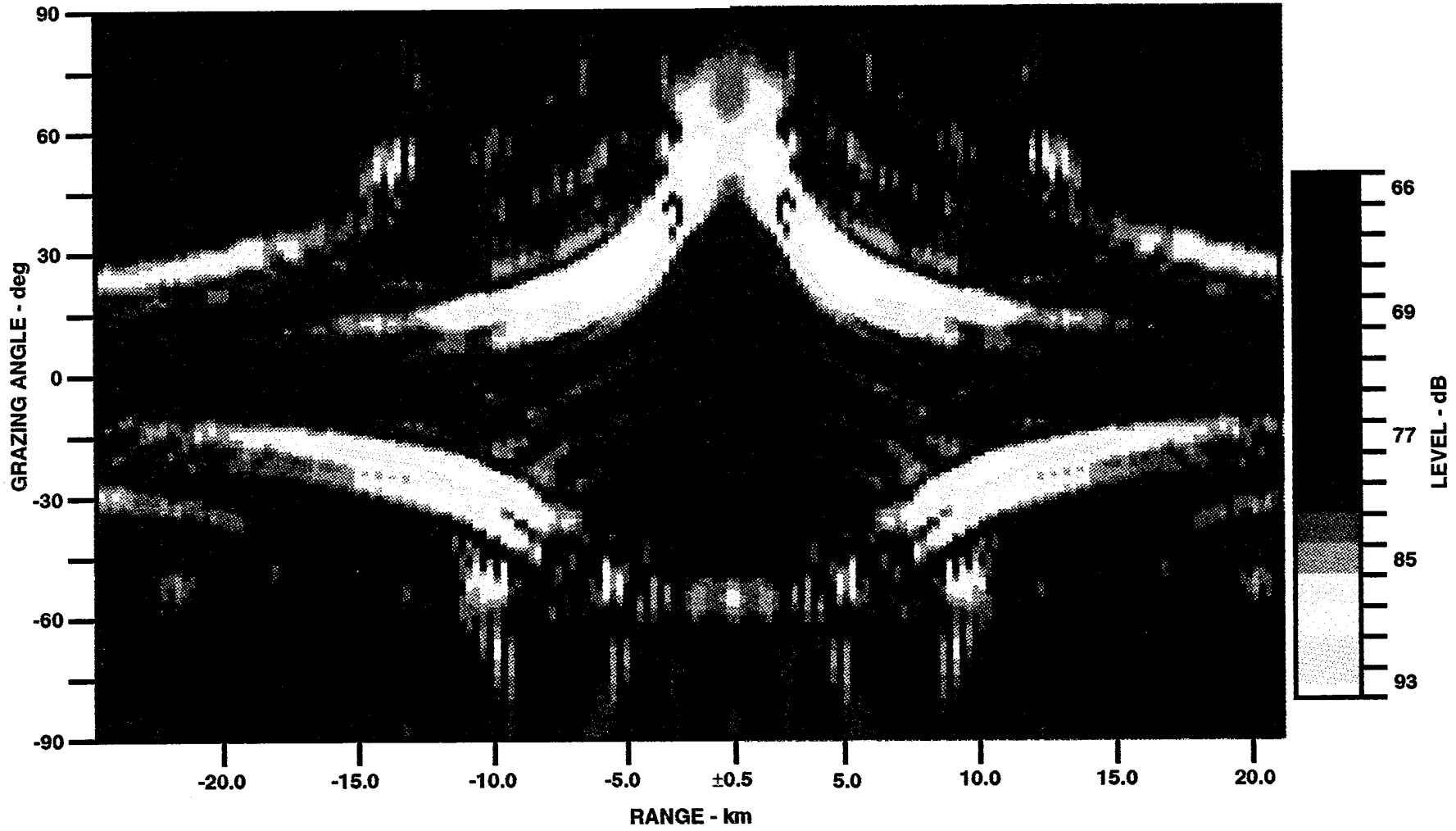

FIGURE 5.8
SHORT RANGE 10 Hz ADIABATIC NORMAL MODE MODELED BEAM LEVELS (GAM 0 SEDIMENT PARAMETERS) versus GRAZING ANGLE AND RANGE

ARL:UT
AS-93-563
SJL - RFG
10-93uncl2

This page intentionally left blank.

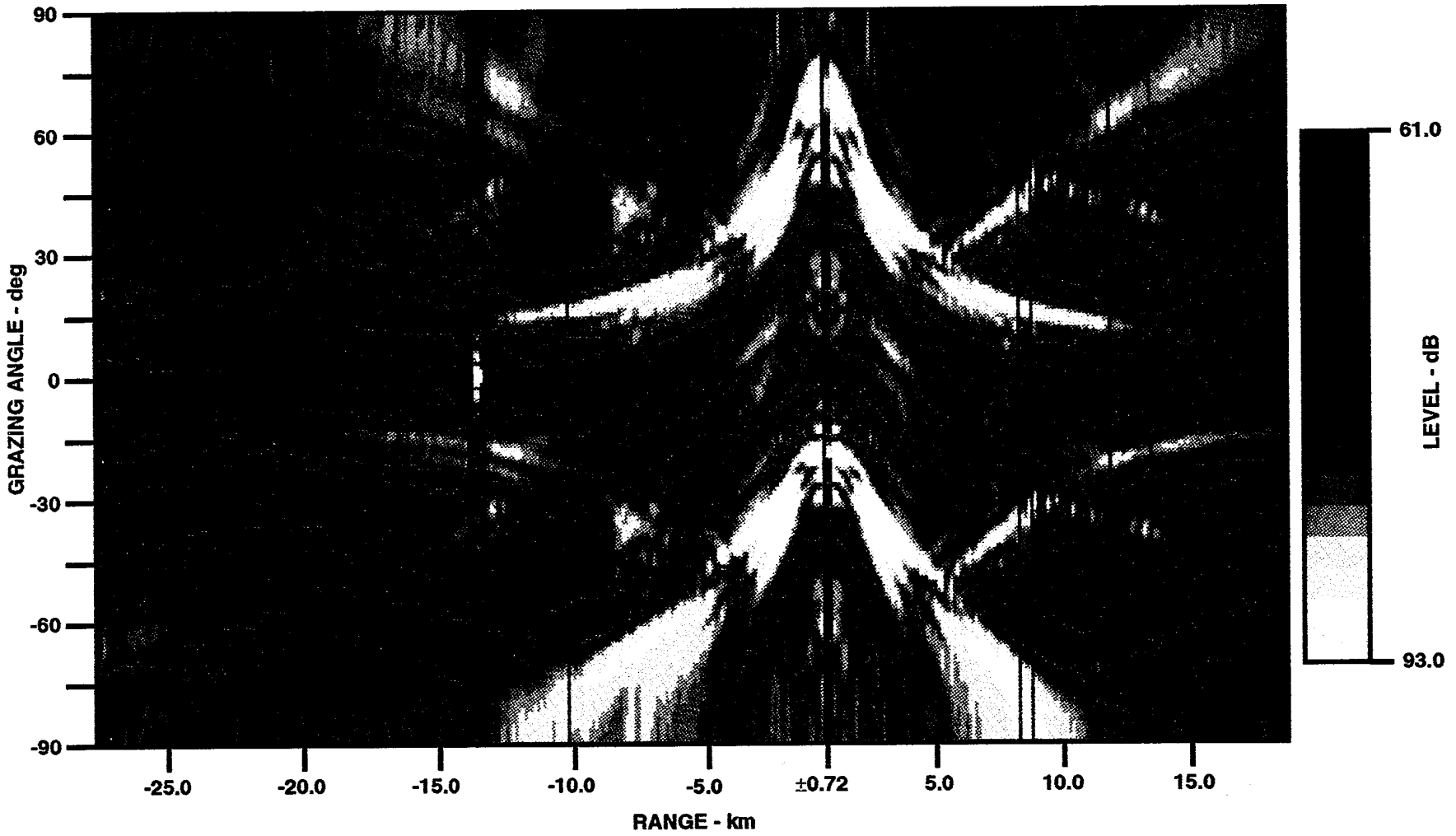

FIGURE 5.9
SHORT RANGE 16 Hz MEASURED BEAM LEVELS versus GRAZING ANGLE AND RANGE

ARL:UT
AS-93-564
SJL - RFG
10-93uncl2

Arrival angles for the peak 7 Hz measured and normal mode calculated beams for 7 and 10 Hz are shown in Figs. 5.10 and 5.11, respectively. Measured and modeled arrival angles are usually the same with the exception of the high angle arrivals at ranges < ~2 km, which are poorly modeled with normal mode calculations. Arrival angles determined with no bottom loss (GAM 0) are also usually equivalent to those calculated with the GAM 1 profile. There are few, but obvious, exceptions when the peak arrival order changes as a result of different coherent interference or different bottom losses applied in the calculations. At ranges between 12.5 and 13.5 km, in Fig. 5.11 for example, there are bottom-surface reflected arrivals at ~50° that were calculated with no bottom loss (GAM 0). However, peak arrival angles calculated with the GAM 1 profile at these same ranges are direct path arrivals at ~15∞ and are virtually indistinguishable from corresponding measurements.

The relatively small differences in measured and modeled arrival angles at both frequencies appear to validate the general properties of the GAM 1 geoacoustic profile. Other direct or single bottom reflecting modeled arrival angles are usually well within 3° of measurements. The few exceptions may usually be accounted for by bathymetry errors, such as those at ranges +13 km < R < +20 km, where in Fig. 2.1 the bathymetry track diverges somewhat from that of the acoustic measurements. The measured bottom-surface peak arrivals in this range interval are at grazing angles that are 3-5∞ greater than the calculations.

Peak TL values corresponding to the 7 and 10 Hz arrival angles in Figs. 5.10 and 5.11 are shown in Figs. 5.12 and 5.13, respectively. For ranges less than ~10 km, the received signal is primarily that of direct arrivals. Note how the measured TL values for direct arrivals at both frequencies in the upper plots are virtually indistinguishable from the calculations at the shortest ranges (~2 km |R| < ~7 km). Recall that the measured omnidirectional levels are also well modeled by corresponding calculations at these ranges for 7 Hz (Fig. 4.4) and 10 Hz (Fig. 4.8). At ranges ~7 km < |R| < ~12 km, additional arrivals begin to have influence on the omnidirectional levels. At these ranges, the measured and modeled arrivals from the surface become more variable with range, and TL of the modeled beams differs by ~ ±2 dB from the beam measurements. This is particularly true at the positive ranges south of the array

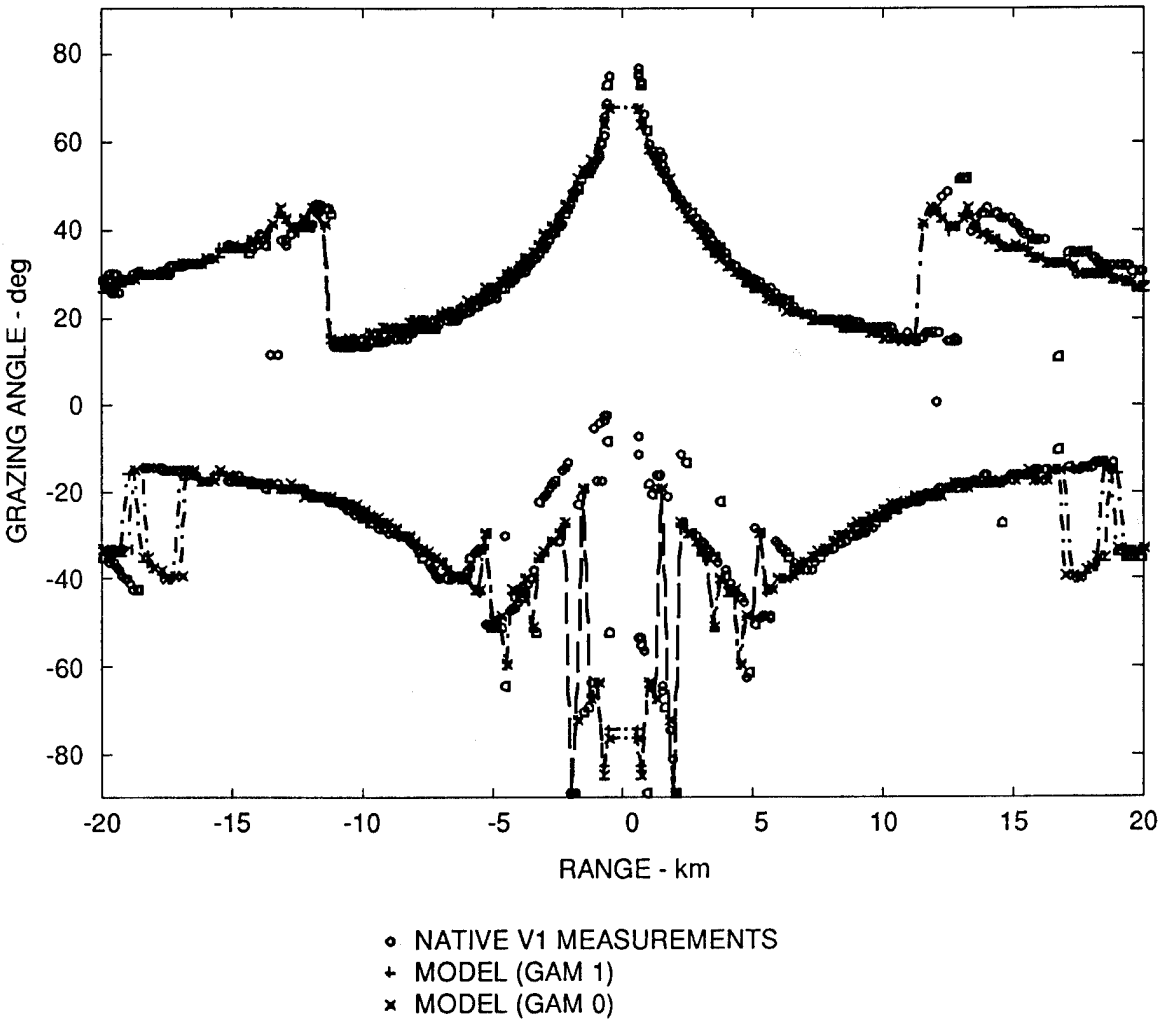

FIGURE 5.10
MEASURED AND MODELED (GAM 0 AND GAM 1 SEDIMENT MODELS) GRAZING ANGLES OF 7 Hz PEAK ARRIVALS FROM THE SURFACE AND FROM THE BOTTOM

ARL - UT
AS-93-565
SJL/RFO
10-93/hd2

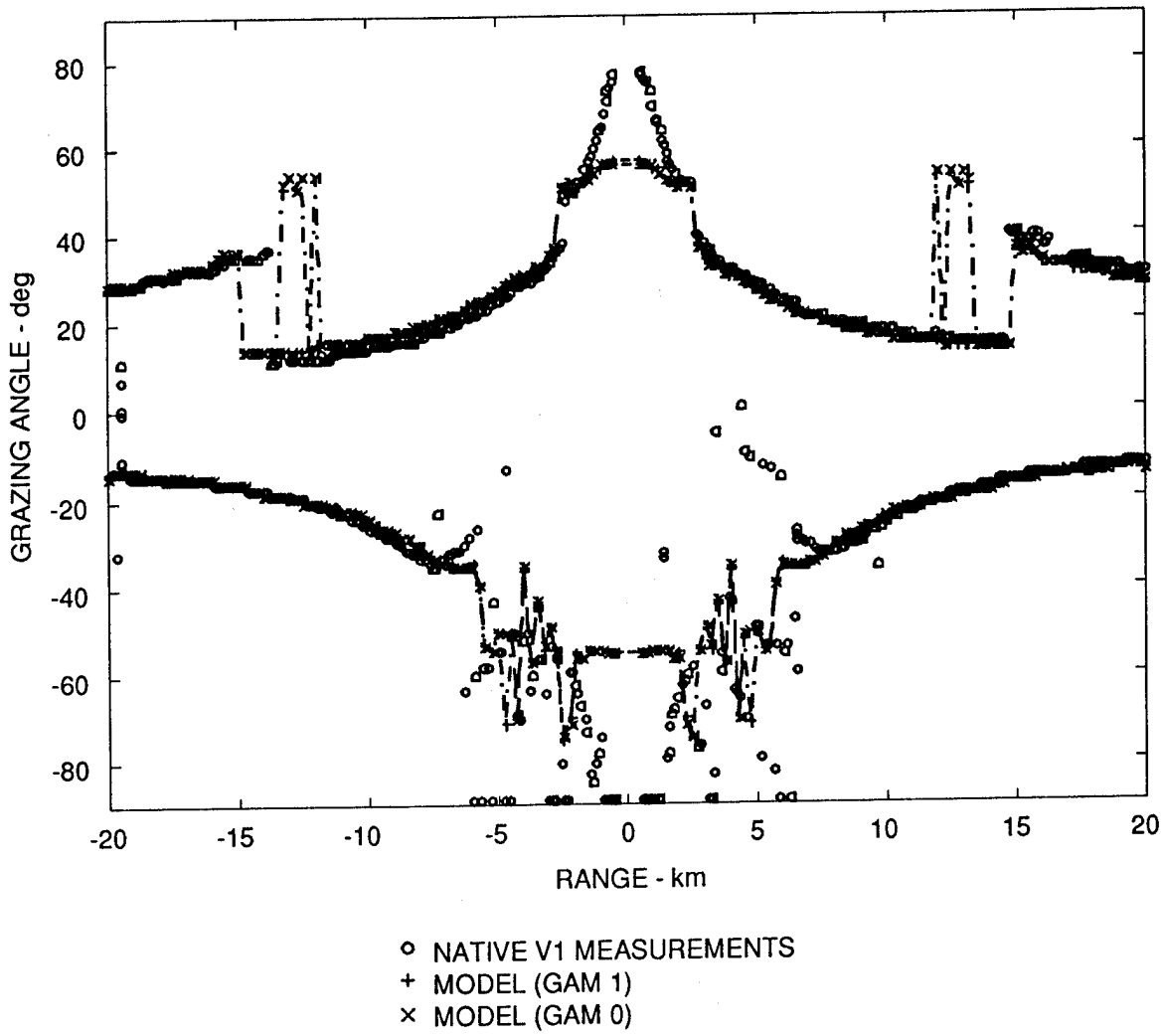

FIGURE 5.11
MEASURED AND MODELED (GAM 0 AND GAM 1 SEDIMENT MODELS) GRAZING ANGLES OF 10 Hz PEAK ARRIVALS FROM THE SURFACE AND FROM THE BOTTOM

ARL - UT
AS-93-566
SJL/RFO
10-93/hd2

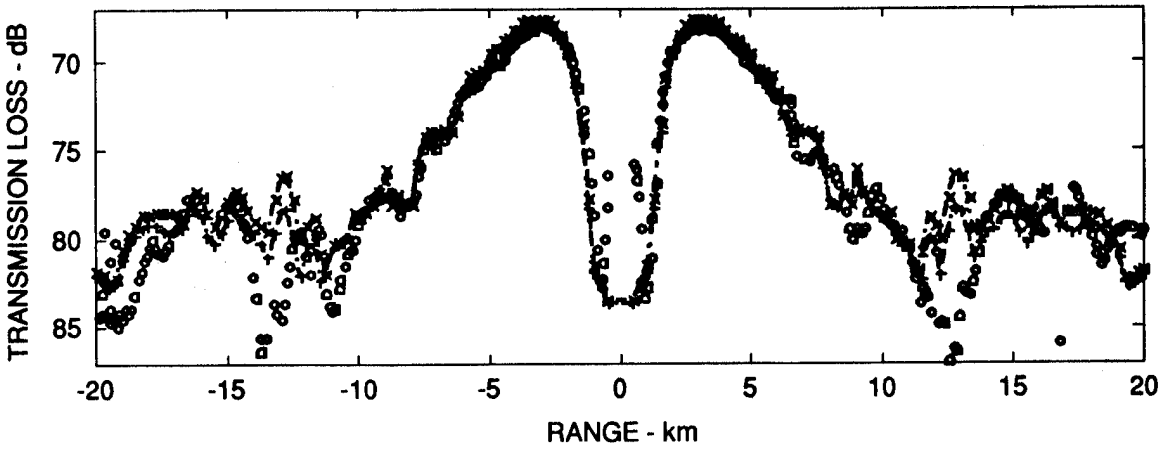

(a) 7 Hz PEAK ARRIVALS FROM THE SURFACE

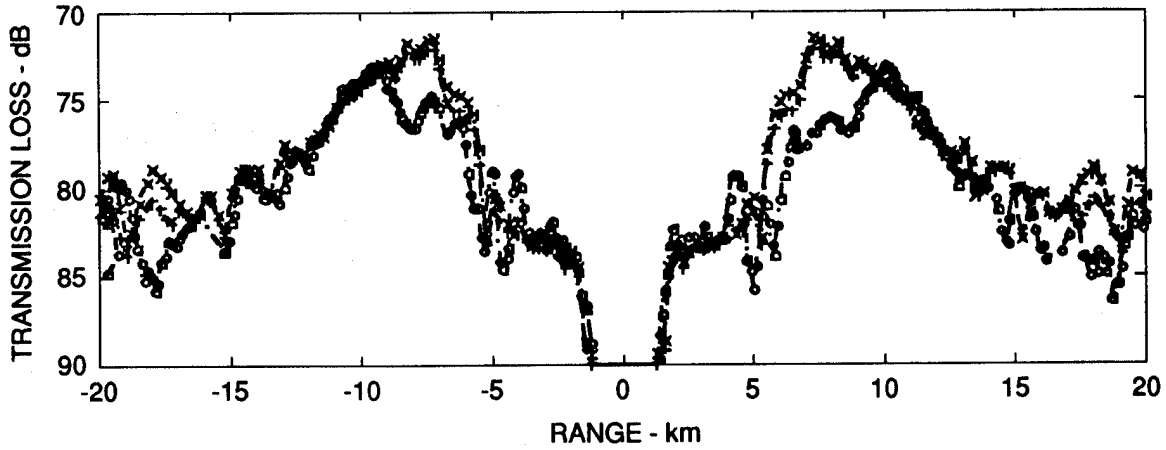

(b) 7 Hz PEAK ARRIVALS FROM THE BOTTOM

- NATIVE MEASUREMENTS
- MODEL (GAM 1)
- MODEL (GAM 0)

FIGURE 5.12
MEASURED AND MODELED
(GAM 0 AND GAM 1 SEDIMENT MODELS)
7 Hz TRANSMISSION LOSS

ARL - UT
AS-93-567
SJL/RFO
10-93/hd2

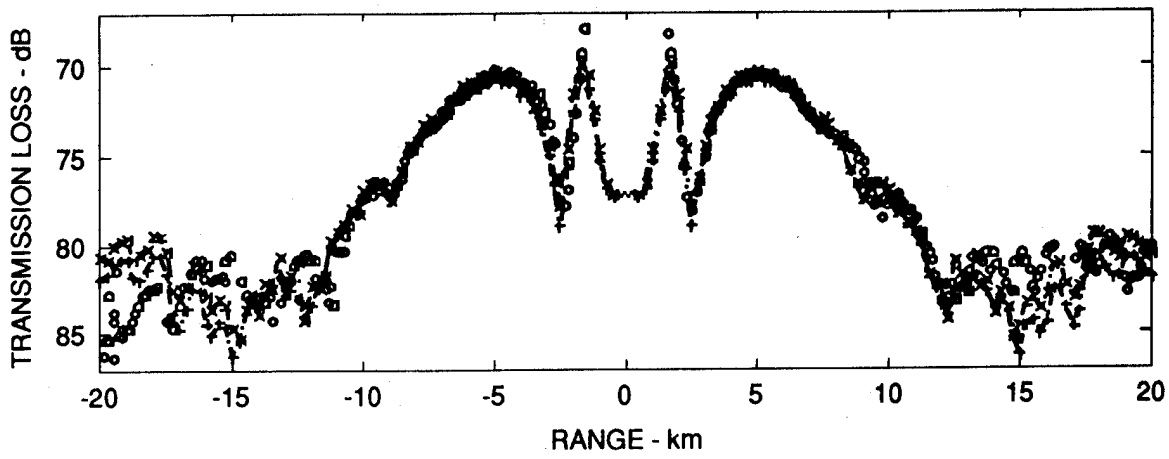

(a) 10 Hz PEAK ARRIVALS FROM THE SURFACE

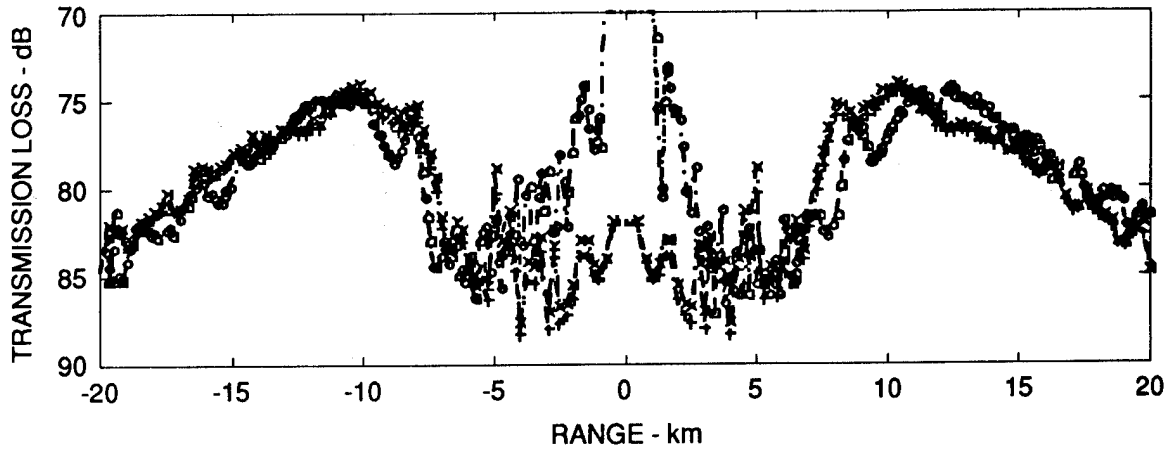

(b) 10 Hz PEAK ARRIVALS FROM THE BOTTOM

- NATIVE MEASUREMENTS
- MODEL (GAM 1)
- MODEL (GAM 0)

FIGURE 5.13
MEASURED AND MODELED
(GAM 0 AND GAM 1 SEDIMENT MODELS)
10 Hz TRANSMISSION LOSS

ARL - UT
AS-93-594
SJL/RFG
10-93/hd2

where greater bathymetry errors are likely (see Fig. 2.1). We attribute this variation to the cumulative result of calculation errors due primarily to bathymetry errors, but the sound velocity and source depth uncertainties may also play a role.

TL corresponding to 7 and 10 Hz arrivals from the ocean bottom are shown in the lower plots of Figs. 5.12 and 5.13. Recall that the values at ranges less than ~6 km are the result of sidelobes from direct arrivals; thus these arrivals are not analyzed. At ranges ~7 km < |R| < ~10 km, the 7 Hz measurements are ~4 dB more lossy than the TL predicted using the GAM 1 bottom profile, and up to 3 dB more lossy for corresponding 10 Hz comparisons. Since these arrivals interact only once with the bottom, we have concluded that GAM 1 is a poor geoacoustic model in its modeling of the bottom loss at these ranges. In Section 6, we will investigate bottom loss in greater detail.

At greater ranges (e.g., ~10 km < |R| < ~20 km), the 7 and 10 Hz TL measurements are somewhat closer to those modeled. However, the more complicated arrival structure and the environmental uncertainties tend to make reliable bottom loss evaluation at these ranges more difficult. At 12-16 km, for example, 10 Hz measurements are about 2 dB less lossy than calculations, falsely indicating acoustic amplification in the bottom, even though the corresponding 10 Hz measured arrival angles in Fig. 5.11 are virtually indistinguishable from the calculations.

This page intentionally left blank.

6. PLANE WAVE BOTTOM LOSS ESTIMATION

In this section we focus on bottom loss as a function of grazing angle associated with single bottom interacting beam arrivals. The transmission loss of the associated measured arrivals is compared with that of respective normal mode calculation using the GAM 1 and GAM 2 bottom profiles shown in Fig. 3.1. Corresponding calculated arrivals based on the GAM 0 profile are used to approximate the geometric spreading loss of the measurements, noting that the respective simulated arrival angles are in excellent agreement with corresponding measured arrival angles. However, the figures shown in this section and Section 7 frequently distinguish between calculated loss at peak angles using the GAM 0 profile, which is labeled "Model (GAM 0)", and the calculated loss using the GAM 0 profile at the peak measurement angles, which is labeled "Spreading Loss Estimate". Plane wave bottom loss calculated directly for the GAM 1 and GAM 2 bottom profiles will also be presented for comparison.

In order to isolate specific arrival orders and examine the angular dependency of the attenuation profile, comparisons of the peak arrivals are analyzed by considering only those cases for which the ranges of the measurements coincide within 130 m of corresponding calculations, and where respective grazing angles are within 3°. The angular dependency at the bottom is determined by projecting the beam arrival angles at the array center to the ocean bottom using Snell's law. Such comparisons of beam arrival versus grazing angle at 7 and 10 Hz are made for single bottom reflected arrivals at ranges ~7 km $\leq$ |R| $\leq$ ~16.5 km.

In Fig. 6.1, the transmission loss of the peak 7 Hz measured arrivals is shown as a function of grazing angle at the bottom. Arrival levels are described well north (Fig. 6.1(a)) and south (Fig. 6.1(b)) of the array by the associated calculations at grazing angles less than 27°. Note that the loss at these angles is accounted for almost entirely by the geometric spreading estimate (GAM 0). This figure also shows that the ~4 dB bottom loss deficiency characterized by the GAM 1 sediment profile at ranges 7-10 km in Fig. 5.11 occurs at grazing angles of 28-36°.

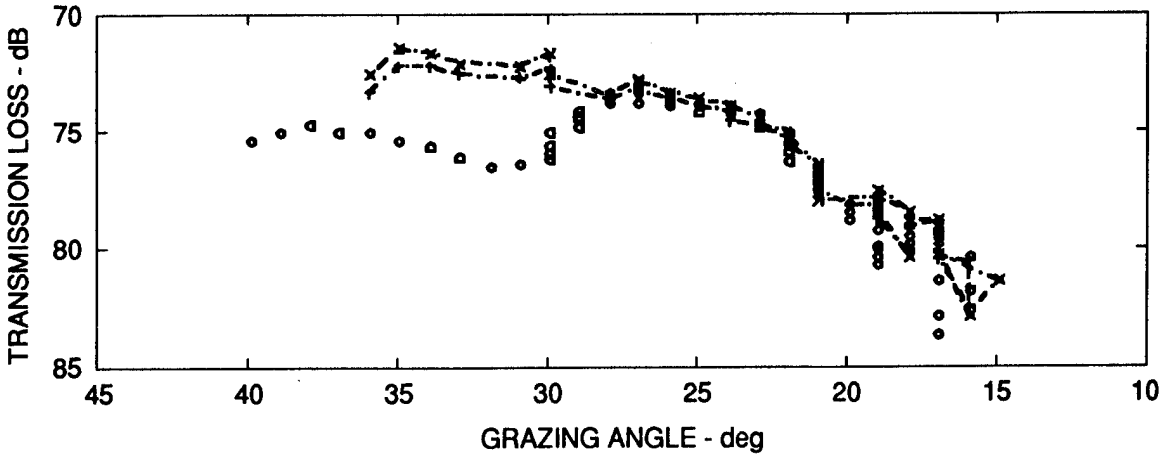

(a) 7 Hz SINGLE-BOTTOM PEAK ARRIVALS 7-16 km NORTH OF V1

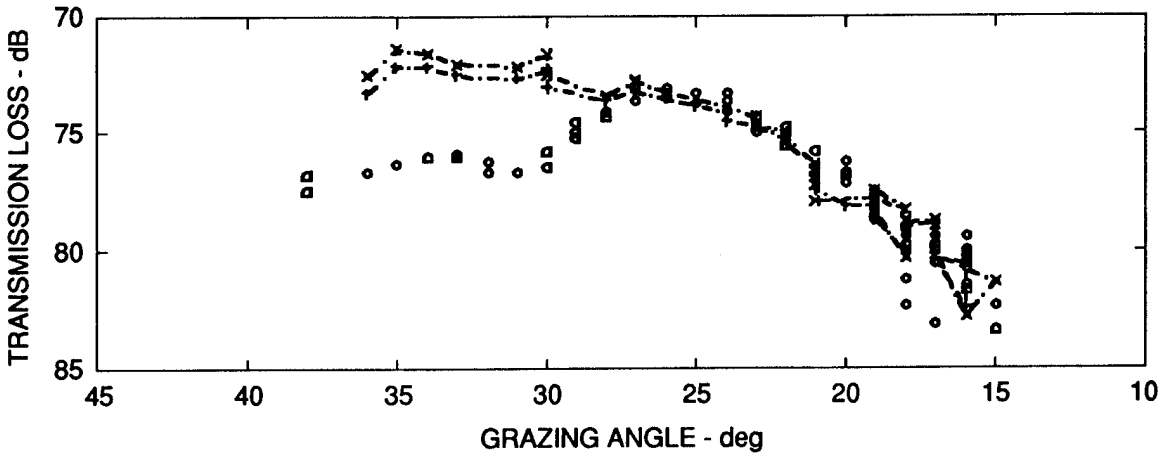

(b) 7 Hz SINGLE-BOTTOM PEAK ARRIVALS 7-16 km SOUTH OF V1

- ∘ NATIVE MEASUREMENTS
- \+ MODEL (GAM 1)
- × MODEL (SPREADING LOSS ESTIMATE)

FIGURE 6.1
MEASURED AND MODELED
(GAM 1 SEDIMENT MODEL AND SPREADING LOSS ESTIMATE)
7 Hz TRANSMISSION LOSS

Measured bottom loss at 7 Hz, estimated by subtracting the spreading loss estimate (GAM 0) from the peak measured arrivals of Fig. 6.1, is shown in Fig. 6.2, along with 7 Hz plane wave bottom loss calculations made directly from the geoacoustic models (GAM 1 and GAM 2). Note that the plane wave bottom loss based on GAM 1 in Fig. 6.2 is consistent with a difference in the calculated peak arrivals based on the GAM 0 and GAM 1 profiles in Fig. 6.1. There is always less than a 1/2 dB difference between the GAM 0 and GAM 1 curves in Fig. 6.1. The GAM 2 profile, which provides a significantly improved simulation of the bottom loss measurements for 28-32° was, in fact, determined numerically by adjusting (primarily) the thickness and depth of the hydrate layer properties given in Ref. 4, so 7 Hz plane wave bottom loss calculations provide good simulation of the corresponding measured bottom loss.

The grazing angles of the calculated peak 7 Hz arrivals based on the GAM 1 and GAM 2, and those of the measured peak arrivals are shown in Fig. 6.3. Both calculated curves accurately simulate the measured peak arrivals, although the GAM 1 profile is slightly better, particularly for the higher arrival orders. TL for the 7 Hz arrivals shown in Fig. 6.3 is shown in Fig. 6.4. Here, the single bottom interacting arrivals are better characterized by GAM 2, particularly at ranges between 7 and 10 km, which suffer a ~4 dB bottom loss deficiency when characterized by the GAM 1. However, arrivals calculated using GAM 2 that interact with the bottom and surface (arriving from the surface at ranges greater than ~12 km) and those that interact twice with the bottom (arriving from the bottom at ranges greater than ~18 km) suffer as much as 8 dB more loss than corresponding measured arrivals.

At 10 Hz, the measured TL of the peak arrivals north of the array are shown in Fig. 6.5(a). Rough agreement with corresponding model simulations for angles less than 27° may be observed, and the model calculations, characterizing the sediment using GAM 1 properties, are ~2-3 dB less lossy at 28-32° than the measurements. At steeper angles (33-35°), the 10 Hz measured bottom arrivals show large variability at these grazing angles. At 33°, for example, peak 10 Hz TL measurements vary from 77 dB to 84 dB. South of the array (Fig. 6.5(b)), 10 Hz TL measurements are poorly modeled by the calculations, at virtually all grazing angles.

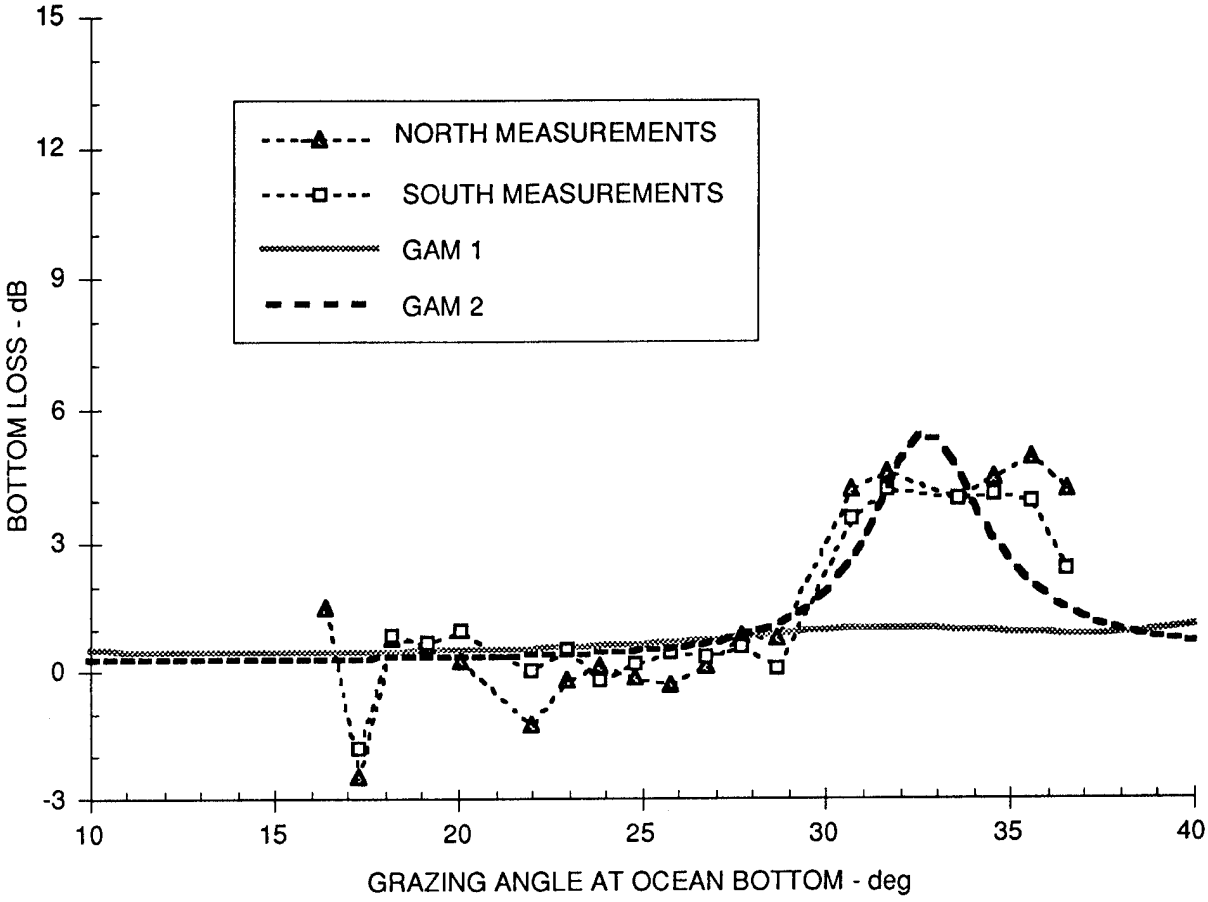

FIGURE 6.2
MEASURED AND MODELED 7 Hz PLANE WAVE BOTTOM LOSS versus GRAZING ANGLE ESTIMATES

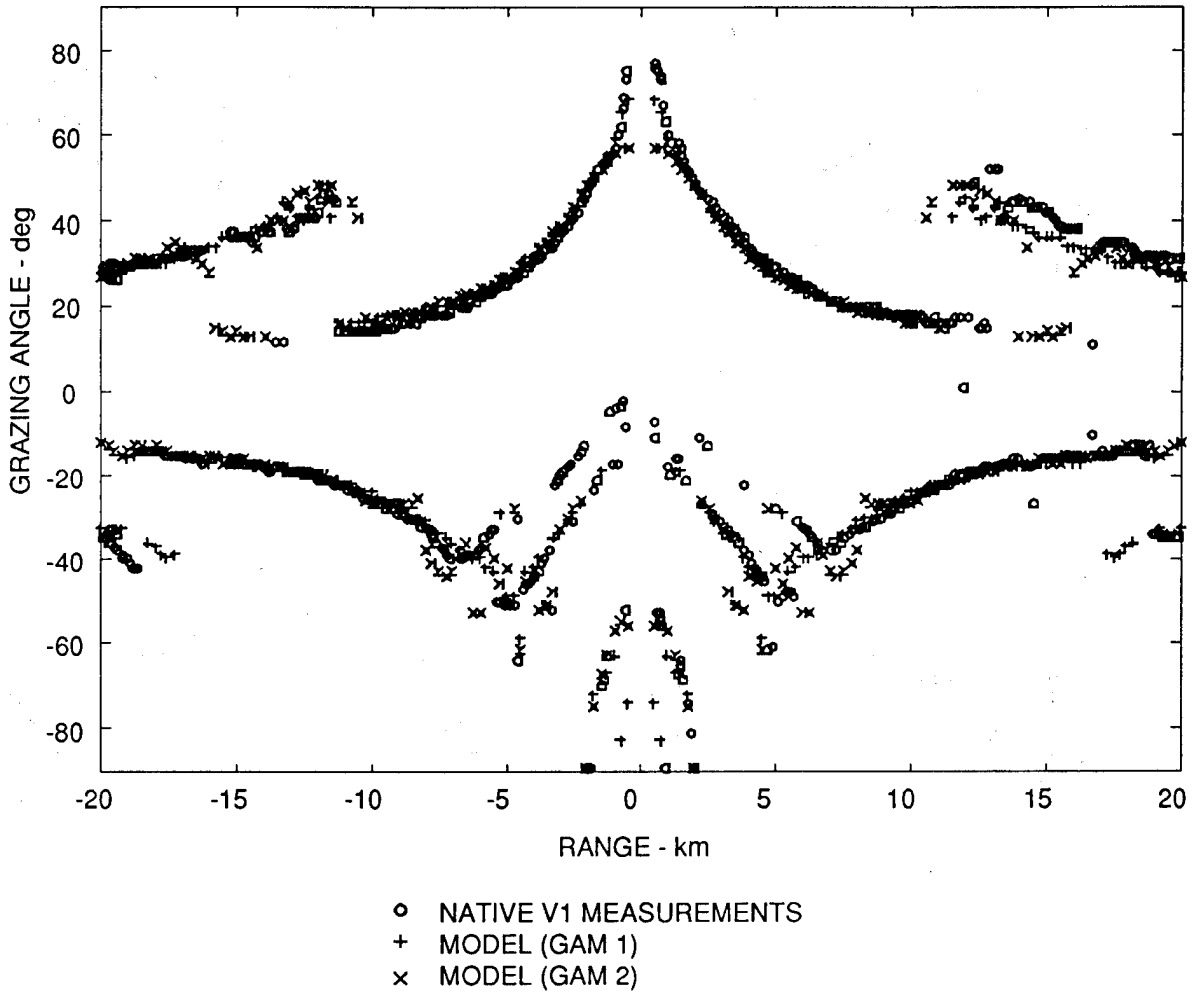

FIGURE 6.3
MEASURED AND MODELED (GAM 1 AND GAM 2 SEDIMENT MODELS) GRAZING ANGLES AT 7 Hz PEAK ARRIVALS FROM THE SURFACE AND FROM THE BOTTOM

ARL - UT
AS-93-570
SJL/RFO
10-93/hd2

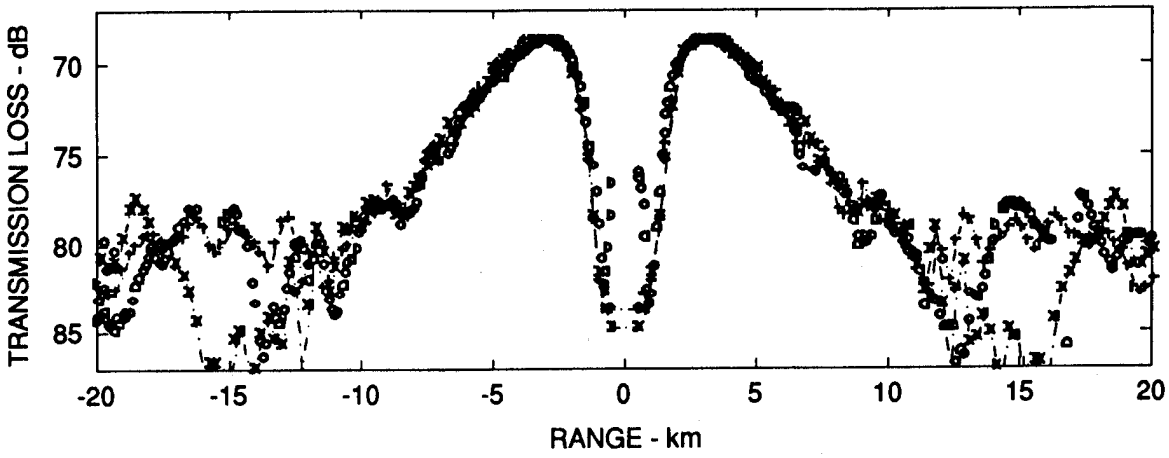

(a) 7 Hz PEAK ARRIVALS FROM THE SURFACE

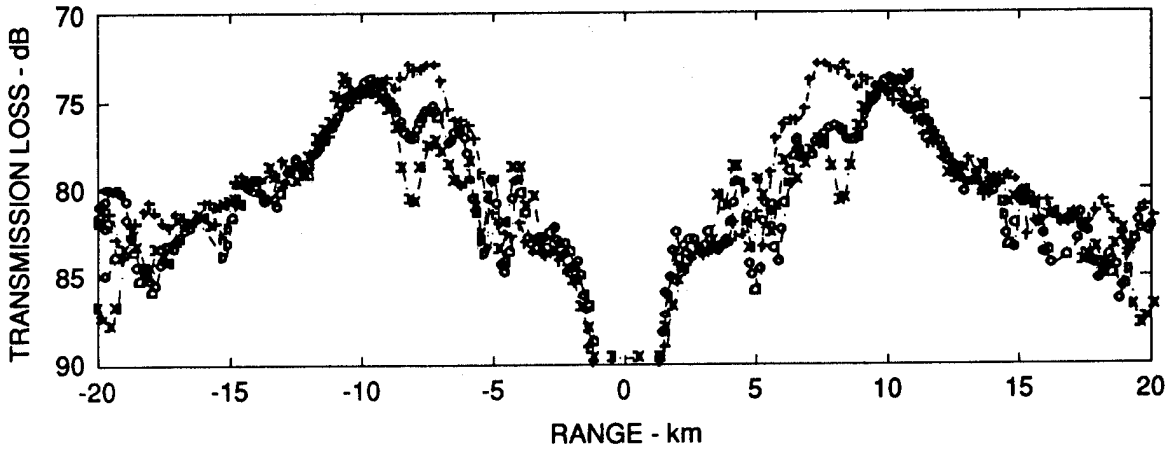

(b) 7 Hz PEAK ARRIVALS FROM THE BOTTOM

- NATIVE MEASUREMENTS
- MODEL (GAM 1)
- MODEL (GAM 2)

FIGURE 6.4
MEASURED AND MODELED
(GAM 1 AND GAM 2 SEDIMENT MODELS)
7 Hz TRANSMISSION LOSS

ARL - UT
AS-93-571
SJL/RFO
10-93/hd2

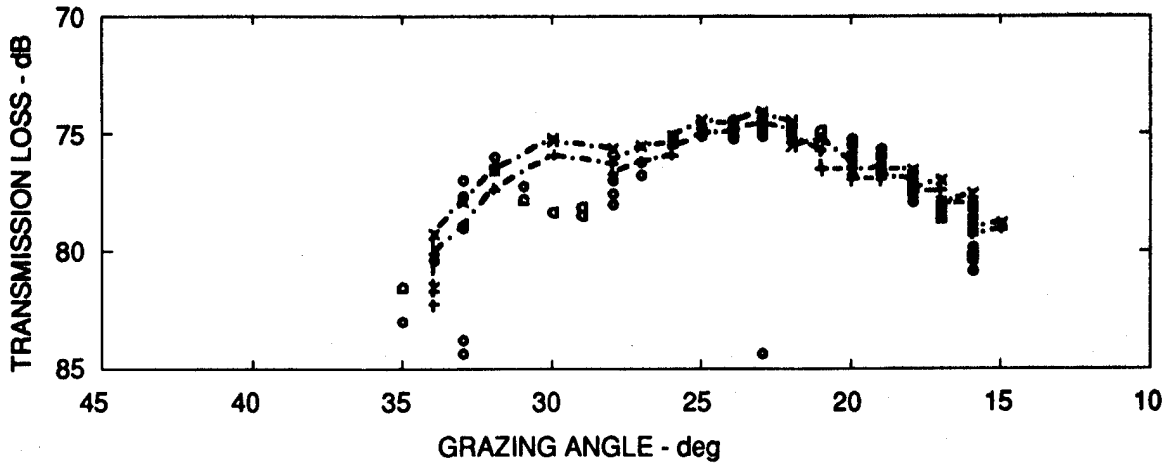

(a) 10 Hz SINGLE-BOTTOM PEAK ARRIVALS 7-16 km NORTH OF V1

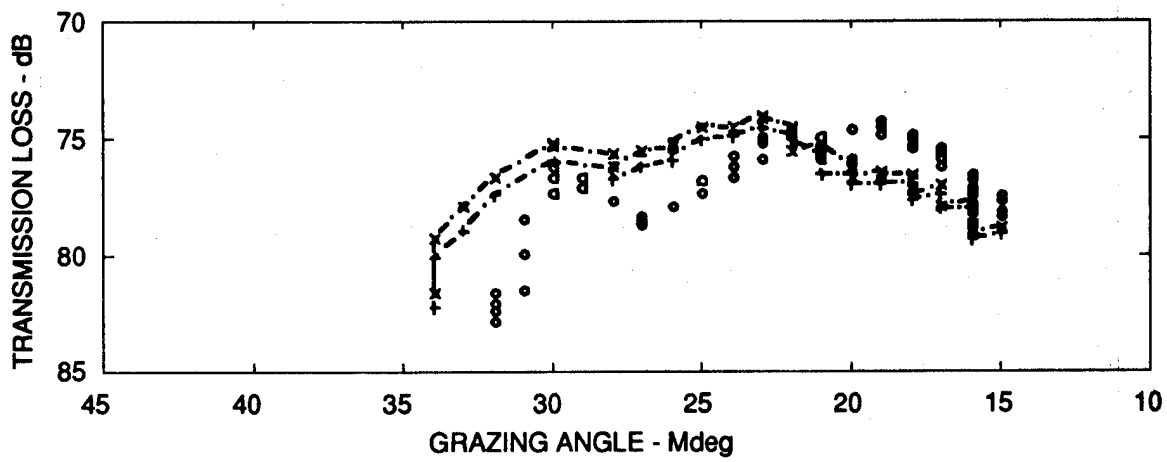

(b) 10 Hz SINGLE-BOTTOM PEAK ARRIVALS 7-16 km SOUTH OF V1

- NATIVE MEASUREMENTS
- MODEL (GAM 1)
- MODEL (SPREADING LOSS ESTIMATE)

FIGURE 6.5
MEASURED AND MODELED
(GAM 1 SEDIMENT MODEL AND SPREADING LOSS ESTIMATE)
10 Hz TRANSMISSION LOSS

ARL - UT
AS-93-572
SJL/RFO
10-93/hd2

Figure 6.6 shows 10 Hz measurements and calculations of bottom loss that are comparable to 7 Hz estimates shown in Fig. 6.2. Plane wave bottom loss calculations at 10 Hz using GAM 1 are less than 2 dB at 10-40°, while those using GAM 2 show a narrow, 12 dB increase at 30°, but are smaller at other angles. The measured bottom loss estimates are considerably scattered, often negative, and are not correlated with either geoacoustic model.

The grazing angles of the calculated 10 Hz peak arrivals which are comparable to the 7 Hz arrivals in Fig. 6.3 are shown in Fig. 6.7. Both 10 Hz calculated curves, which are virtually indistinguishable from each other, accurately modeled the 10 Hz measured peak arrivals. The TL values for these arrivals are shown in Fig. 6.8. The large, narrow peak of the calculated plane wave bottom loss for GAM 2 at 30° (Fig. 6.6) is reduced and spread over angles in the averaging process associated with forming the peak beam calculations (see Fig. 6.8). The single bottom interacting arrivals at ranges between 7 and 10 km are characterized only slightly better by GAM 2 than by GAM 1. Other calculated single bottom interacting arrivals are ~2-3 dB more lossy than the measured arrivals.

We now briefly turn our attention to higher order bottom interactions. The 7 and 10 Hz TL versus grazing angle comparisons at short ranges both north and south of the array are shown in Figs. 6.9 and 6.10, respectively, for single bottom interacting arrivals from the surface in the upper plots, and for twice bottom interacting arrivals from the bottom in the lower plots. These arrivals are more sensitive to bathymetry and sediment property uncertainty than the single bottom interacting arrivals shown in Figs. 6.1 and 6.5. They also show considerable scatter; thus we have not inferred bottom loss estimates from them. At longer ranges, in the next section, we will statistically analyze a larger number of multiple bottom interacting arrivals.

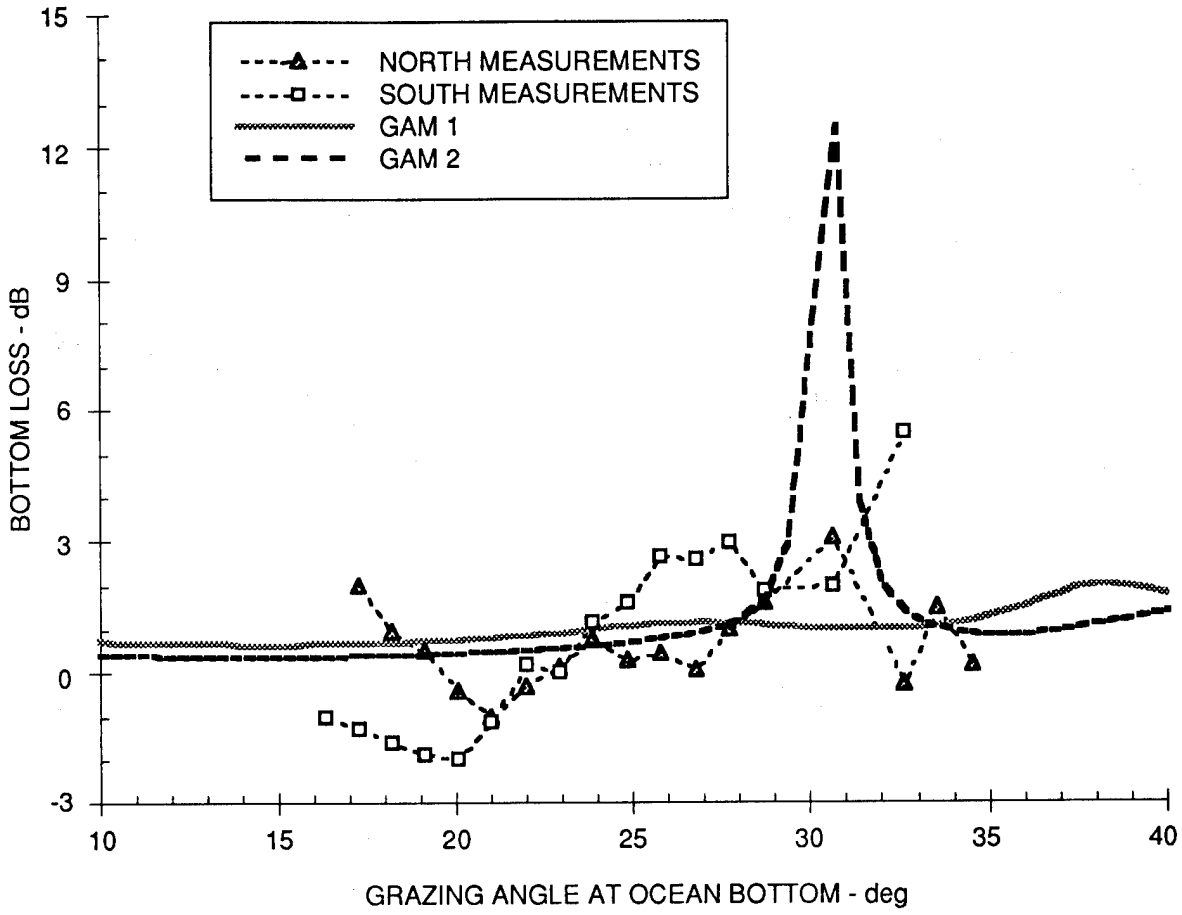

FIGURE 6.6
MEASURED AND MODELED 10 Hz PLANE WAVE BOTTOM LOSS versus GRAZING ANGLE ESTIMATES

ARL - UT
AS-93-573
SJL/RFO
10-93/hd2

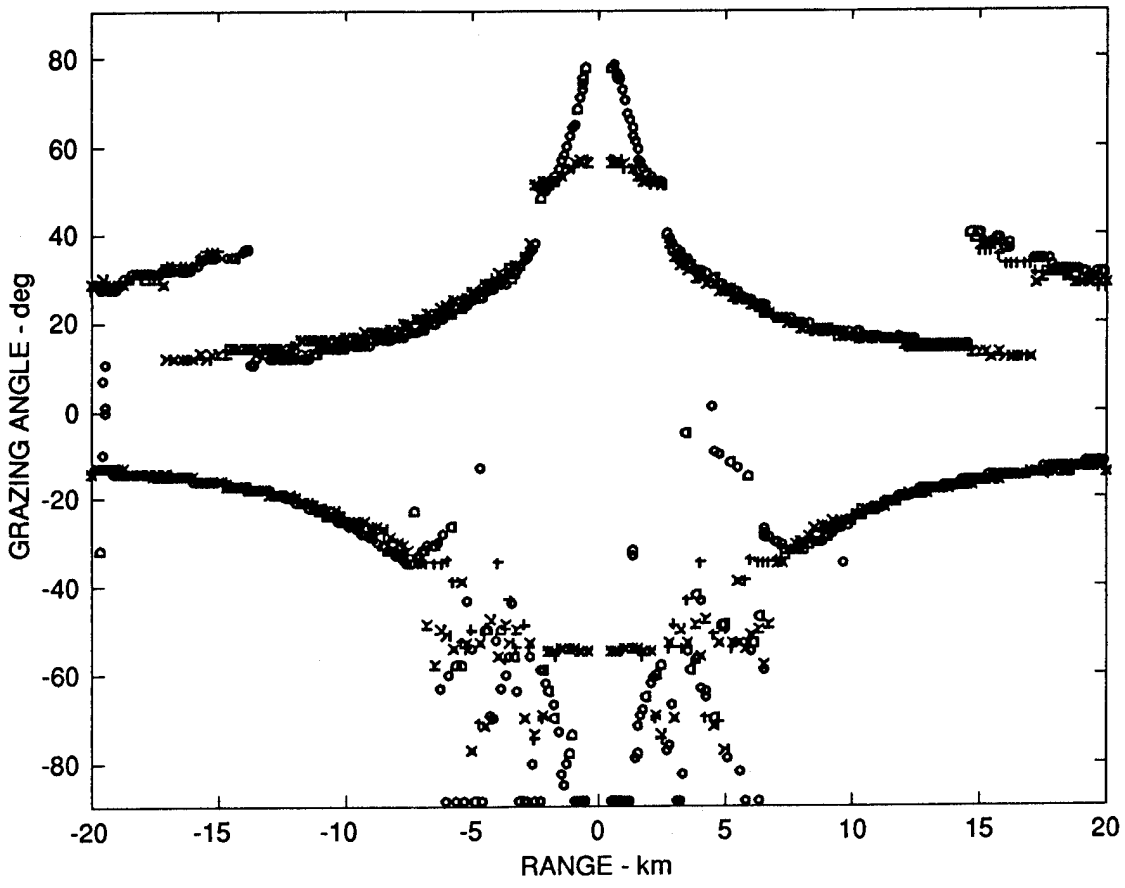

FIGURE 6.7
MEASURED AND MODELED
(GAM 1 AND GAM 2 SEDIMENT MODELS)
GRAZING ANGLES OF 10 Hz PEAK ARRIVALS
FROM THE SURFACE AND FROM THE BOTTOM

ARL:UT
AS-93-574
SJL - RFG
10-93uncl2

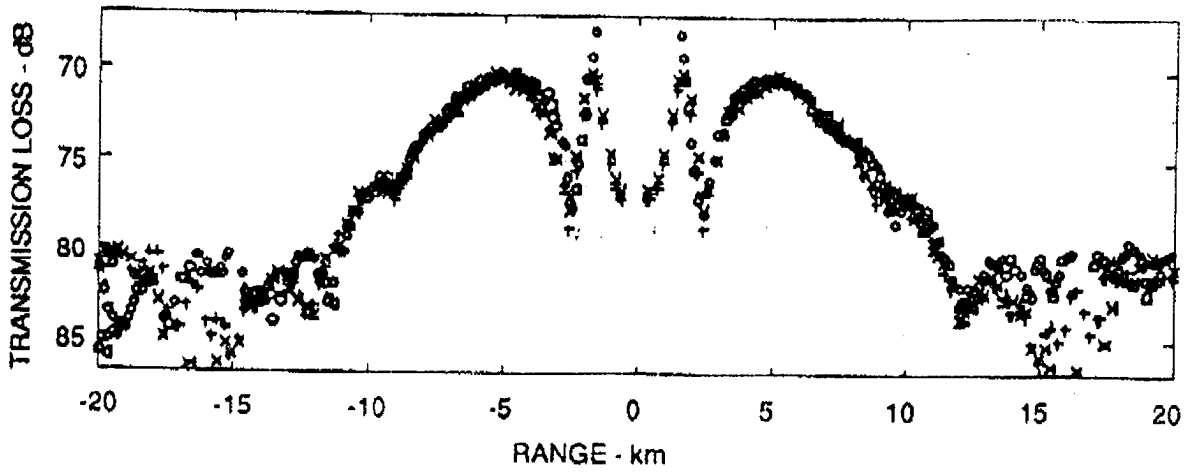

(a) 10 Hz PEAK ARRIVALS FROM THE SURFACE

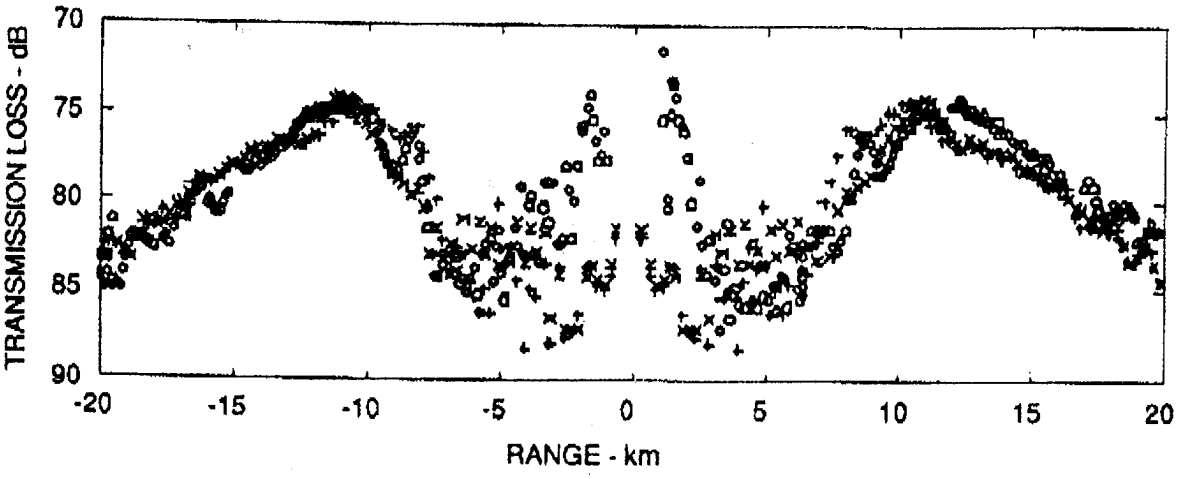

(b) 10 Hz PEAK ARRIVALS FROM THE BOTTOM

- ○ NATIVE MEASUREMENTS
- \+ MODEL (GAM 1)
- × MODEL (GAM 2)

FIGURE 6.8
MEASURED AND MODELED
(GAM 1 AND GAM 2 SEDIMENT MODELS)
10 Hz TRANSMISSION LOSS

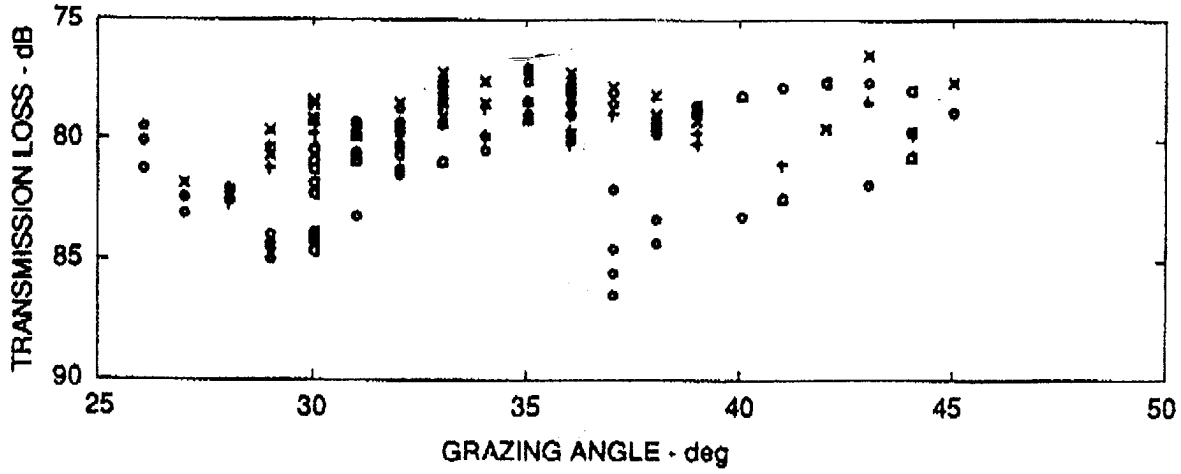

(a) 7 Hz SINGLE-BOTTOM PEAK ARRIVALS FROM THE SURFACE, 13-20 km FROM V1 ARRAY

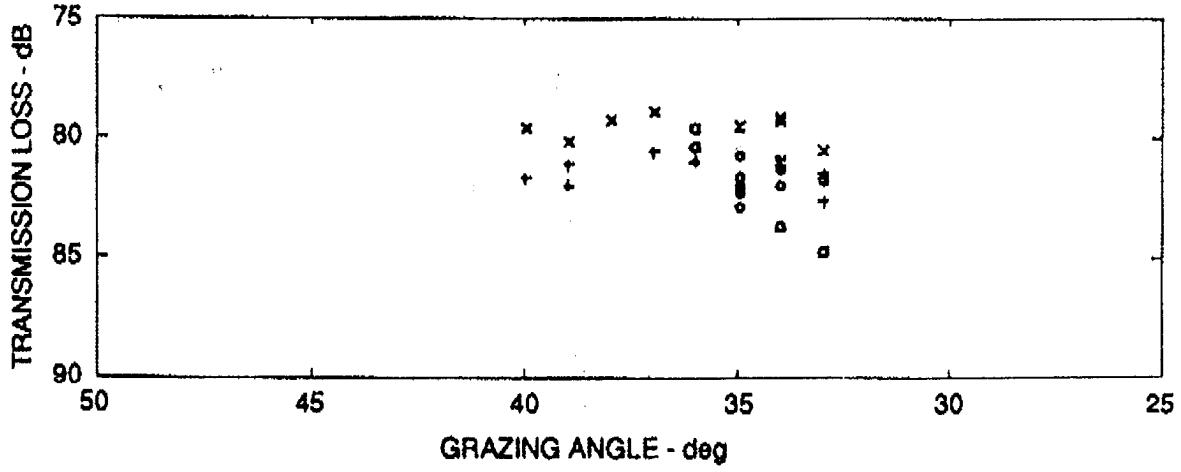

(b) 7 Hz DOUBLE-BOTTOM PEAK ARRIVALS FROM THE BOTTOM, 13-20 km FROM V1 ARRAY

- NATIVE MEASUREMENTS
- MODEL (GAM 1)
- MODEL (SPREADING LOSS ESTIMATE)

FIGURE 6.9
MEASURED AND MODELED
(GAM 1 SEDIMENT MODEL AND SPREADING LOSS ESTIMATE)
7 Hz TRANSMISSION LOSS FOR RANGES OF
13-20 km FROM ARRAY

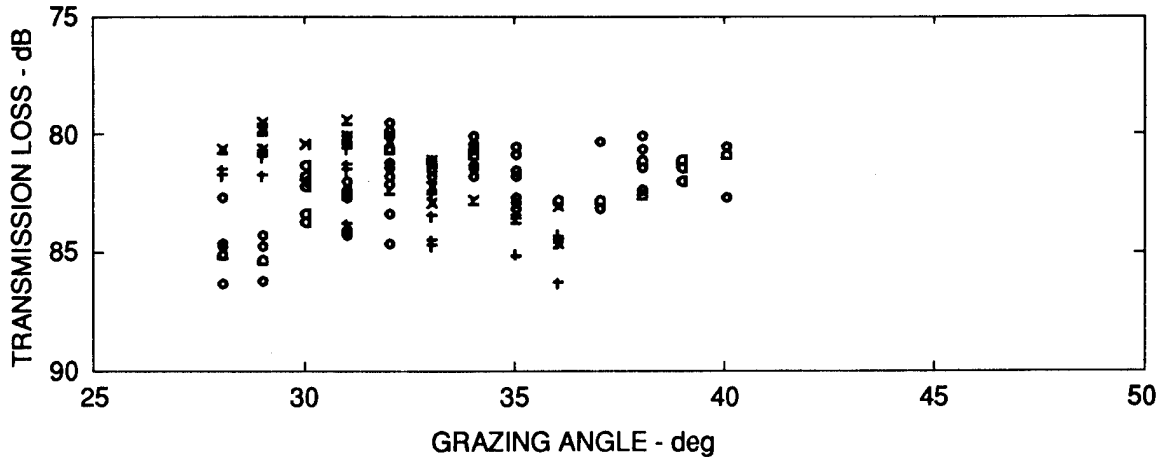

(a) 10 Hz SINGLE-BOTTOM PEAK ARRIVALS FROM THE SURFACE, 13-20 km FROM V1 ARRAY

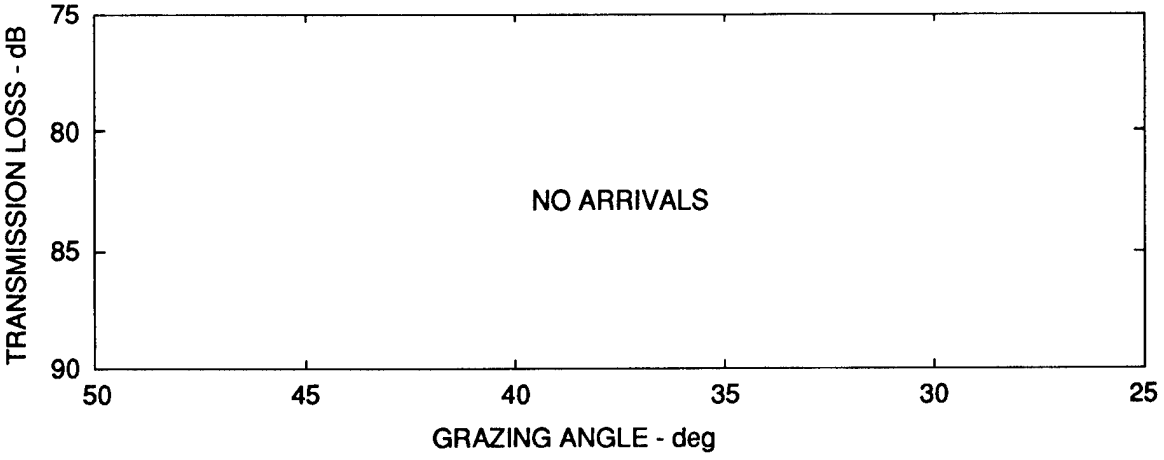

(b) 10 Hz DOUBLE-BOTTOM PEAK ARRIVALS FROM THE BOTTOM, 13-20 km FROM V1 ARRAY

- ∘ NATIVE MEASUREMENTS
- + MODEL (GAM 1)
- × MODEL (SPREADING LOSS ESTIMATE)

FIGURE 6.10
MEASURED AND MODELED
(GAM 1 SEDIMENT MODEL AND SPREADING LOSS ESTIMATE)
10 Hz TRANSMISSION LOSS FOR RANGES OF
13-20 km FROM ARRAY

ARL - UT
AS-93-577
SJL/RFG
10-93/hd2

This page intentionally left blank.

7. LONG RANGE ARRIVAL STRUCTURE

In this section we explore the arrival structure and acoustic bottom loss at longer ranges (35-60 km). The bottom loss increases at these ranges due to increased multiple bottom interactions, and the uncertainty associated with the bottom loss appears to be even greater. Since the increased variation of the bathymetry hinders both arrival angle identification and arrival order classification at longer ranges, we will compare statistical characterizations of the measured and calculated bottom loss.

The 7 and 10 Hz arrival structures are estimated by again forming plane wave beams at each range as shown in Figs. 7.1 and 7.2, respectively. Dominant acoustic energy arrives at grazing angles of 15° to 50°, and usually appears in one of six clusters. Three of these clusters arrive from the surface and three arrive from the bottom. Clusters at 7 Hz are ~10° wide and are generally wider than those at 10 Hz. This is a result of the lower 7 Hz spatial resolution, as indicated by a comparison of the 7 and 10 Hz beam patterns (Fig. 5.1).

One perhaps unexpected feature of the VLF arrival structure apparent in Figs. 7.1 and 7.2 is the absence of signal arrivals at shallow angles. For these arrivals, bottom loss should have minimal effect. However, for the NATIVE environment, we have found the array to be shadowed for arrivals shallower than ~10° when the source is 122 m deep. Plots of the surface interference term shown in Fig. 7.3 illustrate this point. Figure 7.3(a) shows the loss strictly due to surface dipole interference at 7, 10, 16, and 50 Hz for a receiver at the 122 m source depth. From these plots it is clear that 7 and 10 Hz arrivals experience significant loss at shallow grazing angles. The absence of shallow signal arrivals is even more apparent for a receiver 2500 m deep near the center of the array. Here, the shadowing effect due to Snell's law is a dominant factor at angles less than ~10°, as shown in Fig. 7.3(b).

Normal mode calculations corresponding to the measured arrivals (Figs. 7.1 and 7.2) have been estimated by calculating the coherent TL at 7 and 10 Hz using NEMESIS and then subtracting the TL from the 168 dB source level. The levels calculated with no bottom attenuation are shown in

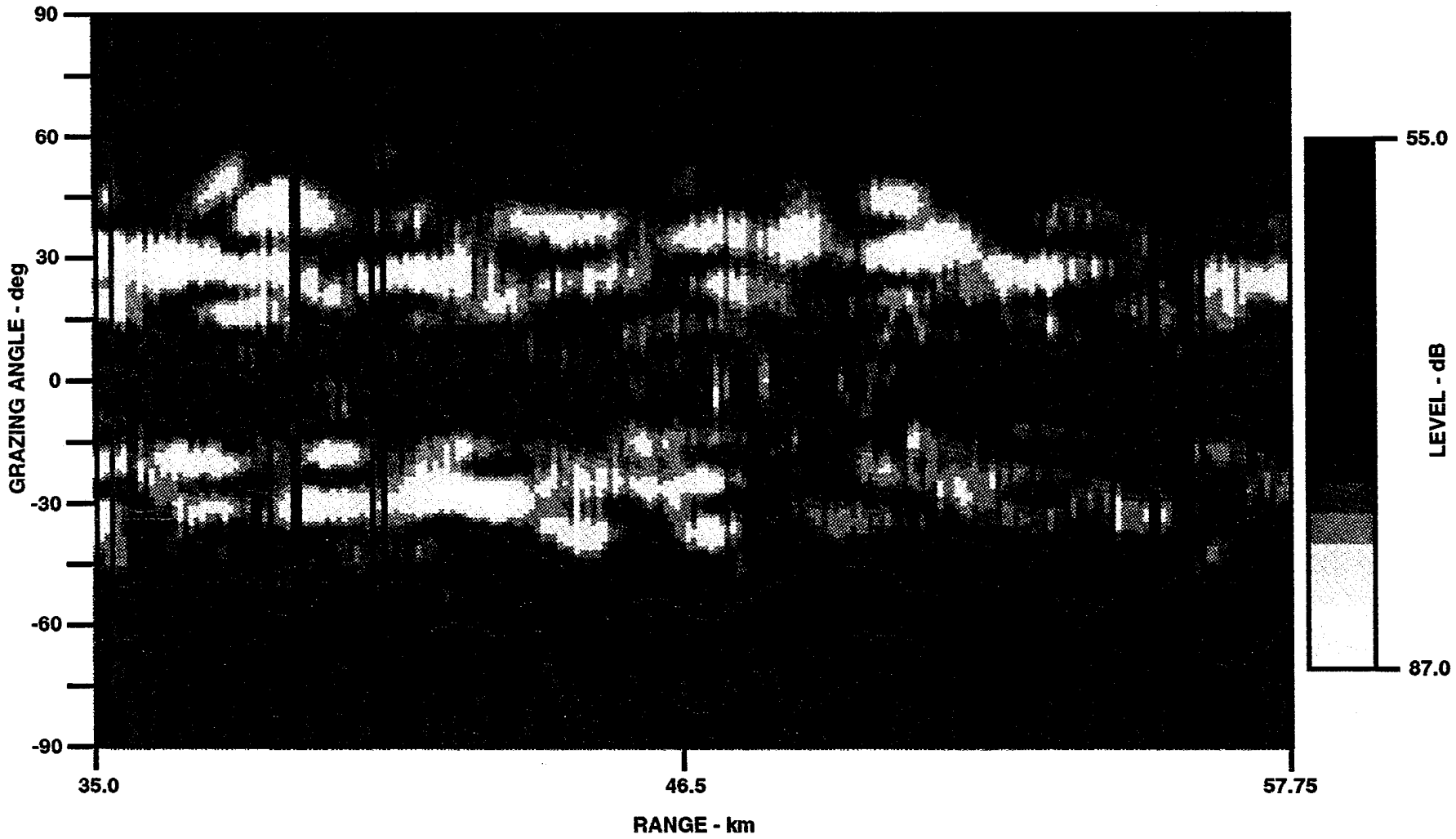

FIGURE 7.1
LONG RANGE 7 Hz MEASURED BEAM LEVELS versus GRAZING ANGLE AND RANGE

ARL:UT
AS-93-578
SJL - RFG
10-93und2

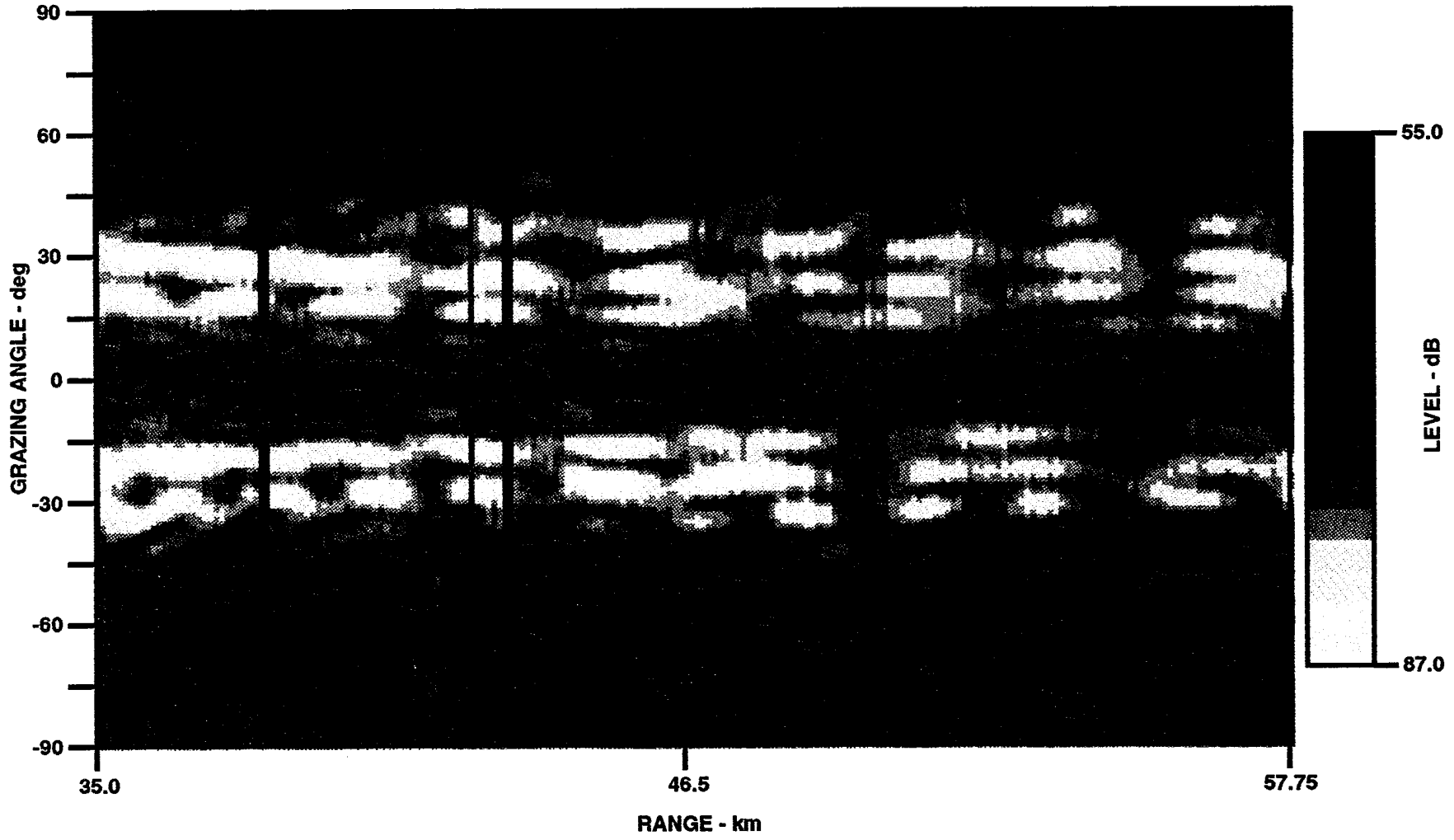

FIGURE 7.2
LONG RANGE 10 Hz MEASURED BEAM LEVELS versus GRAZING ANGLE AND RANGE

ARL:UT
AS-93-595
SJL - RFG
10-93uncl2

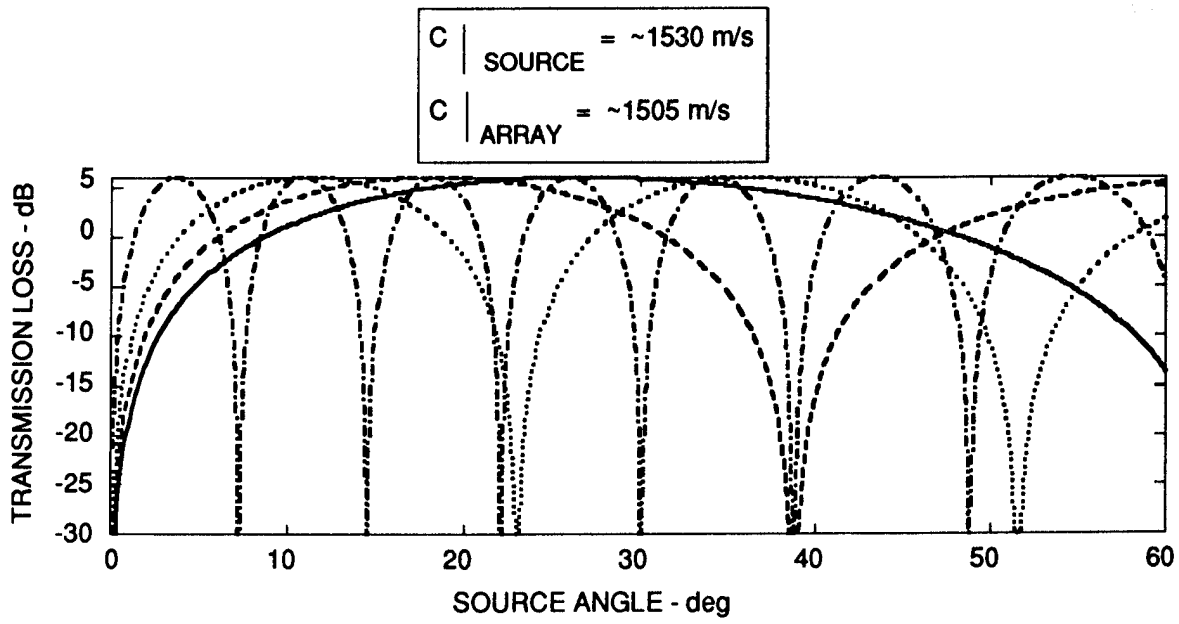

(a) CALCULATED SURFACE INTERFERENCE TERM AT SOURCE DEPTH (122 m)

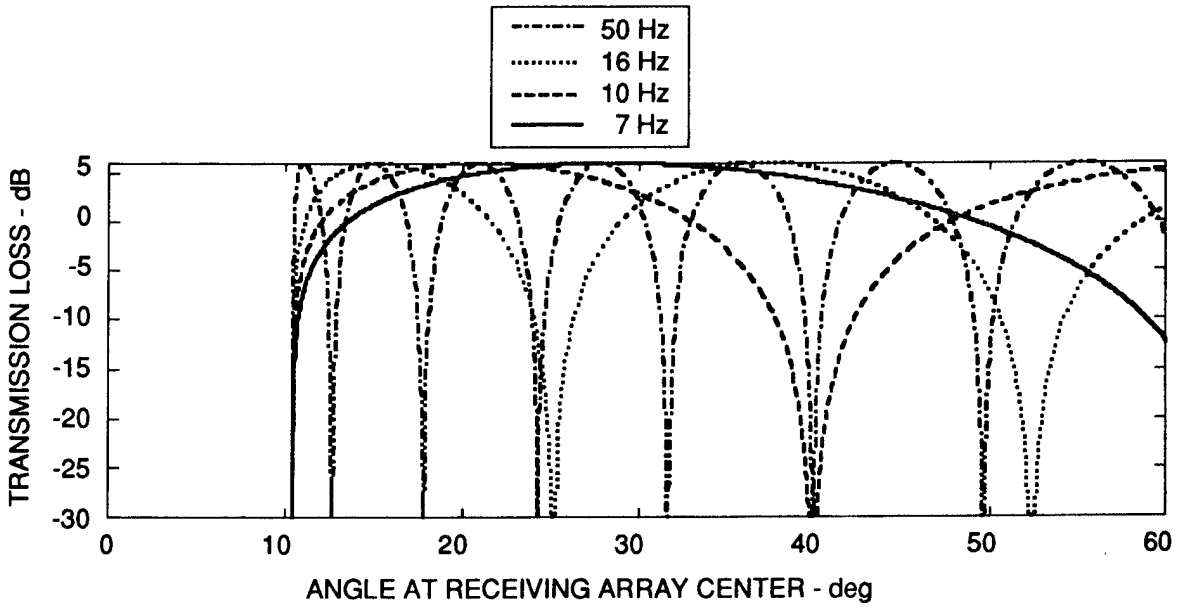

(b) CALCULATED SURFACE INTERFERENCE TERM
NEAR THE ARRAY CENTER DEPTH (2500 m)

FIGURE 7.3
CALCULATED SURFACE INTERFERENCE TERM
AT TWO DEPTHS AND FOUR FREQUENCIES

ARL - UT
AS-93-579
SJL/RFO
10-93/hd2

Figs. 7.4 and 7.5. The prominent features of the calculations favorably describe the measured arrivals in that there are usually three cluster arrivals from both the surface and the bottom which arrive at approximately the same angles as the measurements. Calculations have indicated the three dominant surface and bottom clusters are due to interactions with the ocean bottom two, three, and four times. Due to bathymetry errors, however, the modeled range and central angle of cluster peaks often differ from those of the measurements.

Next we explore long range cw VLF bottom loss by once again quantitatively comparing the peak arrivals of the measurements with model calculations. We note that gas in the hydrate state was not apparent in the seismic reflection data collected during the "long" range portion of Event 1.[4] Thus only two sets of model calculations have been executed: those in which the sediment presents no acoustic loss (GAM 0) and those in which the GAM 1 loss is exhibited. The arrival angles at 7 and 10 Hz are shown in Figs. 7.6 and 7.7, respectively, for the peak measured and calculated beams; the dashed curves are the expected arrival angle for different arrival orders. Note how both the measured and calculated peak grazing angles show several discontinuities as a function of range. This is because the transmission losses corresponding to different arrival orders typically differ by only a few dB at these ranges, and the peak arrivals at ranges only a few (~5) kilometers apart often correspond to different arrival orders.

Coherent TL estimates corresponding to peak angles in Figs. 7.6 and 7.7 are shown in Figs. 7.8 and 7.9, respectively. Note that the TL of the measured and calculated long range beams at both frequencies experience as much as 10 dB variation over any 5 km interval. Also, measured TL for a given arrival order is frequently smaller than that calculated without bottom loss. Model errors in the positions of interference peaks and valleys are compounded at longer ranges, and errors in the modeled arrival order exist in the TL calculations as multiplicative factors of the bottom loss error.

In order to explore bottom loss in the presence of these difficulties, the arrivals have been analyzed by first arranging them into eight groups according to their frequency (7 or 10 Hz), range interval (35-45 km or 45-58 km), and

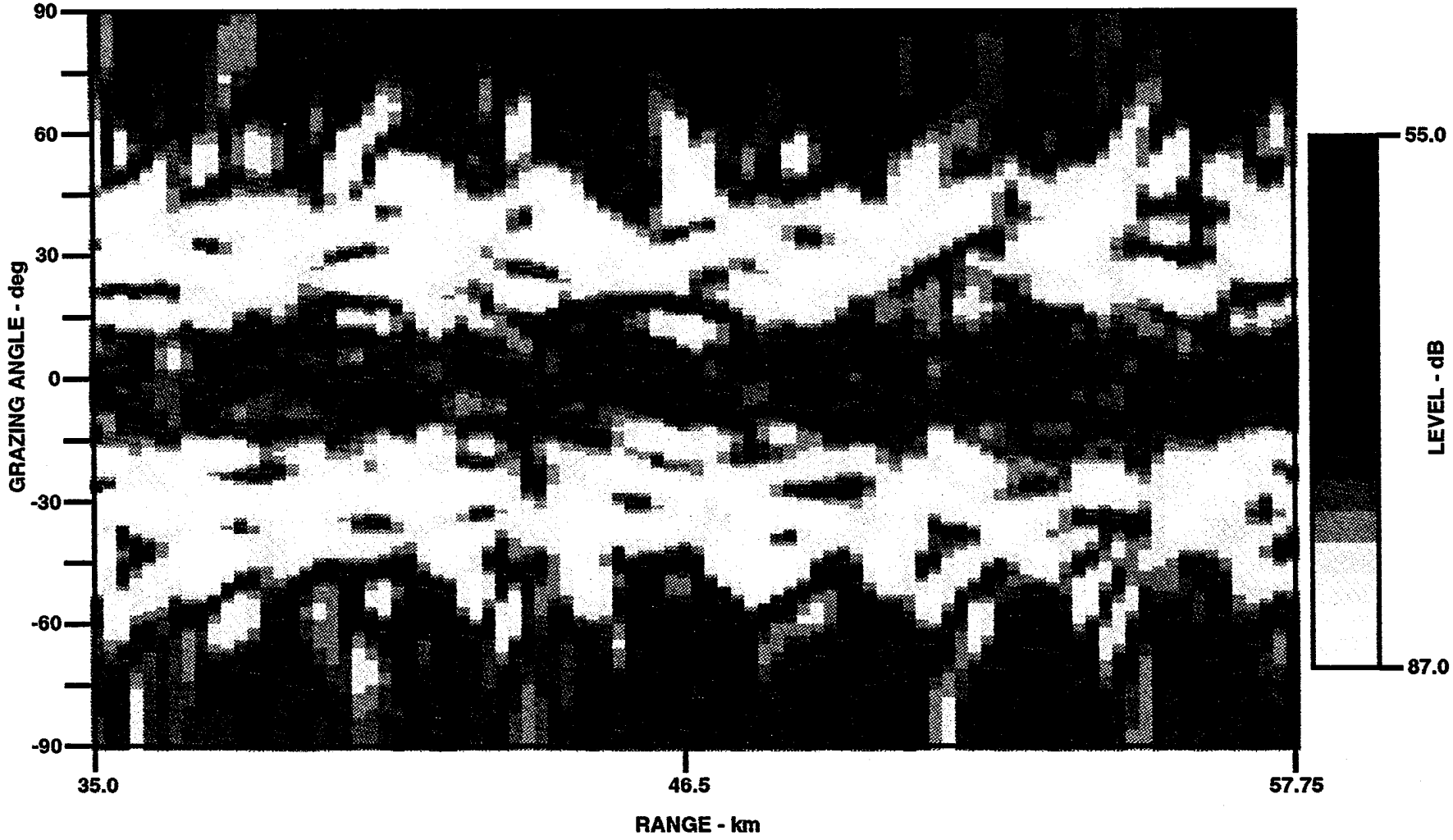

FIGURE 7.4
LONG RANGE 7 Hz ADIABATIC NORMAL MODE MODELED BEAM LEVELS (GAM 0 SEDIMENT PARAMETERS) versus GRAZING ANGLE AND RANGE

ARL:UT
AS-93-580
SJL - RFG
10-93uncl2

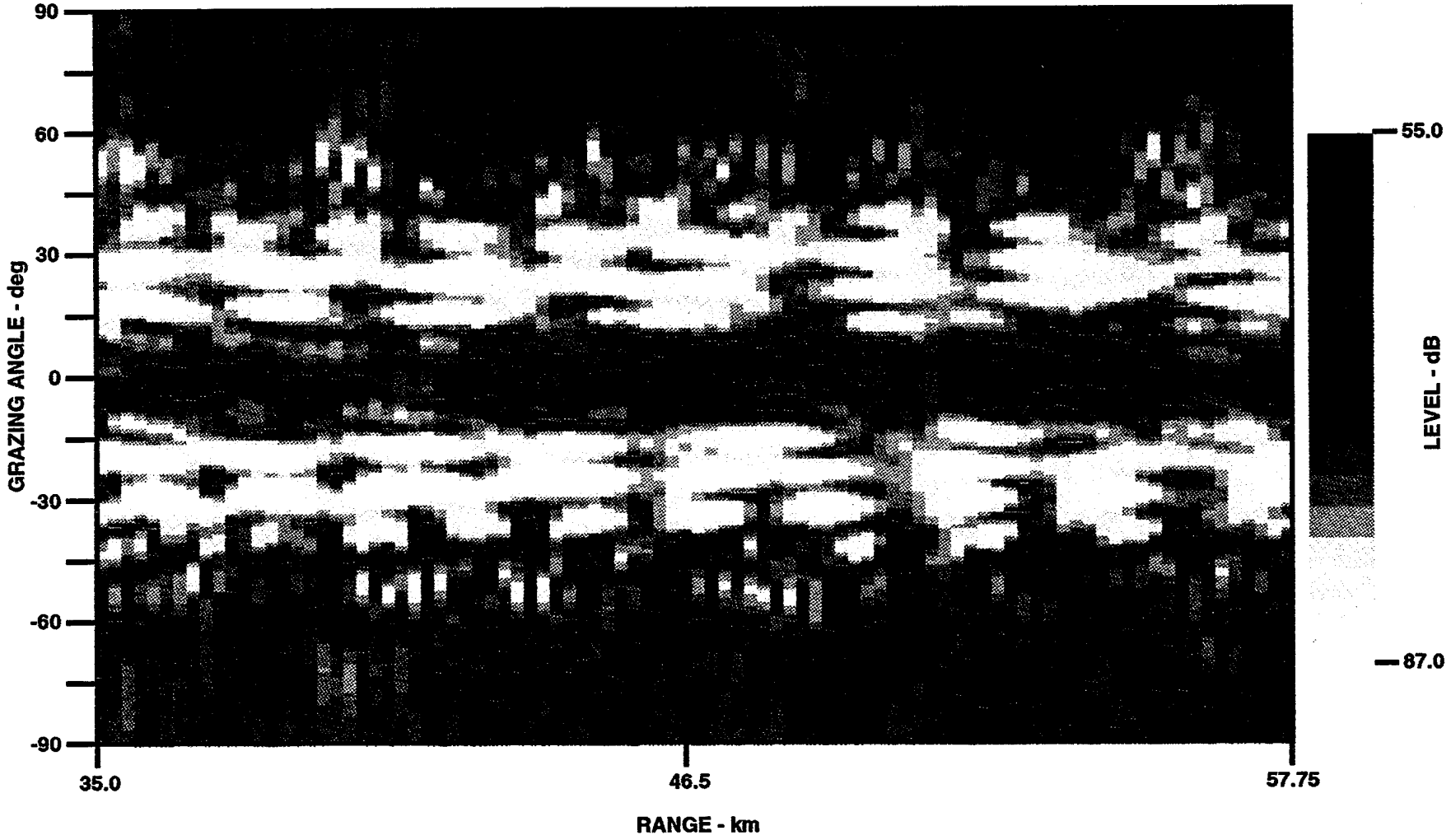

FIGURE 7.5
LONG RANGE 10 Hz ADIABATIC NORMAL MODE MODELED BEAM LEVELS (GAM 0 SEDIMENT PARAMETERS) versus GRAZING ANGLE AND RANGE

ARL:UT
AS-93-581
SJL - RFG
10-93uncl2

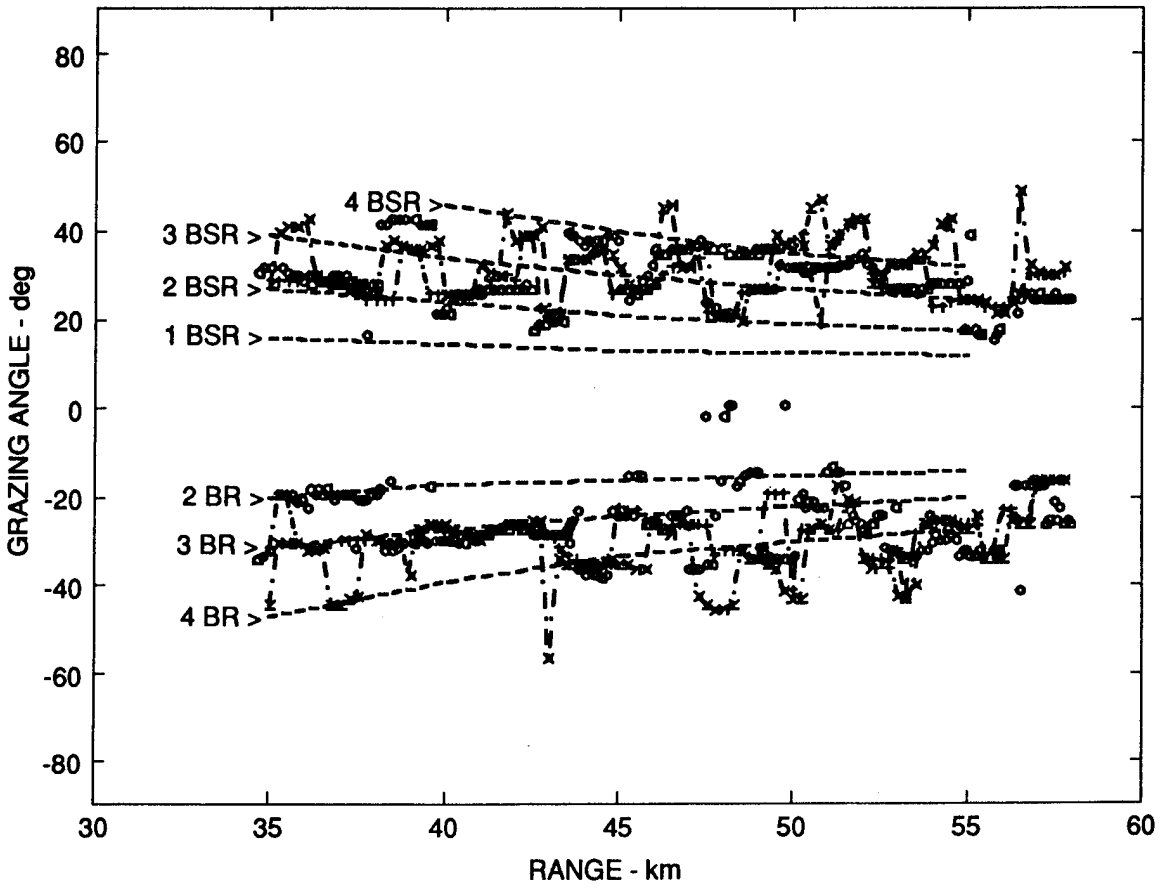

FIGURE 7.6
MEASURED AND MODELED
(GAM 0 AND GAM 1 SEDIMENT MODELS)
GRAZING ANGLES OF 7 Hz PEAK ARRIVALS FROM THE SURFACE
AND FROM THE BOTTOM AT LONG RANGES

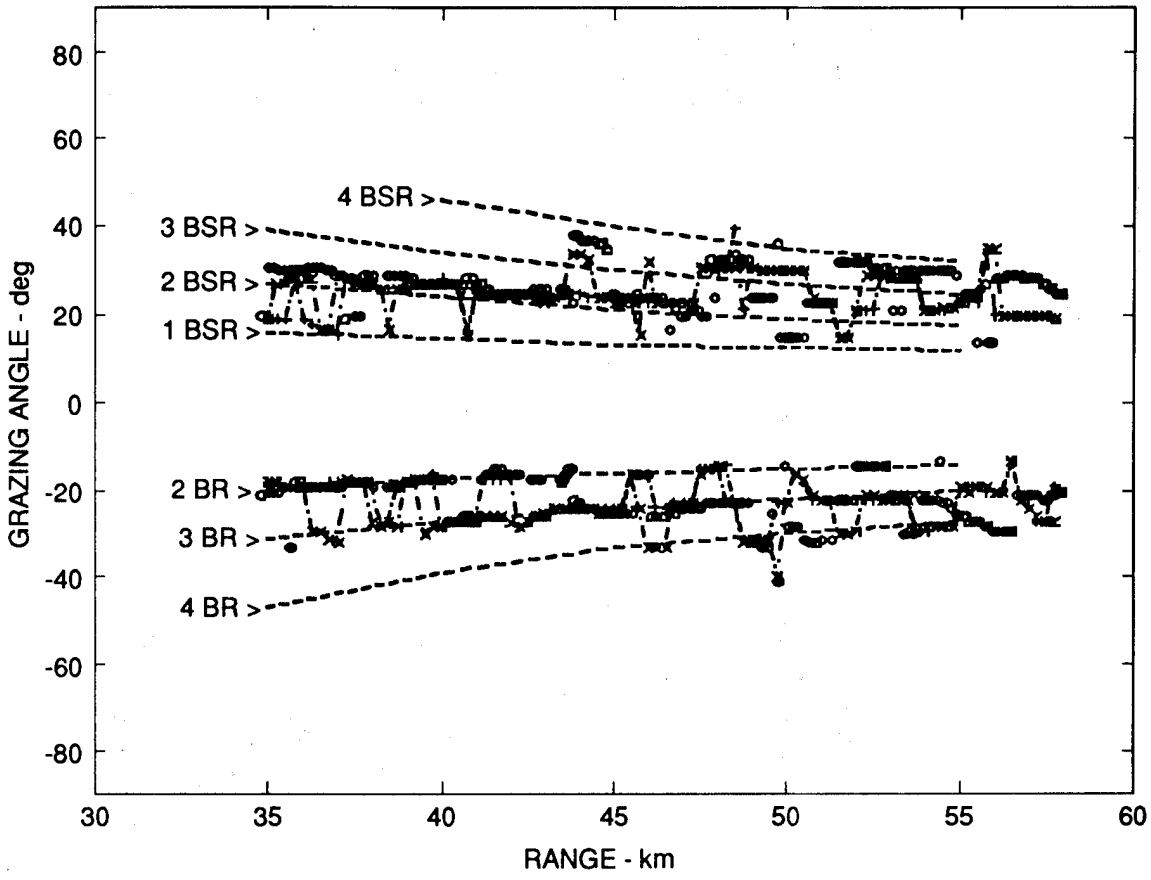

FIGURE 7.7
MEASURED AND MODELED
(GAM 0 AND GAM 1 SEDIMENT MODELS)
GRAZING ANGLES OF 10 Hz PEAK ARRIVALS FROM THE SURFACE
AND FROM THE BOTTOM AT LONG RANGES

ARL - UT
AS-93-583
SJL/RFG
10-93/hd2

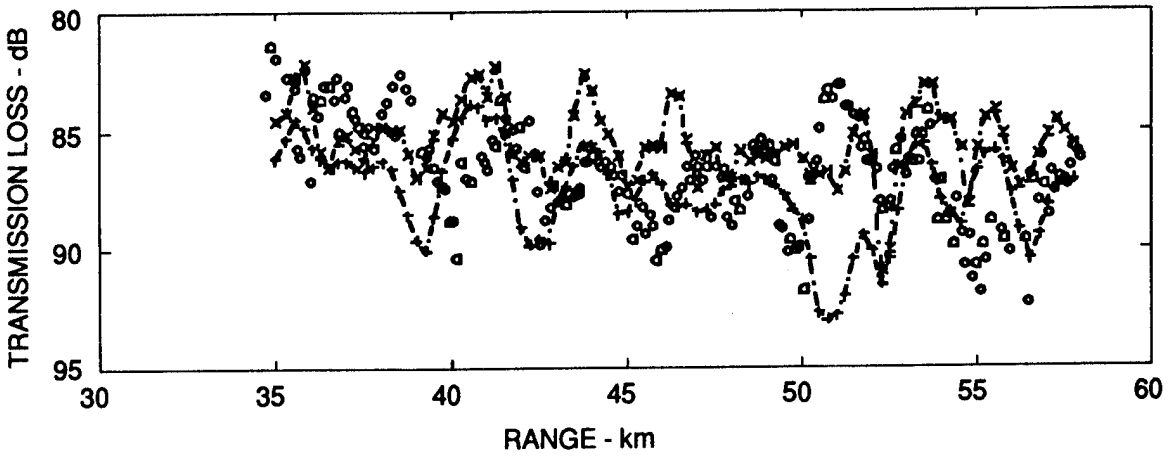

(a) 7 Hz PEAK ARRIVALS FROM THE SURFACE

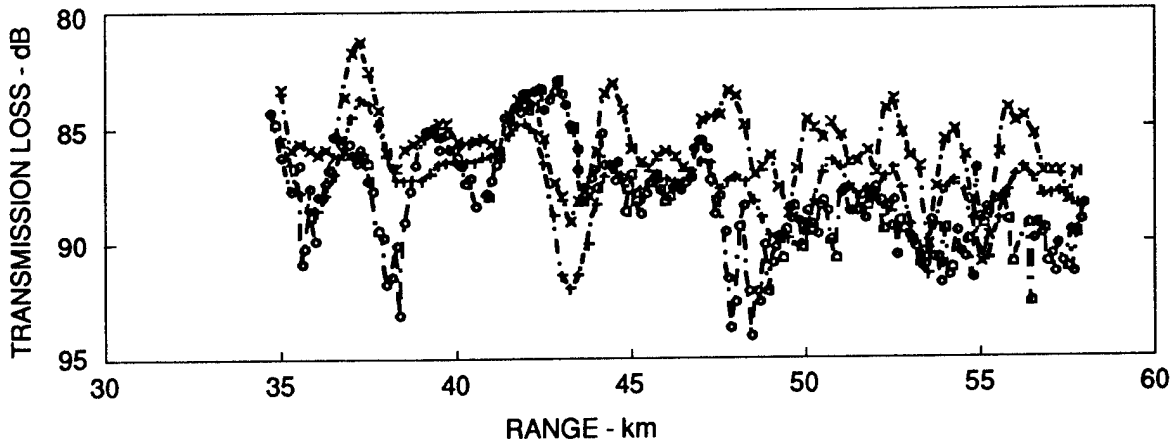

(b) 7 Hz PEAK ARRIVALS FROM THE BOTTOM

- o NATIVE MEASUREMENTS
- \+ MODEL (GAM 1)
- × MODEL (GAM 0)

FIGURE 7.8
MEASURED AND MODELED
(GAM 0 AND GAM 1 SEDIMENT MODELS)
7 Hz TRANSMISSION LOSS

ARL - UT
AS-93-584
SJL/RFO
10-93/hd2

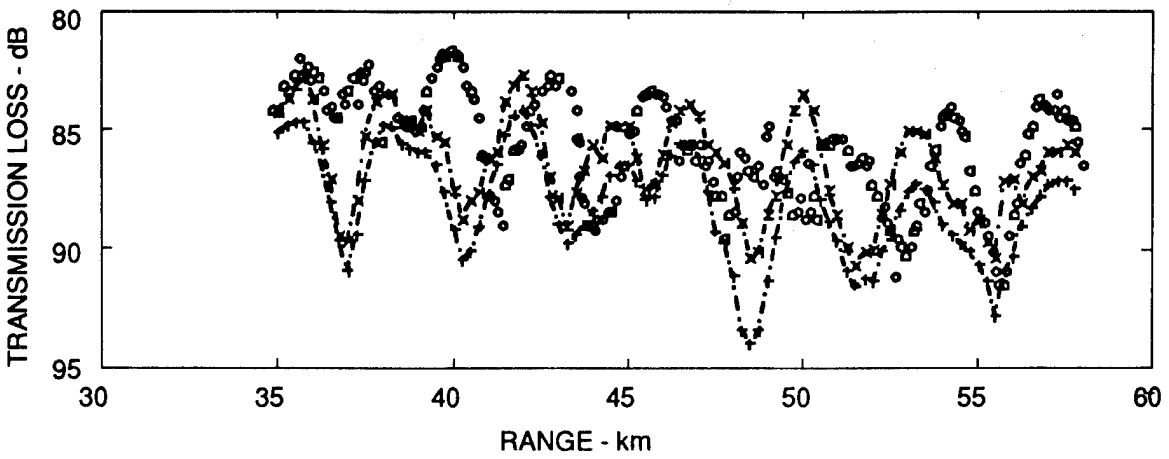

(a) 10 Hz PEAK ARRIVALS FROM THE SURFACE

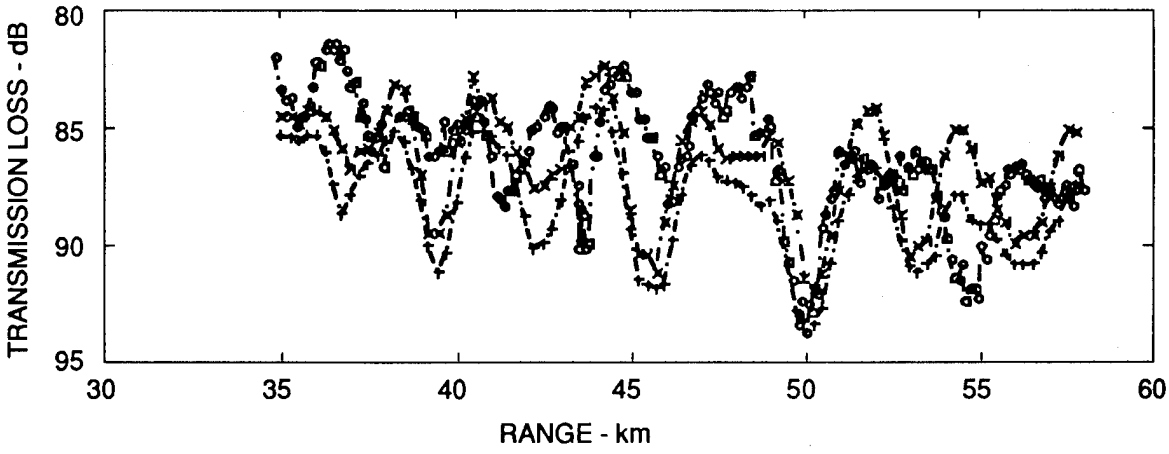

(b) 10 Hz PEAK ARRIVALS FROM THE BOTTOM

o NATIVE MEASUREMENTS
\+ MODEL (GAM 1)
× MODEL (GAM 0)

FIGURE 7.9
MEASURED AND MODELED
(GAM 0 AND GAM 1 SEDIMENT MODELS)
10 Hz TRANSMISSION LOSS

ARL - UT
AS-93-585
SJL/RFO
10-93/hd2

arrival direction (from the surface or from the bottom). Arrival orders in each of the eight possible group permutations were then isolated in the same manner as at shorter ranges: by making measurement/model TL comparisons only for those cases where the ranges of the modeled and measured TL values coincide within 130 m, and where respective grazing angles are within 3°.

Figures 7.10 - 7.17 correspond to each arrival group, where TL versus grazing angle is plotted in the upper plots and the associated cumulative probability of TL is plotted in the lower plots. Note that there is a large scatter of TL versus grazing angle in the top of each figure. A statistical characterization of the measured TL values is shown in each lower plot, with calculated TL values also shown to give perspective. Calculated TL percentiles corresponding to the GAM 1 attenuation profile usually indicate only between ~1 and ~2 dB more loss than calculated TL percentiles which characterize no bottom loss.

The 7 Hz arrivals from the surface and from the bottom in the 35-45 km range interval are shown in Figs. 7.10 and 7.11, respectively. Note that the probability distribution curves characterizing the measured arrivals are close to the corresponding distributions modeled with no bottom loss. However, the same comparisons made in the 45-60 km range interval in Figs. 7.12 and 7.13 show that the measured arrivals are best characterized using the GAM 1 bottom loss. The 10 Hz arrivals from the surface and from the bottom in the 35-45 km range interval are shown in Figs. 7.14 and 7.15, respectively. Here, the probability distribution curves characterizing TL of the measured arrivals indicate ~1 dB less loss than corresponding distributions modeled with GAM 0 bottom loss. Comparisons made in the 45-60 km range interval in Figs. 7.16 and 7.17 show that the measured arrivals are best characterized with GAM 0 bottom loss.

The long range measurements have qualitatively corroborated the bottom loss description observed at shorter ranges in that the 10 Hz bottom loss is lower than that at 7 Hz. Nevertheless, bottom loss predictions of the model calculations are too small relative to the measurement uncertainties to formulate a reliable exact description of the bottom attenuation profile using the long range measurements.

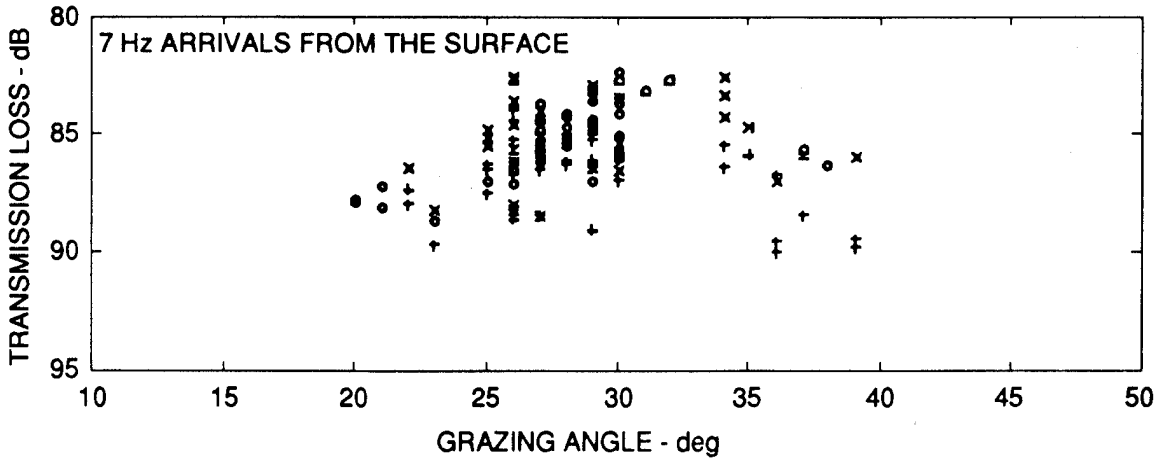

(a) TRANSMISSION LOSS versus GRAZING ANGLE IN THE RANGE INTERVAL 35.3 - 44.6 km

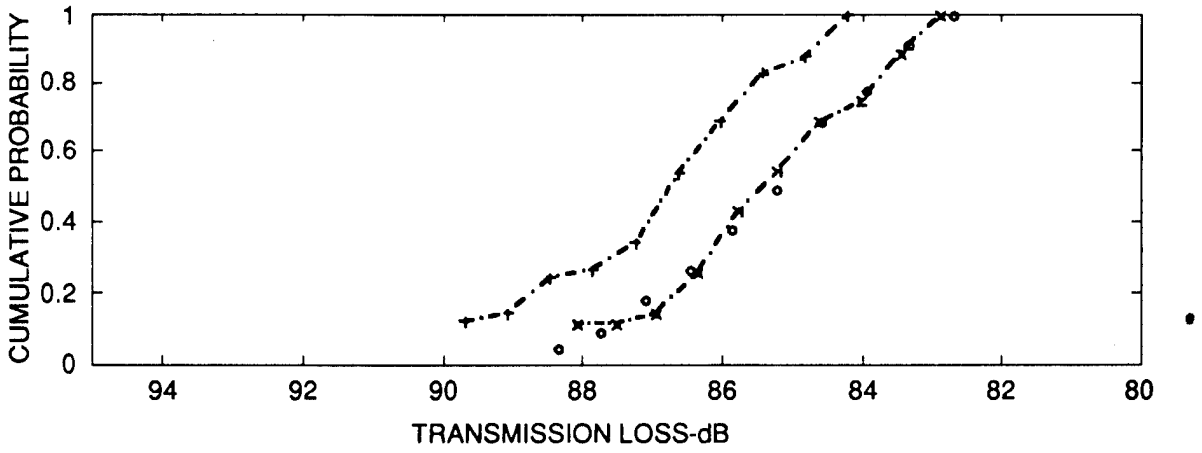

(b) TRANSMISSION LOSS PROBABILITY DISTRIBUTION

- ∘ NATIVE MEASUREMENTS
- + MODEL (GAM 1)
- × MODEL (SPREADING LOSS ESTIMATE)

FIGURE 7.10
TRANSMISSION LOSS versus GRAZING ANGLE AND ASSOCIATED TL PROBABILITY DISTRIBUTION FOR 7 Hz PEAK ARRIVALS FROM THE SURFACE FOR THE 35.3 - 44.6 km RANGE INTERVAL

ARL - UT
AS-93-586
SJL/RFG
10-93/hd2

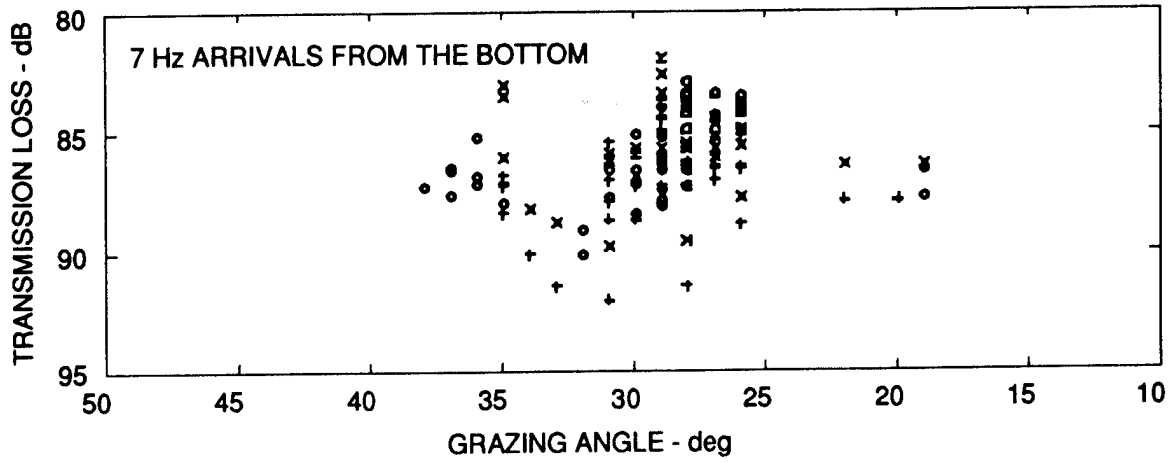

(a) TRANSMISSION LOSS
versus ANGLE IN THE RANGE INTERVAL 35.3 - 44.6 km

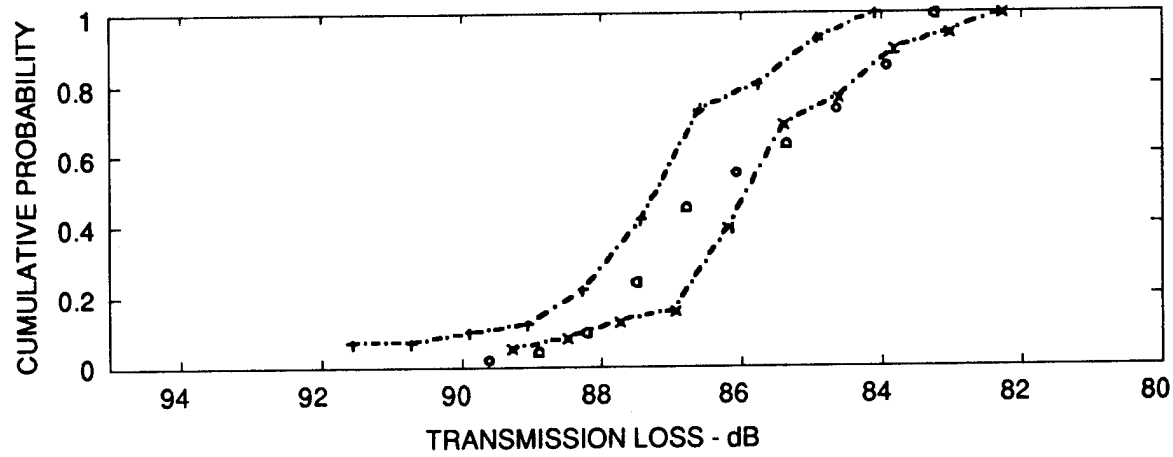

(b) TRANSMISSION LOSS PROBABILITY DISTRIBUTION

o NATIVE MEASUREMENTS
\+ MODEL (GAM 1)
× MODEL (SPREADING LOSS ESTIMATE)

FIGURE 7.11
TRANSMISSION LOSS versus GRAZING ANGLE AND ASSOCIATED TL PROBABILITY DISTRIBUTION FOR 7 Hz PEAK ARRIVALS FROM THE BOTTOM FOR THE 35.3 - 44.6 km RANGE INTERVAL

ARL - UT
AS-93-587
SJL/RFO
10-93/hd2

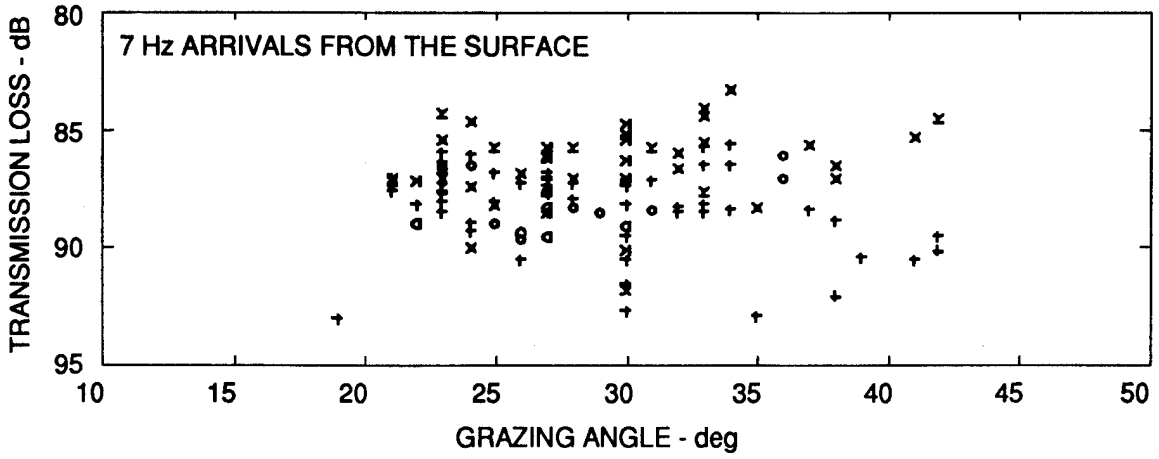

(a) TRANSMISSION LOSS
versus ANGLE IN THE RANGE INTERVAL 45.0-56.31 km

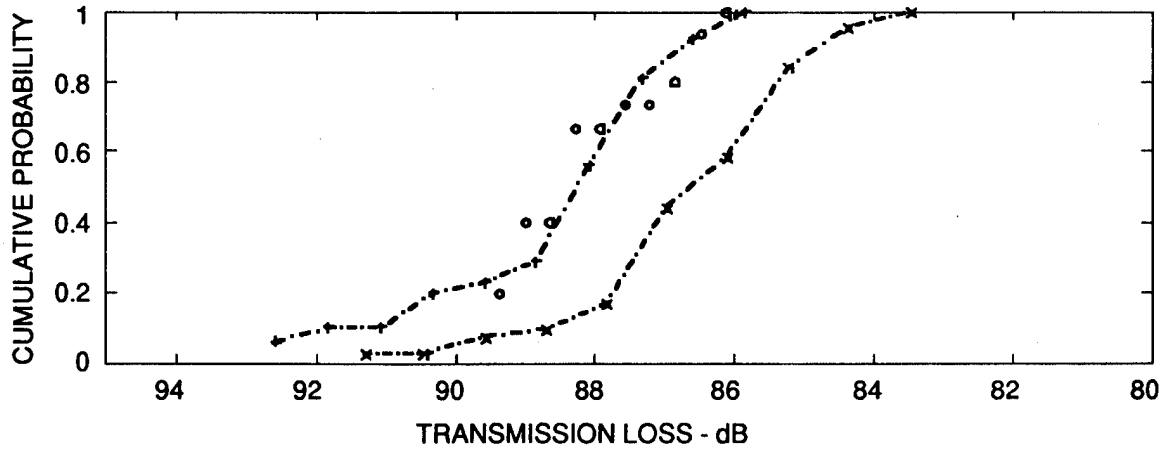

(b) TRANSMISSION LOSS PROBABILITY DISTRIBUTION

- ° NATIVE MEASUREMENTS
- + MODEL (GAM 1)
- × MODEL (SPREADING LOSS ESTIMATE)

FIGURE 7.12
TRANSMISSION LOSS versus GRAZING ANGLE AND ASSOCIATED TL PROBABILITY DISTRIBUTION FOR 7 Hz PEAK ARRIVALS FROM THE SURFACE FOR THE 45.0-56.31 km RANGE INTERVAL

ARL - UT
AS-93-588
SJL/RFO
10-93/hd2

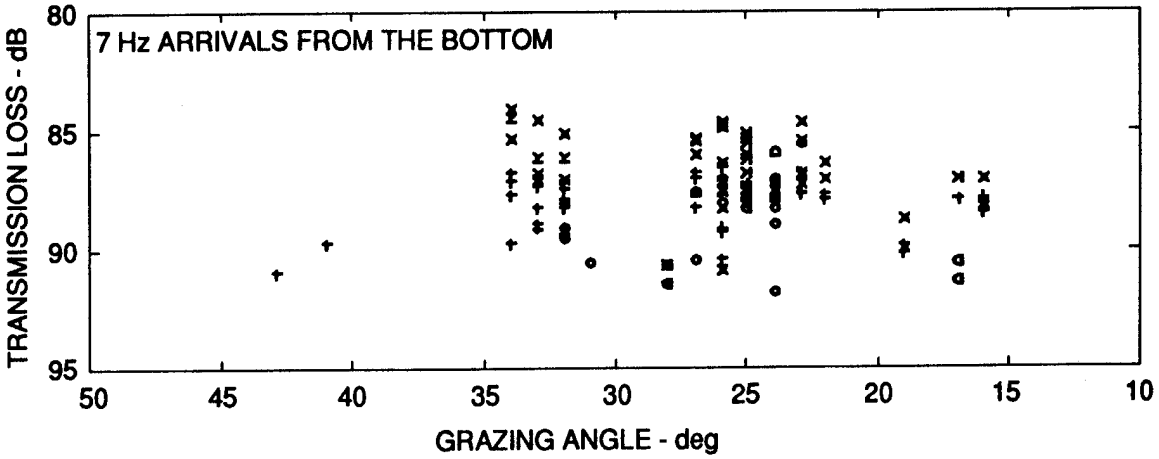

(a) TRANSMISSION LOSS versus GRAZING ANGLE IN THE RANGE INTERVAL 45.0-57.1 km

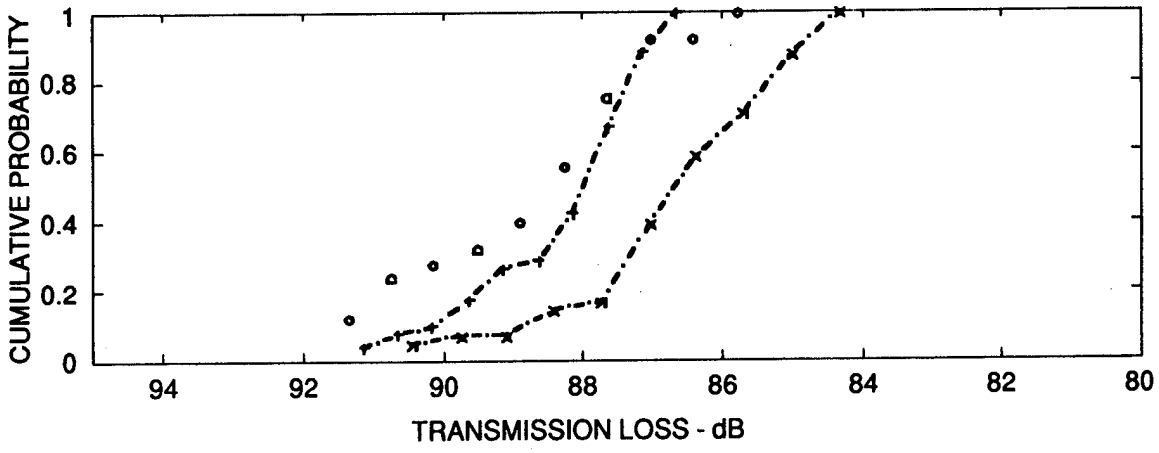

(b) TRANSMISSION LOSS PROBABILITY DISTRIBUTION

- NATIVE MEASUREMENTS
- MODEL (GAM 1)
- MODEL (SPREADING LOSS ESTIMATE)

FIGURE 7.13
TRANSMISSION LOSS versus GRAZING ANGLE AND ASSOCIATED TL PROBABILITY DISTRIBUTION FOR 7 Hz PEAK ARRIVALS FROM THE BOTTOM 45.0-57.1 km RANGE INTERVAL

ARL - UT
AS-93-589
SJL/RFG
10-93/hd2

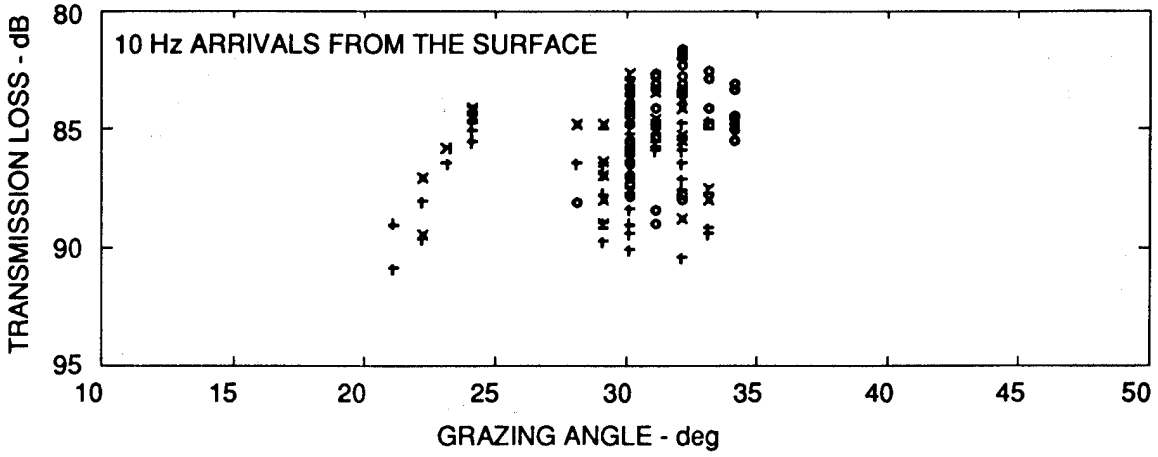

(a) TRANSMISSION LOSS
versus ANGLE IN THE RANGE INTERVAL 37.3 - 44.9 km

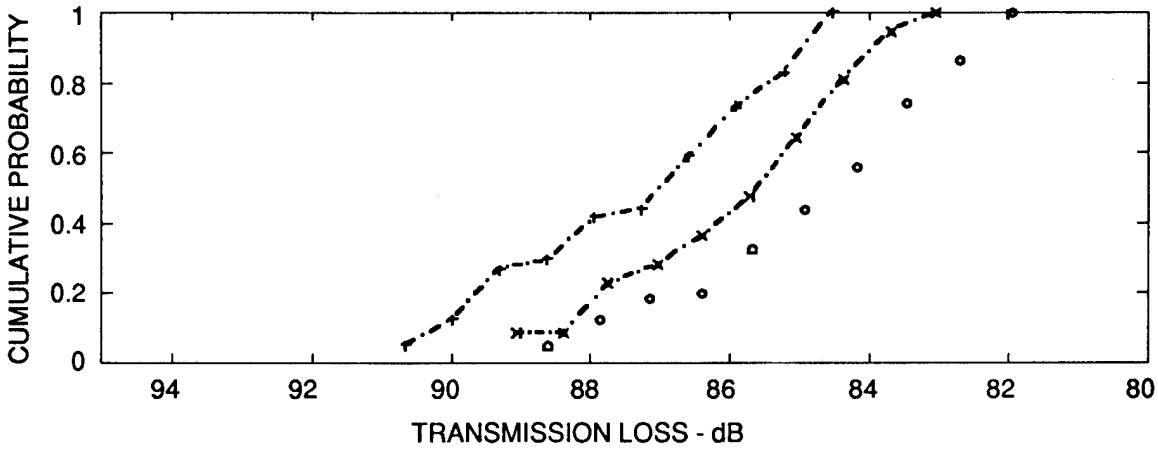

(b) TRANSMISSION LOSS PROBABILITY DISTRIBUTION

o NATIVE MEASUREMENTS
\+ MODEL (GAM 1)
× MODEL (SPREADING LOSS ESTIMATE)

FIGURE 7.14
TRANSMISSION LOSS versus GRAZING ANGLE AND ASSOCIATED TL PROBABILITY DISTRIBUTION FOR 10 Hz PEAK ARRIVALS FROM THE SURFACE FOR THE 37.3 - 44.9 km RANGE INTERVAL

ARL - UT
AS-93-590
SJL/RFO
10-93/hd2

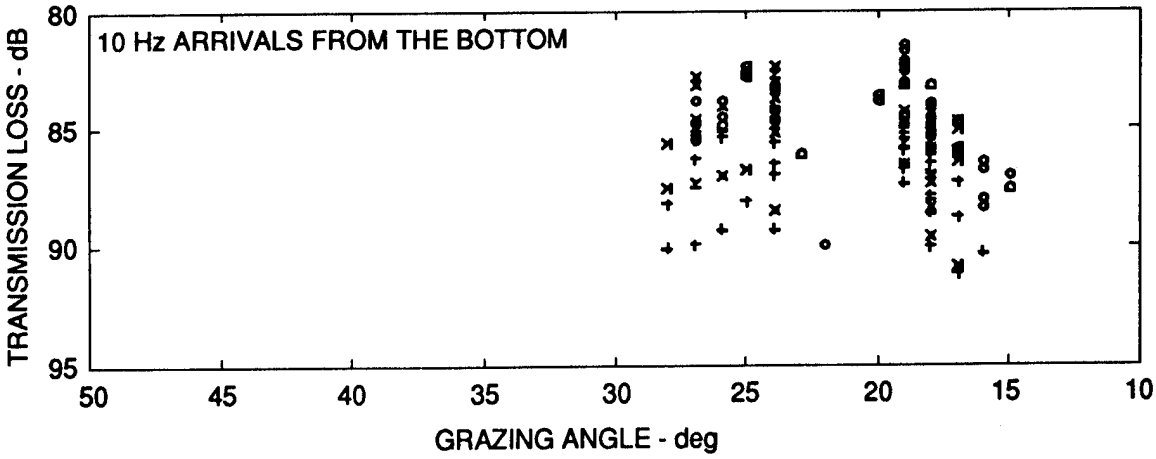

(a) TRANSMISSION LOSS versus GRAZING ANGLE IN THE RANGE INTERVAL 35.1 - 44.9 km

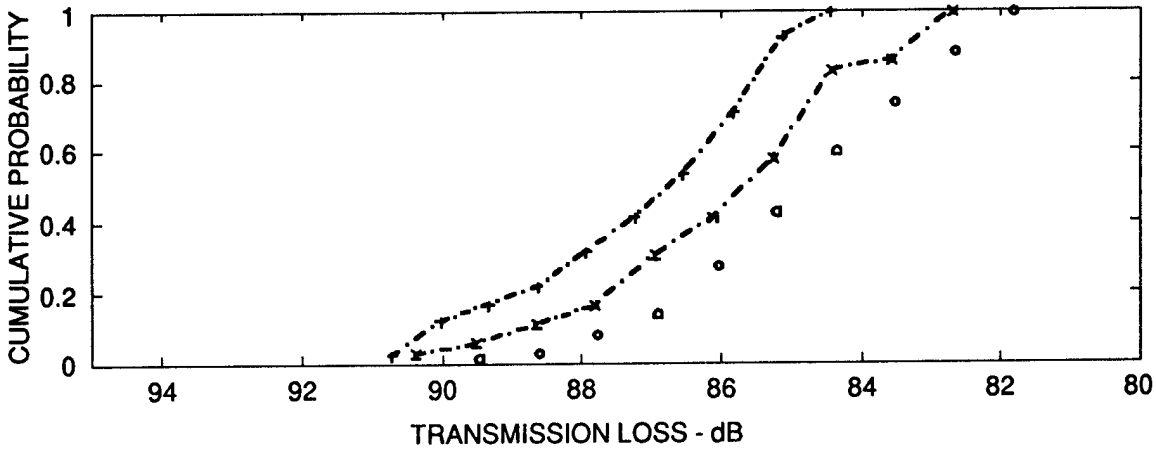

(b) TRANSMISSION LOSS PROBABILITY DISTRIBUTION

- ∘ NATIVE MEASUREMENTS
- + MODEL (GAM 1)
- × MODEL (SPREADING LOSS ESTIMATE)

FIGURE 7.15
TRANSMISSION LOSS versus GRAZING ANGLE AND ASSOCIATED TL PROBABILITY DISTRIBUTION FOR 10 Hz PEAK ARRIVALS FROM THE BOTTOM FOR THE 35.1 - 44.9 km RANGE INTERVAL

ARL - UT
AS-93-591
SJL/RFG
10-93/hd2

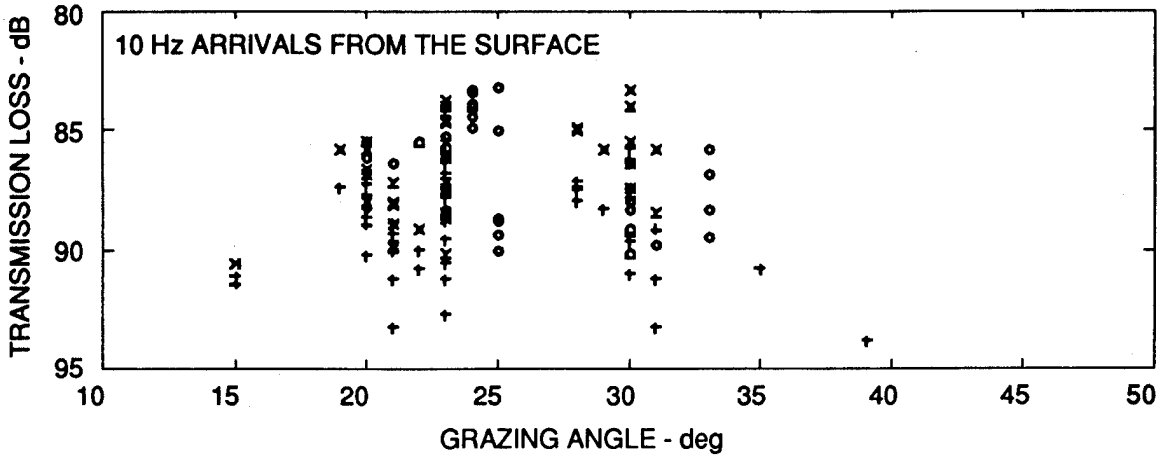

(a) TRANSMISSION LOSS
versus ANGLE IN THE RANGE INTERVAL 45.0 - 55.4 km

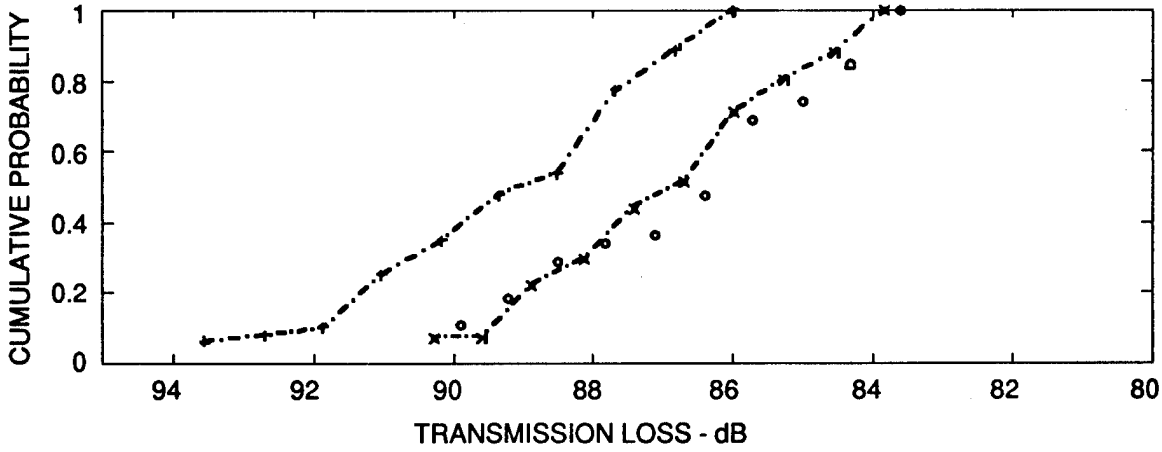

(b) TRANSMISSION LOSS PROBABILITY DISTRIBUTION

o NATIVE MEASUREMENTS
\+ MODEL (GAM 1)
× MODEL (SPREADING LOSS ESTIMATE)

FIGURE 7.16
TRANSMISSION LOSS versus GRAZING ANGLE AND ASSOCIATED TL PROBABILITY DISTRIBUTION FOR 10 Hz PEAK ARRIVALS FROM THE SURFACE FOR THE 45.0 - 55.4 km RANGE INTERVAL

ARL - UT
AS-93-592
SJL/RFO
10-93/hd2

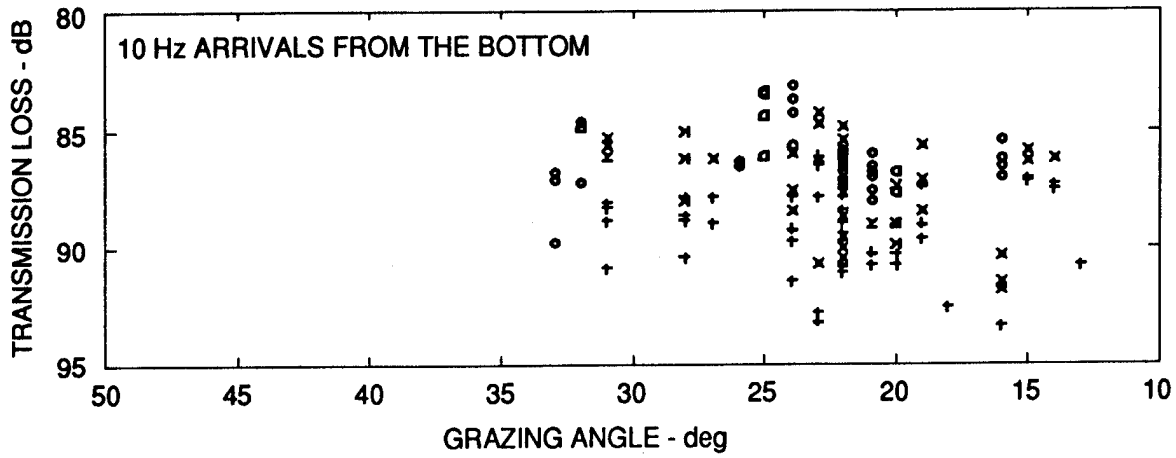

(a) TRANSMISSION LOSS
versus ANGLE IN THE RANGE INTERVAL 45.0-58.0 km

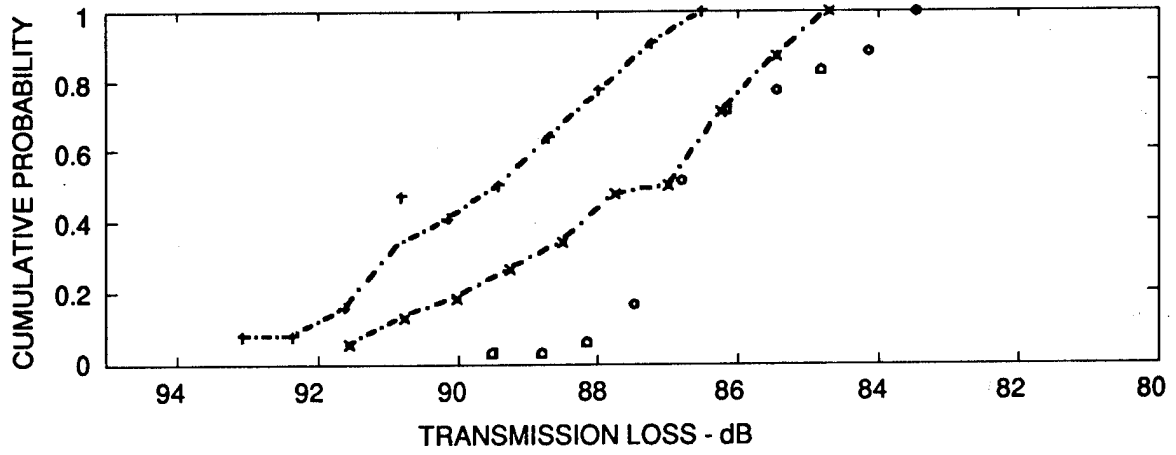

(b) TRANSMISSION LOSS PROBABILITY DISTRIBUTION

o NATIVE MEASUREMENTS
\+ MODEL (GAM 1)
× MODEL (SPREADING LOSS ESTIMATE)

FIGURE 7.17
TRANSMISSION LOSS versus GRAZING ANGLE AND ASSOCIATED TL PROBABILITY DISTRIBUTION FOR 10 Hz PEAK ARRIVALS FROM THE BOTTOM FOR THE 45.0-58.0 km RANGE INTERVAL

ARL - UT
AS-93-593
SJL/RFO
10-93/hd2

8. SUMMARY

Through a careful comparison of the NATIVE I cw measurements with ray and normal mode simulations, the VLF arrival structure and bottom loss have been analyzed. We have observed excellent agreement between measured TL and modeled omnidirectional geometric spreading loss at ranges where direct paths dominate (<7 km), although the agreement is reduced at longer ranges as bottom reflected arrivals become significant. The VLF arrival structure at 7 and 10 Hz has been inspected by means of beam analysis, which shows many features usually associated with a ray description of high frequency signals. Multiple bottom and surface interacting arrivals have been observed in the measurements as well as by both models, and we have analyzed in detail arrivals which encounter the bottom up to four times.

Ray analysis has revealed that negative angle arrivals appearing like bottom interacting energy at the very shortest ranges (<7 km) are actually the result of direct arrivals received on sidelobes. We have performed the bulk of our analysis, however, with adiabatic normal mode calculations. The adiabatic normal mode calculations have allowed us to quantitatively investigate the measured VLF arrivals through a comparison with modeled arrivals.

At ranges less than 20 km, arrivals corresponding to direct, bottom, and bottom-surface interactions are well defined and easily distinguishable, and have arrival structure features that are accurately modeled. At 35-60 km range, the peak arrivals are of irregular order, with the peak arrivals interacting with the bottom between two and four times; yet, all of the arrival orders are approximately equal in level. We have found the long range arrivals are less energetic due to surface interference and shadowing effects at angles shallower than ~10°, and due to spreading and bottom loss at angles steeper than ~40°.

Analysis of the short range bottom interacting measurements using plane wave bottom loss calculations has indicated that a gas hydrate layer is likely the cause of a ~4 dB bottom loss at 7 Hz for grazing angles of 30-34°. At 10 Hz, a higher loss, narrower angular region at about 30° was predicted by the plane wave bottom loss calculation for such a layer. Corresponding beam

calculations at 10 Hz, however, yielded a lower loss, broader angular region than that given by the bottom loss calculations. Unfortunately, the measured bottom loss estimates were considerably scattered, often negative, and did not correlate as well with either geoacoustic model of the sediment at 10 Hz.

Except at angles corresponding to probable interaction with a hydrate layer, VLF bottom loss was low compared to typical values at higher frequency, and consistent with conventional modeled loss calculations corresponding to the hemipalagic geoacoustic parameters in the sediment. At shallow angles, those most relevant to moderate and long range ASW systems, bottom loss is less than 1 dB for single bottom interactions and, to the precision of the measurements, the GAM 1 profile statistically bounds both 7 and 10 Hz bottom loss for multiple bottom interacting arrivals existing at 15-40° grazing angles.

REFERENCES

1. B. R. Gomes et al., "NATIVE I Exercise Plan," NOARL Informal Doc. ID 001:222:90, Naval Oceanographic and Atmospheric Research Laboratory, Stennis Space Center, Mississippi, 9 July 1990.

2. Evan K. Westwood and Paul J. Vidmar, "Eigenray Finding and Time Series Simulation in a Layered-Bottomed Ocean," J. Acoust. Soc. Am. **81**, 912-924 (1987).

3. Ruth Gonzalez and Susan G. Payne, "User's Guide for NEMESIS and PLMODE," Applied Research Laboratories Technical Memorandum 80-6, Applied Research Laboratories, The University of Texas at Austin, May 1980.

4. B. R. Gomes, Sheila McDonnell, and LT Mark Null (USN), "Noise and Transmission Loss in VLF Environments (NATIVE I) Environmental Report," Naval Oceanographic and Atmospheric Research Laboratory, Stennis Space Center, Mississippi, May 1991.

5. Naval Air Development Center, Warminster, Pennsylvania, "NATIVE I Navigation Reconstruction," 4 August 1990.

6. Anthony Brescia and Joseph McCandless, "The Extremely Low Frequency (ELF) Projector Source Level Reconstruction for the NATIVE I Sea Test," NADC Tech. Memo 5044-101290, Naval Air Development Center, Warminster, Pennsylvania, August 1990.

7. K. A. Knevolden and L. A. Barnard, "Hydrates of Natural Gas in Continental Margins," Am. Assoc. Petrol. Geol. Memoir 34, 631-664 (1982).

8. J. M. Daniels and Paul J. Vidmar, "Occurrence and Acoustical Significance of Natural Gas Hydrates in Marine Sediments," J. Acoust. Soc. Am. **72**, 1564-73 (1982).

9. Geoacoustic parameters from Ref. 4 (p. 3G) were adjusted to those of GAM 2 so that 7 Hz plane wave bottom loss calculations provided a good simulation of corresponding measured bottom loss estimates.

20 October 1993

DISTRIBUTION LIST FOR
ARL-TR-93-20
Final Report under Contract N00039-91-C-0082
TD No. 01A1019, NATIVE I VLF Experiment Data Research and Analysis

Copy No.

Commanding Officer
Naval Research Laboratory
Stennis Space Center, MS 39529-5004
1 Attn: J. Ellis
2 B. Gomes
3 J. Newcomb

Commanding Officer
Advanced Environmental Acoustic Support Program
Office of Naval Research Detachment
Stennis Space Center, MS 39529-7050
4 Attn: B. Wheatley (Code 321)
5 E. Chaika (Code 322)

Office of Naval Research
Department of the Navy
Arlington, VA 22217-5000
6 Attn: R. Feden (Code 322)

Chief of Naval Operations
3450 Massachusetts Ave. NW
Naval Observatory
Washington, DC 20392-5421
7 Attn: E. Whitman (N096T)

Commanding Officer
Naval Air Warfare Center/Acoustics Division
Warminster, PA 18974-5000
8 Attn: B. Steinberg

Commanding Officer
Patrol Wings Five
Naval Air Station
Brunswick, ME 04011-5000
9 Attn: CDR M. Worthington (Code N3M)

Distribution List for ARL-TR-93-20 under Contract N00039-91-C-0082,
TD No. 01A1019
(cont'd)

Copy No.	
	National Oceanic and Atmospheric Administration U.S. Department of Commerce Federal Building 4 - Room 2069 Washington, DC 20233
10	Attn: R. Winokur
	Marine Physical Laboratory Scripps Institute of Oceanography San Diego, CA 92152-6400
11	Attn: G. D'Spain
	Science Applications, Inc. 920 Andres Ave. Coral Gables, FL 33134
12	Attn: P. Vidmar
	Planning Systems, Inc. 7925 Westpark Drive McLean, VA 22102
13	Attn: C. Holland
14	Environmental Sciences Group, ARL:UT
15	Nancy R. Bedford, ARL:UT
16	Joan C. Lange, ARL:UT
17	Scott J. Levinson, ARL:UT
18	Stephen K. Mitchell, ARL:UT
19	Library, ARL:UT
20 - 21	Reserve, ARL:UT